



U.S. Department of
Transportation

**Federal Railroad
Administration**

Evaluation of the Degradation of Concrete Ties Using Machine Vision Technology on High-Speed Rail Corridors

Office of Research,
Development
and Technology
Washington, DC 20590



NOTICE

This document is disseminated under the sponsorship of the Department of Transportation in the interest of information exchange. The United States Government assumes no liability for its contents or use thereof. Any opinions, findings and conclusions, or recommendations expressed in this material do not necessarily reflect the views or policies of the United States Government, nor does mention of trade names, commercial products, or organizations imply endorsement by the United States Government. The United States Government assumes no liability for the content or use of the material contained in this document.

NOTICE

The United States Government does not endorse products or manufacturers. Trade or manufacturers' names appear herein solely because they are considered essential to the objective of this report.

REPORT DOCUMENTATION PAGE*Form Approved*
OMB No. 0704-0188

Public reporting burden for this collection of information is estimated to average 1 hour per response, including the time for reviewing instructions, searching existing data sources, gathering and maintaining the data needed, and completing and reviewing the collection of information. Send comments regarding this burden estimate or any other aspect of this collection of information, including suggestions for reducing this burden, to Washington Headquarters Services, Directorate for Information Operations and Reports, 1215 Jefferson Davis Highway, Suite 1204, Arlington, VA 22202-4302, and to the Office of Management and Budget, Paperwork Reduction Project (0704-0188), Washington, DC 20503.

1. AGENCY USE ONLY (Leave blank)		2. REPORT DATE July 2018	3. REPORT TYPE AND DATES COVERED Technical Report – 2011	
4. TITLE AND SUBTITLE Evaluation of the Degradation of Concrete Ties Using Machine Vision Technology on High-Speed Rail Corridors			5. FUNDING NUMBERS DTFR53-12-C-00003	
6. AUTHOR(S) Herbert J. Henderson; Eric T. Sherrock				
7. PERFORMING ORGANIZATION NAME(S) AND ADDRESS(ES) ENSCO, Inc. 5400 Port Royal Road Springfield, VA 22151			8. PERFORMING ORGANIZATION REPORT NUMBER SERV-REPT-0000479 Rev B	
9. SPONSORING/MONITORING AGENCY NAME(S) AND ADDRESS(ES) U.S. Department of Transportation Federal Railroad Administration Office of Railroad Policy and Development Office of Research, Development and Technology Washington, DC 20590			10. SPONSORING/MONITORING AGENCY REPORT NUMBER DOT/FRA/ORD-18/26	
11. SUPPLEMENTARY NOTES COR: Hugh Thompson				
12a. DISTRIBUTION/AVAILABILITY STATEMENT This document is available to the public through the FRA Web site at http://www.fra.dot.gov .			12b. DISTRIBUTION CODE	
13. ABSTRACT (Maximum 200 words) ENSCO, Inc. used machine vision technology to assess concrete tie degradation in Amtrak's high-speed Northeast Corridor (NEC) over a 13-month period. The study examined three aspects of concrete tie degradation: 1) the prevalence of nonconformance types found in the assessed ties, 2) the evolution of concrete tie grades over time, and 3) the rate at which cracks in the assessed ties were found to grow. The assessment of nonconformance prevalence included cracks, chips, crumbling, and missing fasteners. The tie grading scale used in the study ranged from Grade 1–No Material Nonconformances through Grade 5–Ineffective for a population of approximately 26,000 ties and is based on a set of quantifiable parameters discussed in the report. The study's measured crack growth rate data was used to assess whether various parameters (e.g., curvature, posted speed, tie manufacturer, etc.) have a material impact on crack growth rates. The report includes an assessment of the effectiveness of machine vision-based concrete tie inspection as well as several recommendations pertaining to concrete tie maintenance practices.				
14. SUBJECT TERMS Concrete tie, concrete crosstie, tie degradation, cracked tie, concrete tie conditions, tie maintenance, tie replacement, tie inspection, tie grading, tie assessment, Northeast Corridor, concrete tie grades			15. NUMBER OF PAGES 83	
			16. PRICE CODE	
17. SECURITY CLASSIFICATION OF REPORT Unclassified	18. SECURITY CLASSIFICATION OF THIS PAGE Unclassified	19. SECURITY CLASSIFICATION OF ABSTRACT Unclassified	20. LIMITATION OF ABSTRACT Unlimited	

NSN 7540-01-280-5500

Standard Form 298 (Rev. 2-89)
Prescribed by ANSI Std. Z39-18
298-102

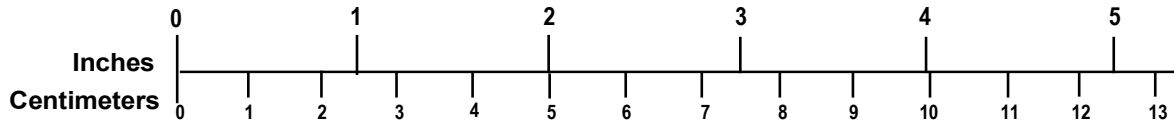
METRIC/ENGLISH CONVERSION FACTORS

ENGLISH TO METRIC

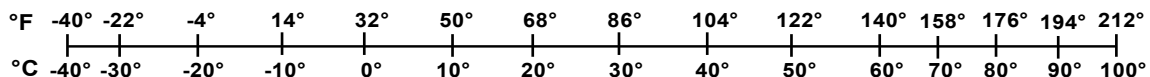
METRIC TO ENGLISH

<p>LENGTH (APPROXIMATE)</p> <p>1 inch (in) = 2.5 centimeters (cm)</p> <p>1 foot (ft) = 30 centimeters (cm)</p> <p>1 yard (yd) = 0.9 meter (m)</p> <p>1 mile (mi) = 1.6 kilometers (km)</p>	<p>LENGTH (APPROXIMATE)</p> <p>1 millimeter (mm) = 0.04 inch (in)</p> <p>1 centimeter (cm) = 0.4 inch (in)</p> <p>1 meter (m) = 3.3 feet (ft)</p> <p>1 meter (m) = 1.1 yards (yd)</p> <p>1 kilometer (km) = 0.6 mile (mi)</p>
<p>AREA (APPROXIMATE)</p> <p>1 square inch (sq in, in²) = 6.5 square centimeters (cm²)</p> <p>1 square foot (sq ft, ft²) = 0.09 square meter (m²)</p> <p>1 square yard (sq yd, yd²) = 0.8 square meter (m²)</p> <p>1 square mile (sq mi, mi²) = 2.6 square kilometers (km²)</p> <p>1 acre = 0.4 hectare (he) = 4,000 square meters (m²)</p>	<p>AREA (APPROXIMATE)</p> <p>1 square centimeter (cm²) = 0.16 square inch (sq in, in²)</p> <p>1 square meter (m²) = 1.2 square yards (sq yd, yd²)</p> <p>1 square kilometer (km²) = 0.4 square mile (sq mi, mi²)</p> <p>10,000 square meters (m²) = 1 hectare (ha) = 2.5 acres</p>
<p>MASS - WEIGHT (APPROXIMATE)</p> <p>1 ounce (oz) = 28 grams (gm)</p> <p>1 pound (lb) = 0.45 kilogram (kg)</p> <p>1 short ton = 2,000 pounds (lb) = 0.9 tonne (t)</p>	<p>MASS - WEIGHT (APPROXIMATE)</p> <p>1 gram (gm) = 0.036 ounce (oz)</p> <p>1 kilogram (kg) = 2.2 pounds (lb)</p> <p>1 tonne (t) = 1,000 kilograms (kg) = 1.1 short tons</p>
<p>VOLUME (APPROXIMATE)</p> <p>1 teaspoon (tsp) = 5 milliliters (ml)</p> <p>1 tablespoon (tbsp) = 15 milliliters (ml)</p> <p>1 fluid ounce (fl oz) = 30 milliliters (ml)</p> <p>1 cup (c) = 0.24 liter (l)</p> <p>1 pint (pt) = 0.47 liter (l)</p> <p>1 quart (qt) = 0.96 liter (l)</p> <p>1 gallon (gal) = 3.8 liters (l)</p> <p>1 cubic foot (cu ft, ft³) = 0.03 cubic meter (m³)</p> <p>1 cubic yard (cu yd, yd³) = 0.76 cubic meter (m³)</p>	<p>VOLUME (APPROXIMATE)</p> <p>1 milliliter (ml) = 0.03 fluid ounce (fl oz)</p> <p>1 liter (l) = 2.1 pints (pt)</p> <p>1 liter (l) = 1.06 quarts (qt)</p> <p>1 liter (l) = 0.26 gallon (gal)</p> <p>1 cubic meter (m³) = 36 cubic feet (cu ft, ft³)</p> <p>1 cubic meter (m³) = 1.3 cubic yards (cu yd, yd³)</p>
<p>TEMPERATURE (EXACT)</p> <p>$[(x-32)(5/9)] \text{ } ^\circ\text{F} = y \text{ } ^\circ\text{C}$</p>	<p>TEMPERATURE (EXACT)</p> <p>$[(9/5) y + 32] \text{ } ^\circ\text{C} = x \text{ } ^\circ\text{F}$</p>

QUICK INCH - CENTIMETER LENGTH CONVERSION



QUICK FAHRENHEIT - CELSIUS TEMPERATURE CONVERSION



For more exact and or other conversion factors, see NIST Miscellaneous Publication 286, Units of Weights and Measures. Price \$2.50 SD Catalog No. C13 10286

Updated 6/17/98

Acknowledgements

This report was made possible with cooperation from the Federal Railroad Administration's (FRA) Office of Research, Development and Technology, Amtrak, and the Computer Vision Laboratory at the University of Maryland, College Park. The authors would like to express their gratitude to Mr. Hugh Thompson at FRA for overseeing the project and to Messrs. Mike Trosino, Joe Mascara, and Steven Sawadasavi, of Amtrak who provided logistical support in coordinating track time necessary to complete this project. The authors would also like to thank the many dedicated Amtrak personnel who assisted on the ground during the imaging surveys conducted under this project. From the University of Maryland, the authors would like to sincerely thank Professor Rama Chellapa and Mr. Xavier Gibert-Serra for image review software development and image database support.

Contents

Executive Summary.....	1
1. Introduction.....	3
1.1 Background.....	3
1.2 Objectives.....	4
1.3 Overall Approach.....	5
1.4 Scope.....	5
1.5 Organization of the Report.....	6
2. Technical Approach.....	7
2.1 Data Acquisition.....	7
2.2 Image Processing and Review.....	11
2.3 Crack Growth Rate Analysis Approach.....	12
2.4 Determination of Statistical Significance.....	15
3. Results.....	21
3.1 Tie Condition Results.....	21
3.2 Growth Rate Results—All Cracks Studied.....	25
3.3 Parametric Growth Rate Results.....	28
3.4 Heuristic Growth Rate and Frequency Results.....	34
4. Assessments.....	38
4.1 Tie Condition Assessment.....	38
4.2 Crack Growth Rate Assessment—All Cracks Studied.....	40
4.3 Parametric Crack Growth Rate Assessment.....	40
4.4 Assessment of Human and Machine Factors.....	43
5. Conclusion.....	45
6. References.....	48
Abbreviations and Acronyms.....	49
Appendix A. Example Images Showing Observed Crack Types.....	50
Appendix B. Tie Rating Guidelines Used in this Study.....	55
Appendix C. Preliminary and Final Software Customization Efforts.....	69

Illustrations

Figure 1-1. Examples of Early and Late Stage Cracking on Two Concrete Ties	4
Figure 2-1. High-Rail Vehicle Used to Collect Track Bed Images	10
Figure 2-2. Track Bed Viewing Software Configured for Side-By-Side Track Bed Viewing....	11
Figure 2-3. Example of an Annotated “Thin” Crack (Width Less Than or Equal to 5 Pixels) ...	12
Figure 2-4. Example of an Annotated “Thick” Crack (Width Greater Than 5 Pixels).....	12
Figure 2-5. Example Frequency Distribution Based on Percentage Growth Rate	14
Figure 2-6. Relationship Between Median Growth Rate and Cumulative Percentage Curve	15
Figure 2-7. Relationship Between RSS Measurement Uncertainty and the Standard Deviation of the Median	17
Figure 3-1. Observed Distribution of Nonconformance Types	21
Figure 3-2. Observed Distribution of Nonconformance Types by Mile.....	22
Figure 3-3. Observed Distribution of Crack Types	22
Figure 3-4. Distribution of Tie Grades Assessed Over 10 Miles of Track Bed Image Data	23
Figure 3-5. Percent Change in the Number of Ties of Each Grade Over a 1-Year Period.....	24
Figure 3-6. Number of Grade 4 or 5 Ties per 39 Feet Versus Tie Location - August 2012.....	25
Figure 3-7. Number of Grade 4 or 5 Ties per 39 Feet Versus Tie Location—September 2013..	25
Figure 3-8. Crack Growth Rate Data for All Cracks Studied Between August 2012 and April 2013 (1,022 Cracks).....	26
Figure 3-9. Crack Growth Rate Data for All Cracks Studied Between August 2012 and September 2013 (2,139 Cracks).....	26
Figure 3-10. Distribution of Crack Growth Rates Among Cracks That Grew	27
Figure 3-11. Crack Growth Rate Versus Curvature.....	29
Figure 3-12. Crack Growth Rate Versus Track Grade	30
Figure 3-13. Crack Growth Rate Versus Posted Speed.....	30
Figure 3-14. Crack Growth Versus Crack Location (Field Versus Gauge Side of Tie).....	31
Figure 3-15. Comparison of Crack Growth Rate Versus Crack Size	32
Figure 3-16. Crack Growth Rate Versus Favorable and Unfavorable Conditions	33
Figure 3-17. Crack Growth Rate Versus Tie Manufacturer	33
Figure 3-18. Crack Growth Rate Versus Position Along the Tie (Tie Manufacturers “A” and “B”).....	34
Figure 3-19. Crack Growth Rate Versus Position Along the Tie (Tie Manufacturer “A” Only)....	35

Figure 3-20. Crack Growth Rate Versus Position Along the Tie (Tie Manufacturer “B” Only)	35
Figure 3-21. Normalized Crack Frequency Versus Position Along the Tie (Tie Manufacturers “A” and “B”).....	36
Figure 3-22. Crack Frequency Versus Position Along the Tie (Tie Manufacturer “A” Only)....	37
Figure 3-23. Crack Frequency Versus Position Along the Tie (Tie Manufacturer “B” Only)....	37
Figure 4-1. Typical Examples of the Nonconformance Types Assessed	38

Tables

Table 2-1. Location of Test Zone Within Amtrak’s AB Line	7
Table 2-2. List of Assessed Track-Related Parameters in the Study’s Test Zone.....	8
Table 2-3. Track and Mile Post Numbers for Detailed Tie Condition Assessment	9
Table 2-4. Track and Mile Numbers for Period 1 Data Set—August 2012 to April 2013	9
Table 2-5. Track and Mile Numbers for Period 3 Data Set—August 2012 to September 2013 .	10
Table 2-6. List of Parameters Included in the Study’s Parametric Growth Rate Assessment.....	13
Table 2-7. Uncertainty in the Growth Rate of a Typical Crack Due to Statistical Sampling.....	18
Table 2-8. Two-Sigma Uncertainties for Parameters Assessed in this Study.....	20
Table 3-1. Summary of Assessed Crack Population Sizes for Periods 1 and 3.....	26
Table 3-2. Percentage of All Cracks Studied That Did and Did Not Grow.....	27
Table 3-3. Sub-Population Sizes for Assessed Parameters.....	28
Table 3-4. Conditions Used to Assess the Impact of Simultaneous Factors on Growth Rate.....	32
Table 4-1. List of Observed Crack Types	39
Table 4-2. Summary of Crack Growth Rates for Assessed Parameters	41
Table 4-3. Growth Rate Spread When Tie Manufacturer “B” Ties are Removed from Data Set	43

Executive Summary

In 2011, ENSCO, Inc. used machine vision technology to assess the degradation in concrete ties on a high-speed rail corridor. In this study funded by the Federal Railroad Administration (FRA), continuous high-resolution images of the track bed were collected on three test dates spread over a 13-month period. Each imaging survey covered the same segment of approximately 100 miles of high-speed track located on the National Railroad Passenger Corporation's (Amtrak) Northeast Corridor (NEC). The track bed images were then reviewed in an office setting with the goal of quantifying and assessing concrete tie degradation over time. Degradation in concrete ties was assessed using two primary approaches.

In the first approach, a population of approximately 115,000 imaged ties was examined for cracks. A set of 2,139 cracks were tracked over 13 months to quantify individual crack growth rates. The growth rate behavior across the entire population of studied cracks was assessed first. An additional assessment then determined whether each of the following parameters influenced the measured crack growth rates:

- Curvature (up to 4.96 degrees)
- Track grade (-0.893 in to 0.546 in)
- Posted speed (30 to 150 mph)
- Tie manufacturer (tie manufacturers "A" and "B")
- Crack location (field or gauge side of tie)
- Crack size (small: 0-3 in, medium: 3-6 in, and large: greater than 6 in)

Conclusions from the crack growth rate assessments indicated that crack growth rates were not alarming. Specifically, during the study's 13-month interval of observation, 65 percent of the cracks studied did not show growth, while 35 percent showed growth. Of the 35 percent that showed growth, the typical increase in crack length was 0.6 in/yr. The results indicated that crack size, crack location, curvature, and tie manufacturer each have a statistically significant influence on crack growth rates, while posted speed and grade do not. Although specific parameters were shown to influence crack growth rate by statistically significant amounts, the overall magnitude of each parameter's influence was overshadowed by the dominant trend that overall crack growth rates were low. As a result, the correlations noted in the study's parametric analysis did not provide stand-alone justifications for recommending changes to existing tie inspection practices.

In the second approach employed by this study, track bed images were used to grade overall tie conditions based on a scale of Grade 1—No Material Nonconformances through Grade 5—Ineffective for a population of approximately 26,000 ties. Tie grades were assessed at two points in time, separated by approximately 13 months, and then they were used to derive annualized tie grade progression rates.

Conclusions from assessing tie grades over the study's 13-month interval of observation were consistent with the non-alarming crack growth rates identified in the study. Specifically, tie grades were observed to advance—i.e., worsen over time—however, the percentage of ties that advanced in grade was slight (only 0.45 percent). Among ties that did advance in grade level,

most (94 percent) did so by one grade level, while a few (6 percent) did so by two grade levels. No ties were observed to advance by more than two grade levels during the study's 13-month observation interval.

The methodology corresponding to both approaches used in this study to evaluate concrete tie degradation involved tracking a large number of concrete ties over time. This was accomplished by employing machine vision technology. In doing so, concrete ties were imaged using high-speed line scan cameras to produce a continuous track bed image. The continuous track bed image served as an input to a machine vision algorithm that detected and numbered the imaged ties. Image review software was then used to assist in manually aligning corresponding tie images from consecutive surveys; approximately 115,000 ties were aligned and assessed to locate cracks. Next, a subset of approximately 26,000 of the aligned ties was manually graded based on a scale of Grade 1–No Material Nonconformances through Grade 5–Ineffective for population of approximately 26,000 ties. Tie grading was accomplished with the assistance of image review software. The software was used again to manually draw detailed outlines around a statistically large population of identified cracks (2,139 cracks), and the area of each crack was computed automatically by software from the manually entered outlines. The crack area, measured at two points in time, was then used to establish the crack growth rate data presented in this report.

Based on the results of this study, it is recommended that high-speed railroads consider potential benefits of focusing concrete tie maintenance activities on ineffective and near-ineffective ties (e.g., Grades 4 and 5), while de-emphasizing maintenance activities on ties exhibiting earlier stages of degradation (e.g., Grades 1, 2, and 3). The use of machine vision technology in examining concrete tie conditions was shown to be effective during this study, and this report recommends that railroads examine the potential efficiency gains that come from assessing concrete ties with machine vision technology.

1. Introduction

The research documented in this report aims to quantify concrete tie degradation rates in high-speed rail over statistically significant population sizes using machine vision technology. The Federal Railroad Administration's (FRA) Office of Research, Development and Technology (RD&T) provided funding to ENSCO, Inc. for work performed and conducted in partnership with the National Railroad Passenger Corporation (Amtrak) in 2011. Software development and database support was provided by ENSCO, Inc., and the Computer Vision Laboratory at the University of Maryland, College Park.

Many corridors that have been planned for the U.S. high-speed rail network will use concrete ties. As a result, procedures for concrete tie inspection and maintenance are becoming increasingly important. This study's primary purpose is to advance the understanding of concrete tie degradation to support corresponding improvements in safety and operating efficiencies for high-speed rail networks. Accomplishing this objective would have been difficult without machine vision technology, which allowed the team to go beyond what would have been practical using traditional on-foot tie inspection practices. Specifically, machine vision technology has enabled the evaluation of statistically large population sizes. As a result, this study provides an initial base of data derived from statistically relevant population sizes to help broaden the understanding of concrete tie degradation in high-speed rail corridors.

1.1 Background

In high-speed passenger lines, daily, weekly, or bi-weekly concrete tie condition assessments are typically made from a high-rail vehicle. These assessments are generally sufficient to identify any gross tie conditions that would cause an immediate threat to rail safety. In order to support long-term track maintenance, more detailed tie condition assessments are commonly performed by walking tie inspectors on a less frequent basis. The frequency of the detailed tie condition assessments typically depends on a compilation of feedback from the high-rail-based tie condition assessments, which may vary from one territory to another.

Walking tie inspections generally requires a team of three railroad personnel. As they walk down the track, two members of the team inspect their respective half of each tie, while the third member acts as a lookout for trains. During a walking tie inspection, which typically covers about seven miles per day, tie conditions are often recorded by hand on log sheets, and nonconforming ties may also be marked with paint. A typical output from a detailed tie condition assessment is a tally of the overall condition of each tie based on a tie grading scale, such as Grade 1–No Visible Defects through Grade 5–Ineffective for a population of approximately 26,000 ties.¹

Today's practice of grading concrete ties is designed to provide an accurate snapshot of current tie conditions for tie replacement planning. However, what is not well documented, particularly for high-speed rail applications, is the time required for a typical Grade 1 tie with a minor

¹ This is in reference to the "Concrete Tie Condition Evaluation and Safety Inspection Procedures" section, authored by J.A. Smak, in the May/June 2009 edition of *Amtrak Engineering Practices, Maintenance-of-Way-100*, an internal corporate resource guide.

nonconformance (left side of Figure 1-1) to progress to a Grade 5 state (right side of Figure 1-1). Similarly, data needed to estimate the time required for a benign, early-stage crack (left side of Figure 1-1) to progress to a later-stage crack of concern (right side of Figure 1-1) is also not readily available.

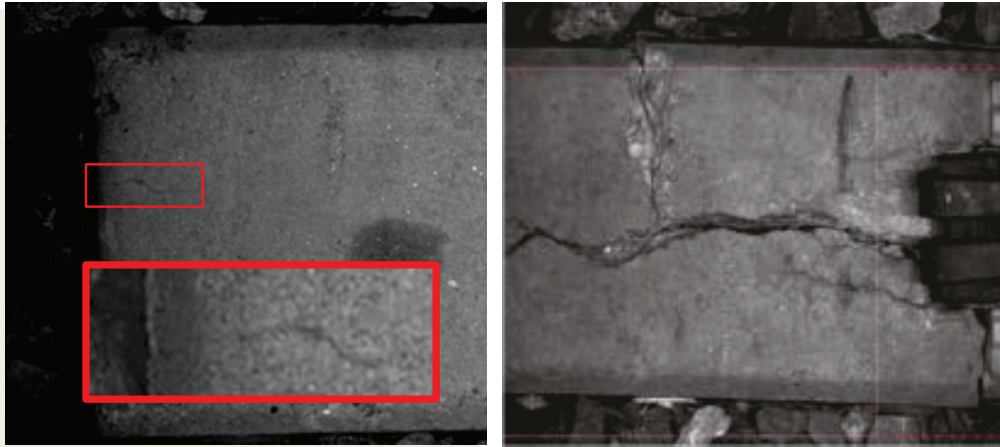


Figure 1-1. Examples of Early and Late Stage Cracking on Two Concrete Ties

While today's concrete tie inspection practices are generally meeting current needs, machine vision technology could lead to significantly improved efficiencies via automated concrete tie inspection. High intensity lighting and machine vision cameras with the high data output rates that can record track bed images at revenue speeds already exist and have been demonstrated to be effective. Additionally, machine vision algorithms that can reliably detect concrete ties in track bed images already exist and have been demonstrated to be effective. In the rail industry, other machine vision algorithms accomplish tasks, such as detecting joint bars, locating cracks in joint bars, and measuring the gap between jointed sections of rail. Ongoing rail-oriented machine vision initiatives include developing algorithms to detect nonconformances including cracks in concrete ties, missing fasteners, and rail head deterioration. Thus, while fully automated concrete tie inspection is not yet a reality, progress toward this end goal is being made.

1.2 Objectives

This study's goal was to use machine vision technology to monitor the progression of concrete tie conditions within a test zone located on Amtrak's Northeast Corridor (NEC). The project's objectives were to:

- Develop a method for quantifying and tracking degradation rates across large numbers of nonconformances in concrete ties in an objective and consistent manner
- Create enhanced software that can efficiently review track bed image data for manually identifying and logging nonconformances in concrete ties
- Provide an enhanced software capability to align and assess track bed image data from multiple test runs conducted over time
- Report survey and analysis results, including measured degradation rates, which will serve as quantified data for tie grading and tie maintenance planning

- Relate operating parameters (including posted speed, curvature, tie manufacturer, grade, and others) to crack growth rates to assess whether one or more of these factors may influence concrete tie degradation

1.3 Overall Approach

In this study, a machine vision system mounted on a high-rail vehicle was used to collect continuous, high-resolution images of the track bed within a pre-selected test zone on the north end of Amtrak's NEC. The study included three separate surveys conducted over a period of 13 months. After the images were collected, a machine vision algorithm automatically detected ties in each track bed image set. Then the image review software was used to manually review the track bed images. During the manual review, cracked ties were identified and aligned across consecutive surveys. Next, the team used the image review software to create an initial image set in which they manually created detailed outlines around each crack in the study. Then the team copied and pasted the crack outlines into a second image set recorded at a later time, and the transferred annotations were manually adjusted so they lined up with each crack outline in the second image set. The image review software was then used to automatically calculate the area of each annotated crack in both images. From this, an annualized crack growth rate was calculated as the change in crack area normalized to a 1-year period.

During the final stage of the crack growth rate analysis, the data was analyzed across a range of parameters to identify the parameters that exert a statistically significant influence on crack growth rate. The assessed parameters included curvature, track grade, posted speed, tie manufacturer, crack size, and crack location with respect to the field or gauge side of the tie.

In addition to the crack growth rate analysis, a two-phase tie condition assessment was conducted using ten miles of track bed image data from the study's test zone. During the first phase, the relative prevalence of four nonconformance types (cracks, chips, crumbling, and missing fasteners) was assessed by counting the instances of each type. During the second phase, a numerical grade was assigned to each tie in the 10-mile data at the beginning and the end of a 13-month period. The tie grade data was used to quantify the rate at which each tie grade progresses to each of the possible higher grades. For example, the data was used to quantify how many Grade 1 ties progress to become Grade 2 ties, how many progress to become Grade 3 ties, and so on.

1.4 Scope

The scope of this project included:

- Developing analysis tools to facilitate manual extraction and utilization of useful information from continuous track bed images recorded using line scan machine vision cameras.
- Enhancing machine vision-based image review capabilities targeted at facilitating the alignment and comparison of multiple images of the same track assets collected over time.
- Characterizing statistically significant samples of individual concrete ties installed on Amtrak's NEC to assess the growth rate of cracks in a high-speed passenger application.

- Determining the influence of infrastructure and operational parameters on observed crack growth rates in a high-speed passenger application.

The results of this study provide a source of information that will help the railroad industry assess the factors contributing to concrete tie degradation, and ultimately the study was designed to support the development of more standardized inspection and maintenance guidelines pertaining to concrete ties, particularly in high-speed applications.

1.5 Organization of the Report

The organization of the report notes the technical approach employed during this research effort discussed in Section 2. Section 3 presents the study's measured results that are related to overall tie conditions, including tie grades. Section 4 presents the assessments of overall tie conditions. Section 5 presents conclusions and recommendations based on the assessments that are presented in Section 4.

Supplemental material is provided in the following appendices:

- Appendix A. Example Images Showing Observed Crack Types
- Appendix B. Tie Rating Guidelines Used in this Study
- Appendix C. Preliminary and Final Software Customization Efforts

2. Technical Approach

This section describes the overall technical approach used in this study. Section 2.1 describes the study's image acquisition phases. Section 2.2 deals with how the images were processed and reviewed. Section 2.3 then describes the approach that the study used to determine crack growth rate. Finally, Section 2.4 describes how measurement and sampling uncertainty were accounted for when assessing the results.

2.1 Data Acquisition

Data collection was performed on several test zones along Amtrak's NEC and included image collection and analysis.

2.1.1 Description of Test Zone

The ties imaged and assessed in this study were installed on Amtrak's NEC near Providence, RI, on Amtrak's AB line.

Table 2-1 lists the start and end locations, as well as the track numbers, for each segment of track included in the study's test zone.

Table 2-1. Location of Test Zone Within Amtrak's AB Line

Approximate Track Start and End Locations	Track Number	Start Mile Post	End Mile Post	Total Miles
Lawn to Kingston Interlocking	1	188	158	29
Transfer to Lawn Interlocking	1	218	189	29
Westerly Yard to Arnold Lumber	2	143	158	15
Lawn to Kingston Interlocking	2	187	159	28
Lawn to Transfer Interlocking	2	189	218	29
TOTAL NUMBER OF MILES				130

The cracks admitted into the study are from a 66-mile subset of the 130 miles of track listed in Table 2-1. Track that was outside of the subset was not used due to data attrition and tie replacement activities that took place during the study's observation interval.

The study's test zone included ties manufactured by two tie manufacturers as well as a range of curvatures, track grades (degree of incline), and posted speeds. One aspect of this study studies whether or not each of these parameters has a material impact on crack growth rates. For reference, Table 2-2 lists each of these parameters and the corresponding range of parameter values found in the study's test zone.

Table 2-2. List of Assessed Track-Related Parameters in the Study’s Test Zone

Parameters
Tie Manufacturer Tie Manufacturer “A” – Installed 1979 Tie Manufacturer “B” – Installed 1994
Curvature Non-Tangent Track ($> 0^\circ$ to 9.93°) Tangent Track (0°)
Track Grade Neutral Grade ($ \text{Grade} \leq 116$) Non-Neutral Grade ($ \text{Grade} > .116$)
Posted Speed High Range ($> 125 - 150$ mph) Low Range ($30 - \leq 125$ mph)

2.1.2 Test Dates and Analysis Periods

This section provides background information on the image data sets used in this study, including the relationship between the image data sets and the various tie condition assessments conducted under this study.

The results of this study were derived from three image data sets collected on the following dates:

- Survey 1 – August 6 to August 10, 2012
- Survey 2 – April 15 to April 19, 2013
- Survey 3 – September 23 to September 26, 2013

Collectively, the three survey dates listed above combine to establish the following three analysis periods:

- Period 1 – August 2012 to April 2013 (between imaging Surveys 1 and 2)
- Period 2 – April 2013 to September 2013 (between imaging Surveys 2 and 3)
- Period 3 – August 2012 to September 2013 (between imaging Surveys 1 and 3)

In this study, track bed images were used to assess concrete tie degradation using two approaches. In the first approach, the progression of tie grades was evaluated on a scale of Grade 1–No Material Nonconformances through Grade 5–Ineffective for a population of approximately 26,000 ties during Period 3 (listed above), and the evaluation was based on approximately 26,000 ties located within the ten miles of track listed in Table 2-3.

The results from the first approach are provided in Section 3.1.

Table 2-3. Track and Mile Post Numbers for Detailed Tie Condition Assessment

Track-Mile Post	
1-199	1-210
1-203	1-211
1-207	1-212
1-208	1-213
1-209	2-161

The second approach involved measuring crack growth rates across a statistically large population of cracks. The corresponding growth rate comparisons are presented in Section 3.3 and these comparisons are based on growth rate data corresponding to Periods 1 and 3 listed above.²

Table 2-4 lists the track and mile numbers where crack growth rates corresponding to Period 1 were assessed, and Table 2-5 lists the track and mile numbers where crack growth rates corresponding to Period 3 were assessed.³

Table 2-4. Track and Mile Numbers for Period 1 Data Set—August 2012 to April 2013⁴

Track	Mile								
1	189	2	143	2	171	2	183	2	198
1	191	2	144	2	173	2	184	2	206
1	192	2	160	2	176	2	186	2	208
1	193	2	161	2	177	2	190	2	209
1	210	2	163	2	181	2	191		
1	211	2	170	2	182	2	192		

² Original planning for this aspect of the study called for assessing growth rates over all three periods listed above, however, plans were changed due to significant tie replacement activity that took place in the study’s test zone during Period 2. The tie replacement activities resulted in a need to replace annotated cracks in the study’s data set. The replaced cracks were those that could no longer be tracked because the corresponding ties were removed from the study’s test zone. The opportunity cost of this rework effort was that time and resources were no longer sufficient to assess growth rates during all three periods listed above.

³ Based on original plans, the same track and mile numbers would have been used to evaluate tie degradation during all three periods listed above; however, because of the tie replacement activities referenced above, the data sets for Periods 1 and 3 are largely different.

⁴ Underlining is used in Table 2-4 to indicate the track and mile numbers shared in common between Period 1 and Period 3.

Table 2-5. Track and Mile Numbers for Period 3 Data Set—August 2012 to September 2013

Track	Mile								
1	192	1	209	2	163	2	193	2	202
1	193	1	210	2	164	2	194	2	203
1	194	1	211	2	165	2	195	2	205
1	198	1	212	2	166	2	196	2	206
1	199	1	213	2	167	2	197	2	207
1	201	2	159	2	186	2	198	2	209
1	203	2	160	2	190	2	199	2	210
1	207	2	161	2	191	2	200	2	211
1	208	2	162	2	192	2	201	2	213

2.1.3 Image Collection

The images collected in this study were acquired by a monochrome track bed imaging system mounted on a high-rail vehicle (Figure 2-1). Each collected image is a continuous, line scanned picture spanning the full width of each tie with a nominal 0.43 mm pixel size at the tie surface. Images were collected at speeds between 15 and 25 mph during both daytime and nighttime operations, and the image data was tagged with milepost location information entered by a forward-looking observer during Surveys 1 and 2. Survey 3 used automatic milepost insertion based on real-time Global Positioning System (GPS) coordinates. The machine vision inspection technology used for this research is based on technology originated through FRA-sponsored research and development of the automated optical joint bar inspection system used throughout the North American rail industry (Tajaddini, 2006).



Figure 2-1. High-Rail Vehicle Used to Collect Track Bed Images

2.2 Image Processing and Review

This section includes alignment of images collected from surveys and measurement of crack growth area of aligned images

2.2.1 Image Alignment Process

To assess crack growth rates, image files from consecutive surveys were aligned on a tie-by-tie basis. To facilitate the process of aligning track bed images, automatic tie detection software located each tie in the image sets for each survey and each detected tie was assigned a set of GPS coordinates that were recorded during the imaging process. Next, ties at the beginning and end of each mile of image data were aligned based on minimizing the distance between the assigned GPS coordinates. This approach typically resulted in ± 20 feet of registration error. Finally, optimal tie-to-tie registration was achieved by manually aligning the starting and ending points for each one-mile section of track. Manual alignments were made using a side-by-side track bed viewing application, as shown in Figure 2-2.

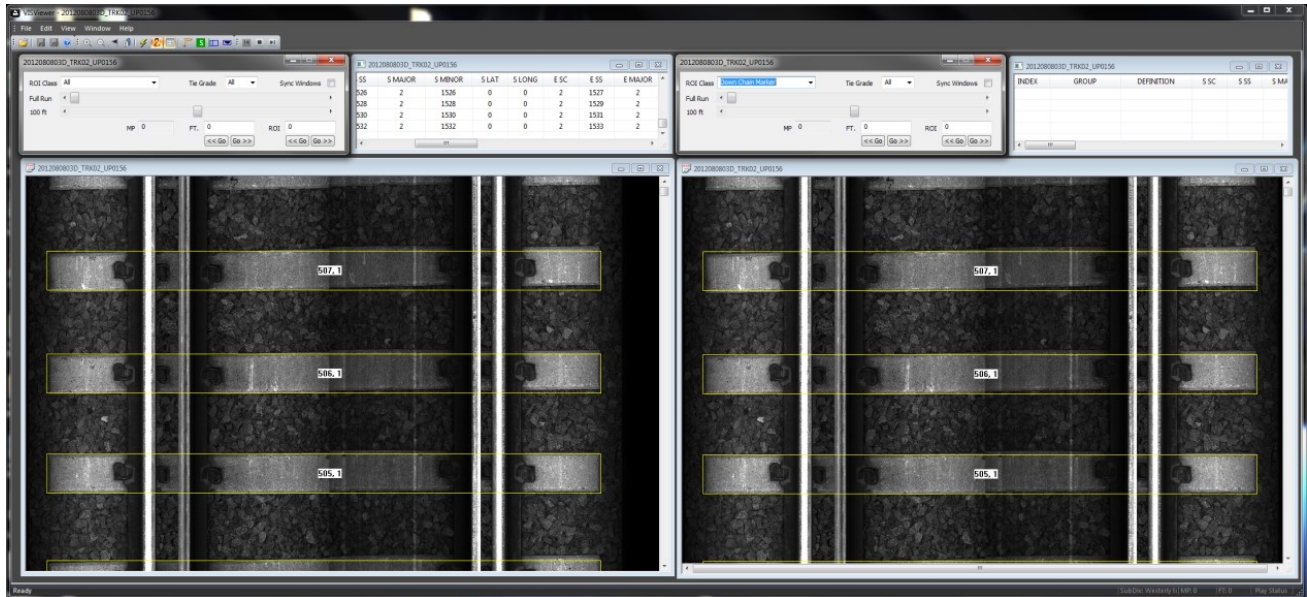


Figure 2-2. Track Bed Viewing Software Configured for Side-By-Side Track Bed Viewing

2.2.2 Crack Area Determination

To measure crack areas, the team began the process by using software jointly developed by ENSCO and the Computer Vision Laboratory at the University of Maryland, College Park to draw a detailed outline around, or along, each crack of interest. Cracks with an average width of approximately 5 pixels or less were captured by drawing a single poly-line down the estimated centerline of the crack (see Figure 2-3). Cracks wider than about 5 pixels were captured by drawing an outline around the perimeter of the crack (see Figure 2-4).

Next, the area of each crack was computed automatically by counting the number of pixels enclosed within (or along) an annotation and multiplying this total by the nominal area of a single pixel.

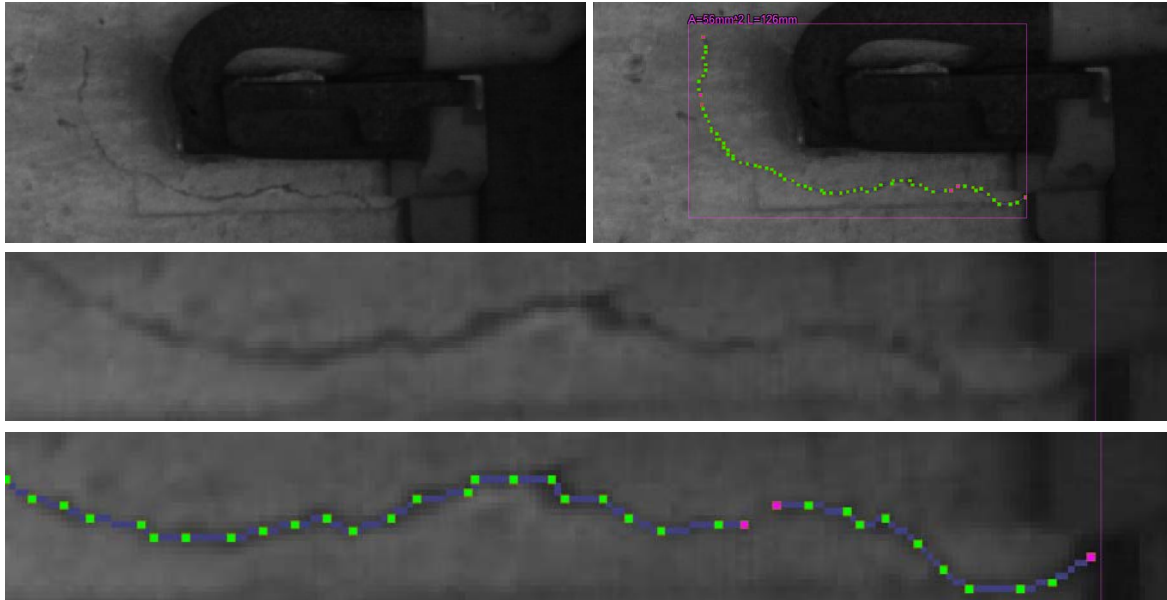


Figure 2-3. Example of an Annotated “Thin” Crack (Width Less Than or Equal to 5 Pixels)

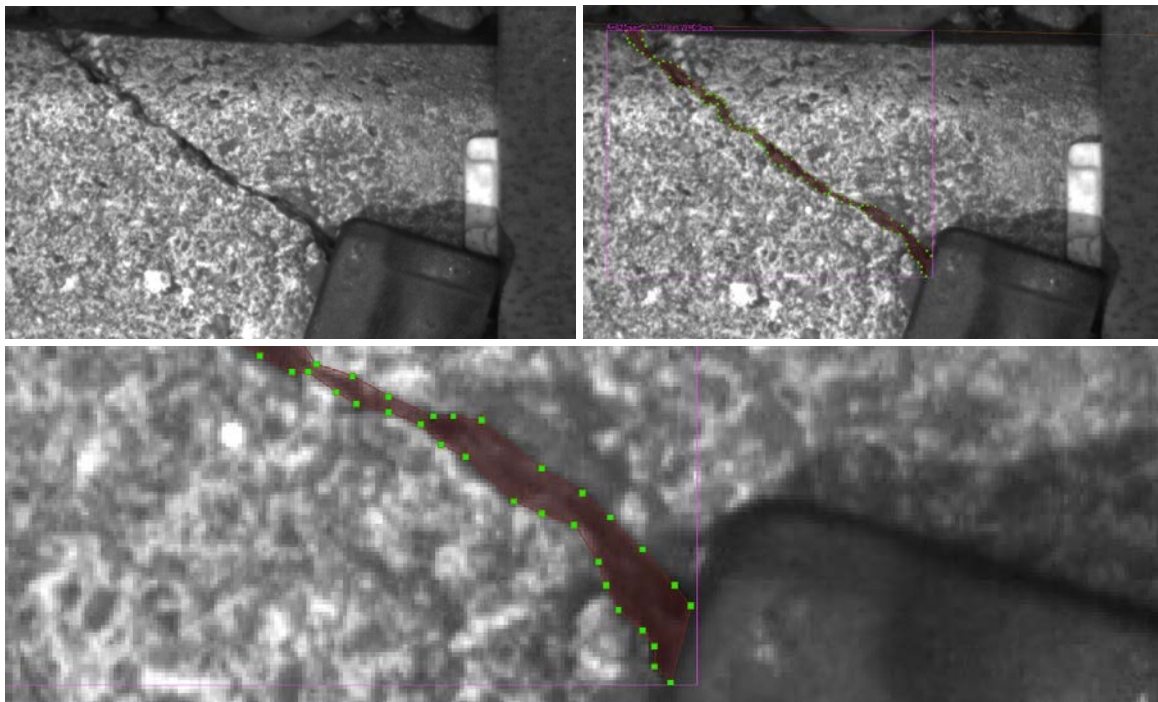


Figure 2-4. Example of an Annotated “Thick” Crack (Width Greater Than 5 Pixels)

2.3 Crack Growth Rate Analysis Approach

Section 2.3.1 presents the overall approach used to analyze crack growth rate data, while the remaining sub-sections describe how crack growth rates are calculated, presented, and compared in the results section of this report.

2.3.1 Overall Crack Growth Rate Analysis Approach

In this study, crack growth rates were analyzed from two perspectives. First, macroscopic growth rate behavior was studied across a statistically large population of cracks located throughout the study’s test zone. Then the team examined whether each parameter listed in

Table 2-6 has a statistically significant influence on crack growth rate. Except for “Combined Factors,” the parameters listed in

Table 2-6 are self-explanatory. The “Combined Factors” parameter is included as part of assessing crack growth behavior in a “worst case” scenario. Further details about the “Combined Factors” parameter are discussed in Section 3.3.4. The details mentioned in the remaining subsections under Section 2.3 pertain to both of the analysis perspectives described above.

Table 2-6. List of Parameters Included in the Study’s Parametric Growth Rate Assessment

Parameter
Combined Factors Worst Case Best Case
Crack Size Small Crack $\leq 35 \text{ mm}^2$ Medium Crack $> 35 \text{ to } \leq 70 \text{ mm}^2$ Large Crack $> 70 \text{ mm}^2$
Curvature Non-Tangent Track ($> 0^\circ$ to 9.93°) Tangent Track (0°)
Tie Manufacturer Tie Manufacturer “B” Tie Manufacturer “A”
Field vs. Gauge Gauge Side Field Side
Track Grade Neutral Grade ($ \text{Grade} \leq .116$) Non-Neutral Grade ($ \text{Grade} > .116$)
Posted Speed High Range ($> 125 - 150 \text{ mph}$) Low Range ($30 - \leq 125 \text{ mph}$)

2.3.2 Crack Growth Rate Calculation

In this report, crack growth rate is calculated and reported as an annualized growth rate (AGR). A crack’s annualized growth rate indicates the increase in a crack’s area (normalized to a 1-year period) and is reported in units of mm^2/year . The equation used to determine annualized growth rate given two crack area measurements (in mm^2) spaced in time by Δt (in years) is as follows:

$$AGR = (\text{Final Crack Area} - \text{Initial Crack Area})/\Delta t \quad (1)$$

2.3.3 Growth Rate Presentation Format

The first of two primary formats used in this report to present crack growth rate data is a normalized frequency distribution. The figure below (Figure 2-5) shows a typical normalized frequency distribution for a sub-population of crack growth rate data. In Figure 2-5, the left-most vertical bar indicates that about 14 percent (read from the left vertical axis, which shows percentages in decimal form) of the cracks in this sub-population grew at an annualized rate greater than zero but not more than 3 mm²/year (read from the horizontal axis). Similarly, each remaining bar in the graph indicates the relative percentage (or normalized frequency) of cracks that grew by the corresponding rate shown under the bar along the horizontal axis. A normalized frequency distribution like Figure 2-5 is an intermediate format needed to produce the second format that is used to compare crack growth rates between two or more crack populations.

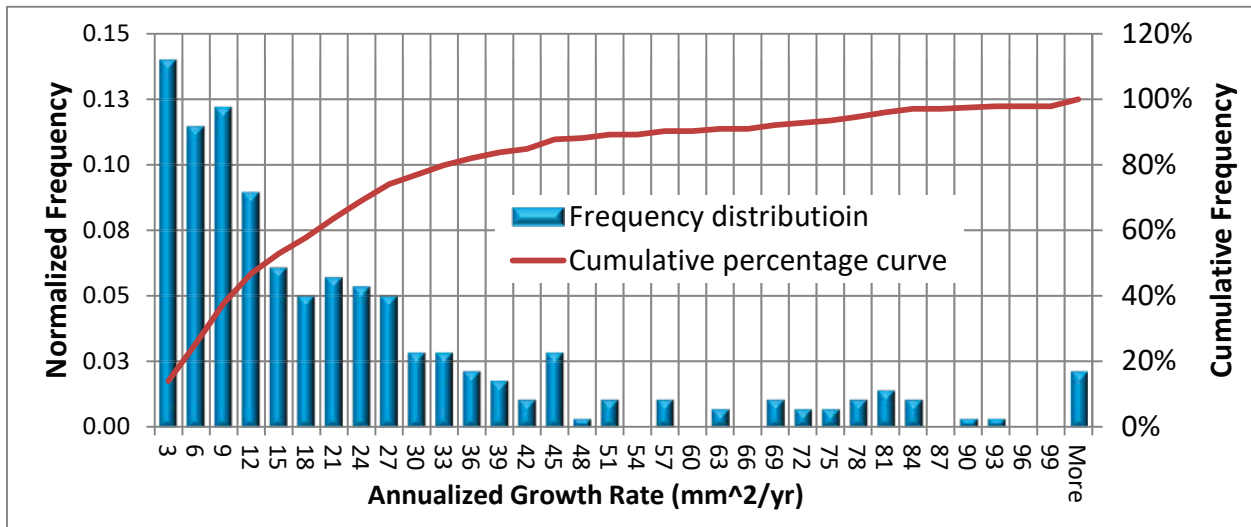


Figure 2-5. Example Frequency Distribution Based on Percentage Growth Rate

The second format used in this report to compare crack growth rate data is a cumulative percentage curve, or cumulative probability distribution. A cumulative percentage curve is the integral (i.e., the running total) of a normalized frequency distribution. Figure 2-5 includes an example of a cumulative percentage curve corresponding to the normalized frequency distribution shown in the same figure. A cumulative percentage curve summarizes an entire population of data and provides a format that can be used to quantitatively compare two or more populations (as discussed the next section).

2.3.4 Crack Growth Rate Metric

When this report assesses whether a given parameter influences crack growth rate more or less than another parameter, the median is used to quantitatively compare two or more parameters of interest. Formally, the median is defined as the 50th percentile within a population (Figure 2-6). The median is a measure of the horizontal position (or location) of a population of data. In this report, the median growth rate within a population of cracks is used to represent the population’s growth rate behavior as a single parameter. This allows a sub-population of many cracks to be

represented by a hypothetical “typical crack.” In this report, a “typical crack” for a given sub-population is one that grows at the sub-population’s median growth rate.

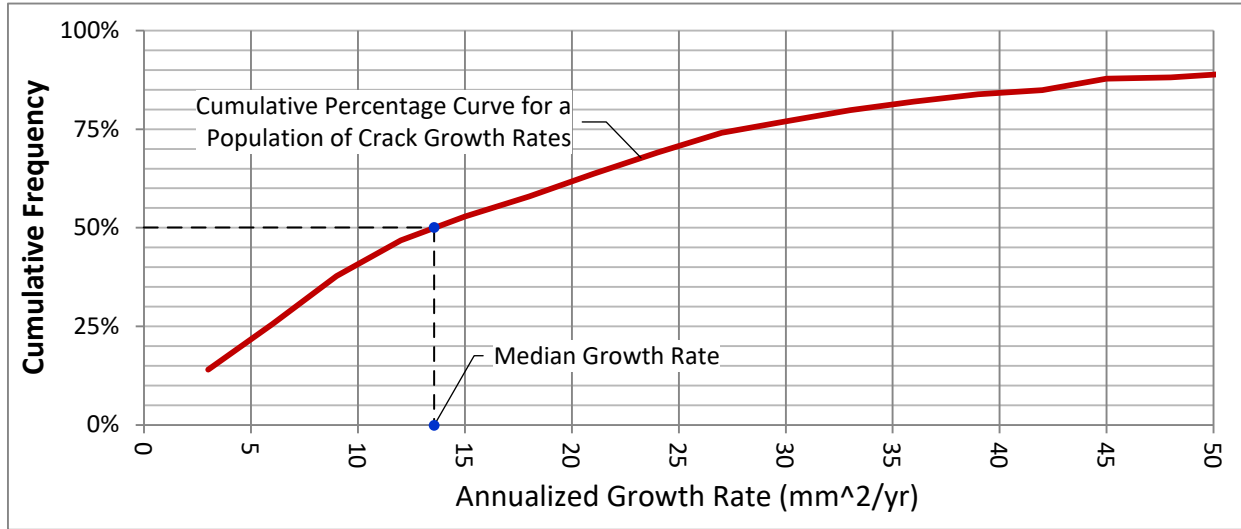


Figure 2-6. Relationship Between Median Growth Rate and Cumulative Percentage Curve

2.4 Determination of Statistical Significance

One aspect of this study assesses the potential impact of various parameters (e.g., curvature, posted speed, etc.) on crack growth rate. In order to draw statistically relevant conclusions, the impact of uncertainty (error) on growth rate must be considered. The following subsections describe:

- How measurement uncertainty in crack growth rate was estimated
- How statistical sampling uncertainty was estimated
- How measurement uncertainty and statistical sampling uncertainty were combined
- How results are compared to determine whether a given parameter has a statistically significant influence on crack growth rate

2.4.1 Measurement Uncertainty

This section describes how uncertainty in the growth rate of a single crack is estimated. Uncertainty in the crack growth rate data is primarily attributable to two independent factors:

1) Using manual review techniques to correctly assess crack boundaries in an image

In this study, crack area is derived by manually drawing a detailed outline around a crack’s boundary using a software application. Changes in crack contrast due to variations in elements, such as lighting conditions, concrete moisture content, and surface contaminants introduce a need to apply judgment when estimating a crack’s true boundary during the annotation process. These factors have a larger impact as crack size decreases. For smaller cracks (crack area ≤ 35 mm²), the uncertainty is approximately 5 percent, for medium cracks (35 mm² < crack area ≤ 70 mm²) it is approximately 2.5 percent, and for large cracks (crack area > 70 mm²) it is approximately 1 percent.

Averaging these values yields approximately 2.8 percent error traceable to non-perfect annotations.

2) Scale repeatability during the imaging process

The track bed images in this study were collected using a high-rail based machine vision system. Scale (size) repeatability during imaging decomposes into two uncorrelated components: 1) scale error due to vertical motion of the imaging platform, and 2) encoder errors moving along the track. Scale errors due to vertical platform motion are estimated to contribute 1 percent to the square root of the sum of the squares (RSS) error budget. Encoder errors along the direction of travel are calibrated over 400 feet with ± 1 -foot accuracy, contributing another 0.25 percent to the RSS error budget. Encoder (or wheel) slippage is another potential source of scale error along the direction of travel, however, encoder slippage is negligible over the width of a single tie.

Combining the non-negligible error sources listed above using a conventional RSS approach yields a total estimated uncertainty in crack area determination of 2.98 percent. Using a conventional RSS approach again, the corresponding uncertainty in crack growth (i.e., the difference between two crack area measurements) is then 4.2 percent. Crack growth is reported as an annualized growth rate, annualizing the rate involves multiplying 4.2 percent by the ratio of 12 months divided by 13 months, where 12 months corresponds to 1 year, and 13 months is the interval of observation. This yields an estimated uncertainty of 3.9 percent in the annualized growth rate. To convert this percentage error to an expected absolute error, an assumption for crack size is required. The assumption used in this analysis is $70 \text{ mm}^2/\text{yr}$, which corresponds to the boundary between a medium and large crack. Based on this assumption, the estimated RSS measurement error in crack growth rate is $2.7 \text{ mm}^2/\text{yr}$.

As described earlier in Section 2.3.4, this study compares the growth rate behavior of two or more crack populations by assigning each population a single parameter (the median crack growth rate within a given sub-population, also referred to herein as the “growth rate for a typical crack”). In order to properly account for measurement uncertainty, the uncertainty in growth rate corresponding to a single crack must be translated to a corresponding uncertainty in the median crack growth rate. To accomplish this, a conventional Monte Carlo simulation was conducted to establish a relationship between the measurement error in the growth rate for a single crack (the x-axis of Figure 2-7) and the standard deviation of the median (the y-axis of Figure 2-7).

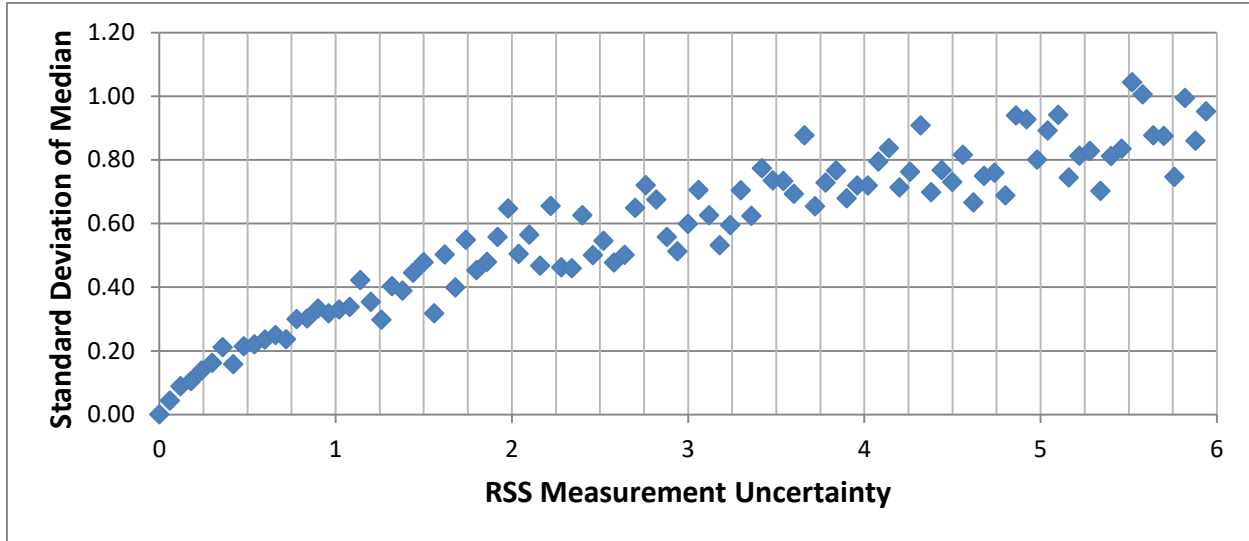


Figure 2-7. Relationship Between RSS Measurement Uncertainty and the Standard Deviation of the Median

Effectively, the graph of Figure 2-7 translates the uncertainty in growth rate for a single crack (an x-axis value) into a corresponding standard deviation in the median crack growth rate (a corresponding y-axis value). From above, the estimated RSS uncertainty for crack growth rate is estimated to be 2.7 mm²/yr. Using Figure 2-7, an RSS measurement uncertainty of 2.7 mm²/yr translates into a standard deviation in the median of approximately 0.6 mm²/yr. In Section 2.4.4, it will be shown how the standard deviation in the median crack growth rate is combined with statistical sampling uncertainty (described in the next section) to yield overall uncertainty in the growth rate of a typical crack.

2.4.2 Statistical Sampling Uncertainty

This section describes how uncertainty in crack growth rate due to statistical sampling was estimated. Statistical sampling uncertainty is important in this study because it is not possible to know with full confidence whether or not an available sub-population of crack growth rate data exactly represents all possible sub-populations. In this study, the median (or 50th percentile point) is the parameter used to compare various sub-populations of crack growth rate data. Thus, an assessment of how statistical sampling impacts the median of a population is needed. To make this assessment, this well-known approximation for the standard deviation of the sample median was used:

$$\sigma \approx \frac{1}{2\sqrt{n}f(x_m)} \quad (2)$$

Equation 2 requires two inputs: 1) a value “n” equal to the number of samples in the population of crack growth rates being assessed, and 2) the median value “f(x_m)” within the normalized frequency distribution corresponding to the population of crack growth rates being assessed.

Because statistical sampling uncertainty depends on the size and shape of the population being analyzed, sampling uncertainty must be evaluated for each parameter of interest (e.g., curvature, posted speed, etc.). Table 2-7 summarizes the estimated statistical sampling uncertainty for each sub-population of crack growth rate data analyzed in this report. In compiling the results listed

in Table 2-7 using Equation 2, values of “n” for each sub-population of interest were pulled from Table 3-3, and values for “ $f(x_m)$ ”, or the median value, were estimated from the plotted frequency distribution corresponding to each parameter, as presented in Section 3.3.

Table 2-7. Uncertainty in the Growth Rate of a Typical Crack Due to Statistical Sampling

Parameter	Estimated Sampling Uncertainty (mm ² /yr)
Combined Factors	
Worst Case	0.77
Best Case	0.29
Crack Size	
Small Crack ≤ 35 mm ²	0.45
Medium Crack < 35 to ≤ 70 mm ²	0.35
Large Crack > 70 mm ²	0.24
Curvature	
Non-Tangent Track	0.57
Tangent track	0.20
Tie Manufacturer	
Tie Manufacturer “A”	0.23
Tie Manufacturer “B”	0.60
Field vs. Gauge	
Gauge Side	0.61
Field Side	0.21
Track Grade	
Neutral Grade ($ Grade \leq 116$)	0.33
Non-Neutral Grade ($ Grade > 116$)	0.33
Posted Speed	
High Range ($>125 - 150$ mph)	0.27
Low Range ($30 - \leq 125$ mph)	0.48

2.4.3 Combining Measurement and Sampling Uncertainty

The previous two sections describe how measurement and sampling uncertainty impact the median crack growth rate within a given sub-population. This section describes how the previously discussed components of uncertainty are combined to establish a net uncertainty in the AGR for a typical crack.

Measurement and sampling uncertainty are uncorrelated, so they are combined using a conventional RSS approach. The result is a net uncertainty in the AGR for a single, representative crack (i.e., a typical crack) within a given sub-population. The next paragraph walks through the process of combining measurement and sampling uncertainty for two sub-populations of crack data.

In this example, sub-populations of crack growth rate data corresponding to cracks located on tangent (straight) and non-tangent (curving) track are used. Uncertainty in the median growth

rate due to measurement error was estimated to be 0.6 mm²/yr for all sub-populations (see Section 2.4.1). From Table 2-7, the sampling uncertainty corresponding to the sub-population of cracks on tangent track is 0.2 mm²/yr. Combining 0.6 mm²/yr measurement uncertainty with 0.2 mm²/year sampling uncertainty using an RSS approach yields a net uncertainty of 0.63 mm²/yr in the AGR for a typical crack on tangent track. Returning to Figure 2-7, the sampling uncertainty for non-tangent track is 0.57 mm²/yr. Combining 0.6 mm²/yr measurement uncertainty with 0.57 mm²/yr sampling uncertainty yields a net uncertainty of 0.83 mm²/yr in the AGR for a typical crack on non-tangent track. In the next section, the examples presented here are continued to demonstrate how a given parameter is assessed to determine if the parameter has a statistically significant impact on crack growth rate.

2.4.4 Method Used to Compare Crack Growth Rates

This section describes how crack growth rates are compared to determine whether a given parameter impacts growth rate in a statistically significant manner. The example presented is a continuation of the example started in the previous section.

From measured data (presented later), the median growth rate (median AGR) for a sub-population of cracks on tangent track is 5.3 mm²/yr. Also from measured data, the median growth rate for a sub-population of cracks on non-tangent (curving) track is 8.9 mm²/yr. This means that, among cracks that grew, a typical crack on curving track grew 3.6 mm²/yr faster ($8.9 - 5.3 = 3.6$) than a typical crack on tangent track. The value of 3.6 in this example is referred to in this report as a Growth Rate Spread. The raw growth rates of 5.3 mm²/yr and 8.9 mm²/yr used in this example are reported as the “Growth Rate of a Typical Crack.”

The Growth Rate Spread value of 3.6 mm²/yr calculated above suggests that cracks grow faster on curving track than they do on tangent track. However, to have more confidence in this conclusion, the impact of uncertainty must be considered. In the previous section, the net uncertainty in growth rate for cracks on tangent track is 0.63 mm²/yr and for non-tangent track it is 0.83 mm²/yr. The RSS combination of these two uncertainties, or 1.05 mm²/yr, is the net uncertainty in the corresponding growth rate spread. The value of 1.05 mm²/yr in this example corresponds to the net uncertainty in the standard deviation of the median growth rate spread. To establish a two-sigma uncertainty, this standard deviation value is multiplied by two to yield a final two-sigma uncertainty of 2.1 mm²/yr.

Now the question of whether curving track impacted crack growth rates in a statistically significant manner can be answered. To answer this question, the measured Growth Rate Spread for the curvature parameter of 3.7 mm²/yr is compared to the two-sigma uncertainty of 2.1 mm²/yr. Because the measured Growth Rate Spread exceeds the two-sigma uncertainty, the data indicates that curvature has a statistically significant impact on the growth rate of cracks in this study’s test zone.

While this example is based on a single parameter (i.e., curvature), it is representative of the analysis applied to the other parameters considered under this study. For reference, Table 2-8 lists the two-sigma uncertainty in Growth Rate Spread for each of the parameters assessed under this study. Later, the values listed in Table 2-8 are used to assess whether each listed parameter exhibited a statistically significant influence on crack growth rates.

Table 2-8. Two-Sigma Uncertainties for Parameters Assessed in this Study

Parameter	Two-Sigma Uncertainty in Growth Rate Spread (mm ² /yr)
Combined Factors Worst Case Best Case	2.4
Crack Size Small Crack ≤ 35 mm ² Medium Crack < 35 to ≤ 70 mm ² Large Crack > 70 mm ²	2.0
Curvature Non-Tangent Track ($> 0^\circ$ to 9.93°) Tangent Track (0°)	2.1
Tie Manufacturer Tie Manufacturer "A" Tie Manufacturer "B"	2.1
Field vs. Gauge Gauge Side Field Side	2.1
Track Grade Neutral Grade ($ \text{Grade} \leq 116$) Non-Neutral Grade ($ \text{Grade} > 116$)	1.9
Posted Speed High Range (>125 - 150 mph) Low Range (30 - ≤ 125 mph)	2.0

3. Results

This section presents the graphed and tabulated results obtained during the study. The results are divided into four sections. Section 3.1 conveys the general condition of ties found in the study's test zone, including both nonconformance types and prevalence information. This section also quantifies the distribution of ties by grade (on a scale of Grade 1–No Material Nonconformances to Grade 5–Ineffective for a population of approximately 26,000 ties) and presents data showing the progression of tie grades over time.

Section 3.2 presents the crack growth rates among all cracks considered in this study, while Section 3.3 focuses on growth rate comparisons made between various sub-populations of crack growth rate data derived from the total population. The results from Section 3.3 are intended to help assess whether or not various parameters (e.g., curvature, posted speed, etc.) have a material impact on crack growth rate. Section 3.4 compares crack frequency and growth rates versus position along the tie to support heuristic assessments of whether crack location has an impact on crack prevalence and/or crack growth rates.

3.1 Tie Condition Results

This section presents results obtained by inspecting track bed image data corresponding to approximately 26,000 concrete ties located within the ten miles of track that was listed in Table 2-3. The subsections under this heading display tie condition results from track bed images collected during the first imaging survey (August 2012), except for Section 3.1.4, which presents results that show how tie grades progressed between the first and third imaging surveys (i.e., between August 2012 and September 2013).

3.1.1 Prevalence of Observed Nonconformance Types

The graph in Figure 3-1 presents the distribution of four nonconformance types (e.g., cracks, chips, missing fasteners, and crumbling) within 10 miles of track in the study's test zone. There was a total population of 2,232 nonconformances dispersed across approximately 26,000 ties in the zone.

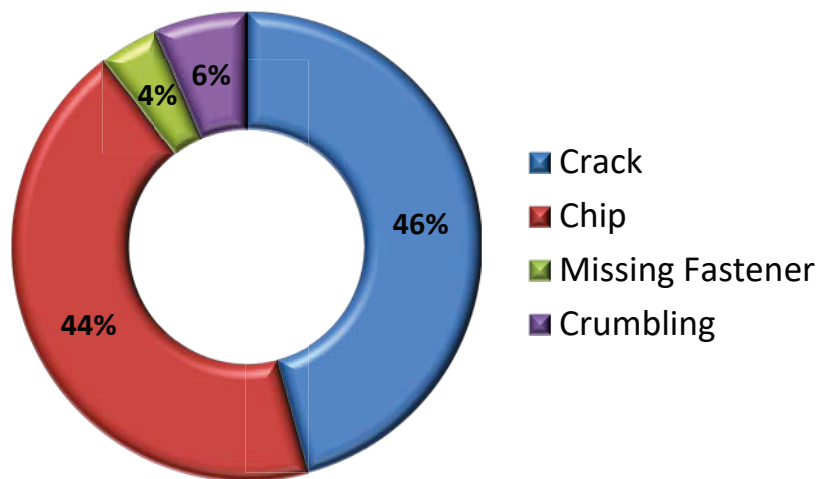


Figure 3-1. Observed Distribution of Nonconformance Types

Figure 3-2 shows the number of nonconformances by type on a per-mile basis within 10 miles of track bed image data. The results of Figure 3-2 are derived from the same 10 miles of track bed image data used in Figure 3-1.

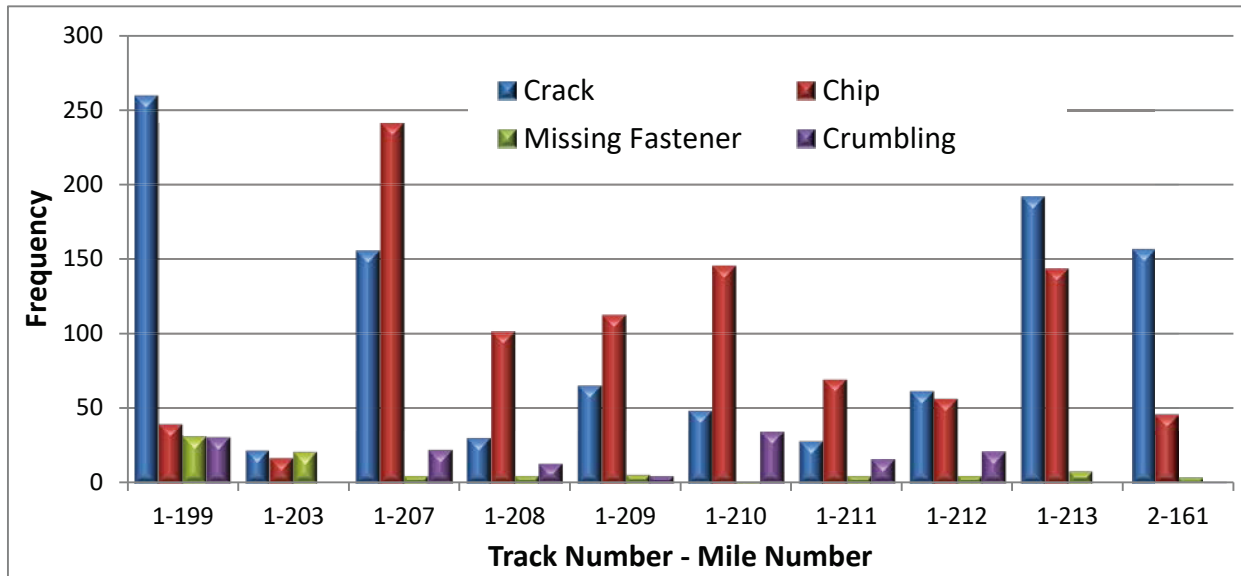


Figure 3-2. Observed Distribution of Nonconformance Types by Mile

3.1.2 Prevalence of Observed Crack Types

Figure 3-3’s graph classifies approximately 1,000 cracks within the study’s test zone into 1 of 10 categories. An image showing a typical crack from each category is provided in Appendix A.

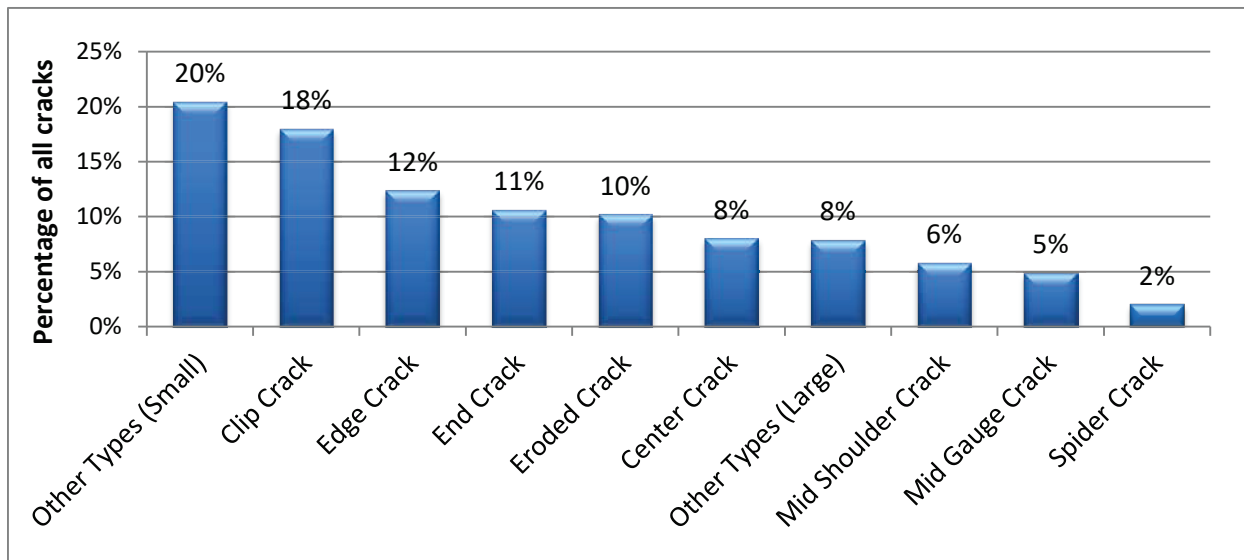


Figure 3-3. Observed Distribution of Crack Types

3.1.3 Distribution of Tie Grades

The chart in Figure 3-4 presents the distribution of ties by grade across 10 miles of track in the study’s test zone. Appendix B includes the tie rating guidelines used to grade the ties

represented in Figure 3-4. The results of Figure 3-4 correspond to the ten miles of track listed earlier in Table 2-3.

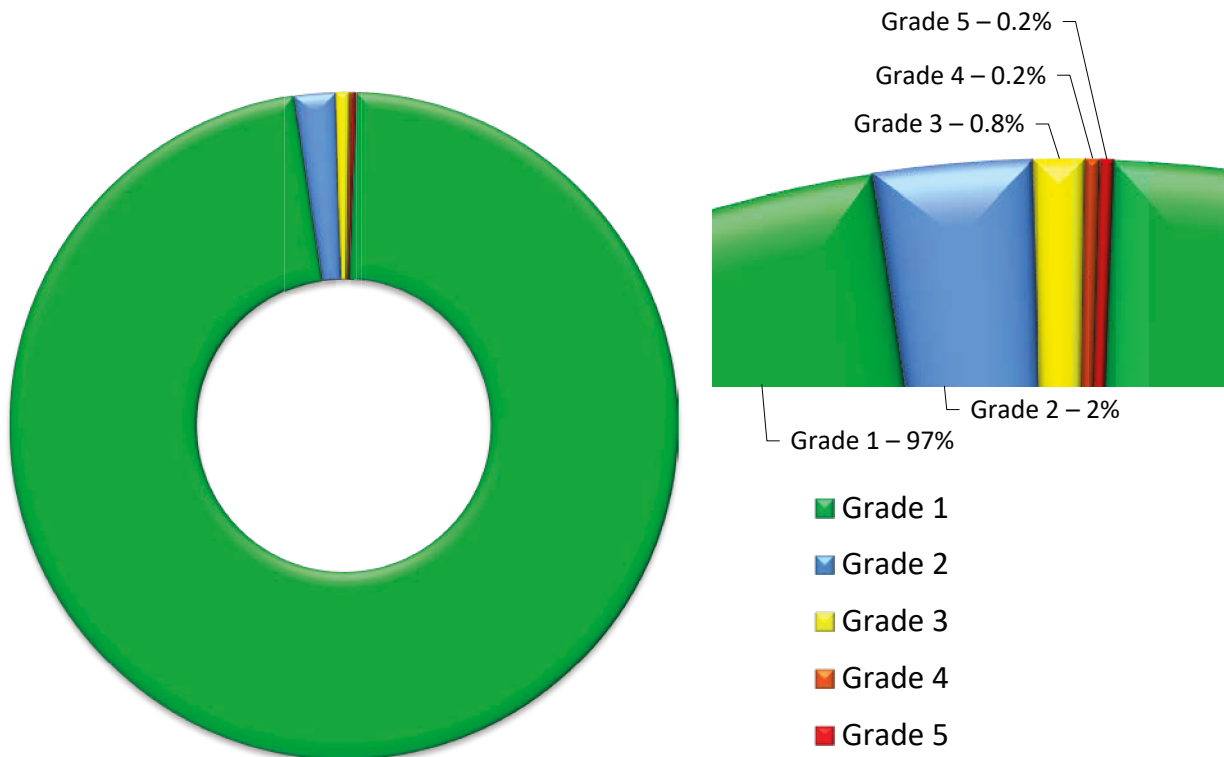


Figure 3-4. Distribution of Tie Grades Assessed Over 10 Miles of Track Bed Image Data

3.1.4 Evolution of Tie Grades Over Time

The data presented in this subsection describes how the tie grades evolved over time and it was derived by grading the ties in each of the ten miles listed in Table 2-3 at two points in time. The two points in time occurred approximately 13 months apart, and the tie grading scale was based on Grade 1–No Material Nonconformances to Grade 5–Ineffective for a population of approximately 26,000 ties. The percentage of ties that changed from each grade to each higher grade was then determined and presented as a series of bar graphs shown in Figure 3-5, further clarified next.

Figure 3-5 includes four bar graphs stacked one on top of the other. The top bar graph shows how Grade 1 ties progressed in grade over an annualized period. Specifically, the top bar graph shows the percentage of Grade 1 ties that progressed to each of the higher grades listed horizontally across the bar graph. Similarly, the second bar graph from the top of Figure 3-5 shows how Grade 2 ties progressed over time. Finally, the third and fourth bar graphs shown in Figure 3-5 show how ties with initial Grades of 3 and 4 (respectively) progressed over time.

The first graph at the top of Figure 3-5 indicates that 0.23 percent of the Grade 1 ties (55 out of ~26,000 ties) advanced in grade. Of the 55 Grade 1 ties that advanced, 0.22 percent (32 out of ~26,000 ties) advanced to Grade 2 and 0.01 percent (3 out of ~26,000 ties) advanced to Grade 3. Finally, no Grade 1 ties advanced to Grade 4 or Grade 5.

The second bar graph indicates that 6.5 percent of pre-existing Grade 2 ties (34 out of 520 ties) advanced in grade during the study period. Of the advancing Grade 2 ties, 6.2 percent (32 out of 520 ties) became Grade 3 ties, while 0.3 percent (2 out of 520 ties) became Grade 4 ties. Among the advancing Grade 2 ties, none became Grade 5 ties.

The third bar graph from the top in Figure 3-5 indicates that 3.8 percent of Grade 3 ties (8 out of 208 ties) advanced to a higher grade during the study’s 13-month observation interval. Of the advancing Grade 3 ties, 3.0 percent (6 out of 208 ties) advanced to Grade 4, while 0.8 percent (2 out of 208 ties) advanced to Grade 5.

The last bar graph in Figure 3-5 indicates that 5.8 percent of the pre-existing Grade 4 ties (3 out of 52 ties) advanced to become Grade 5 ties. In Figure 3-5 no bar graph is shown to indicate advancing Grade 5 ties because the grading scale ends at Grade 5, however, in principle, Grade 5 ties are ultimately replaced and, therefore, cycle back to Grade 1 ties.

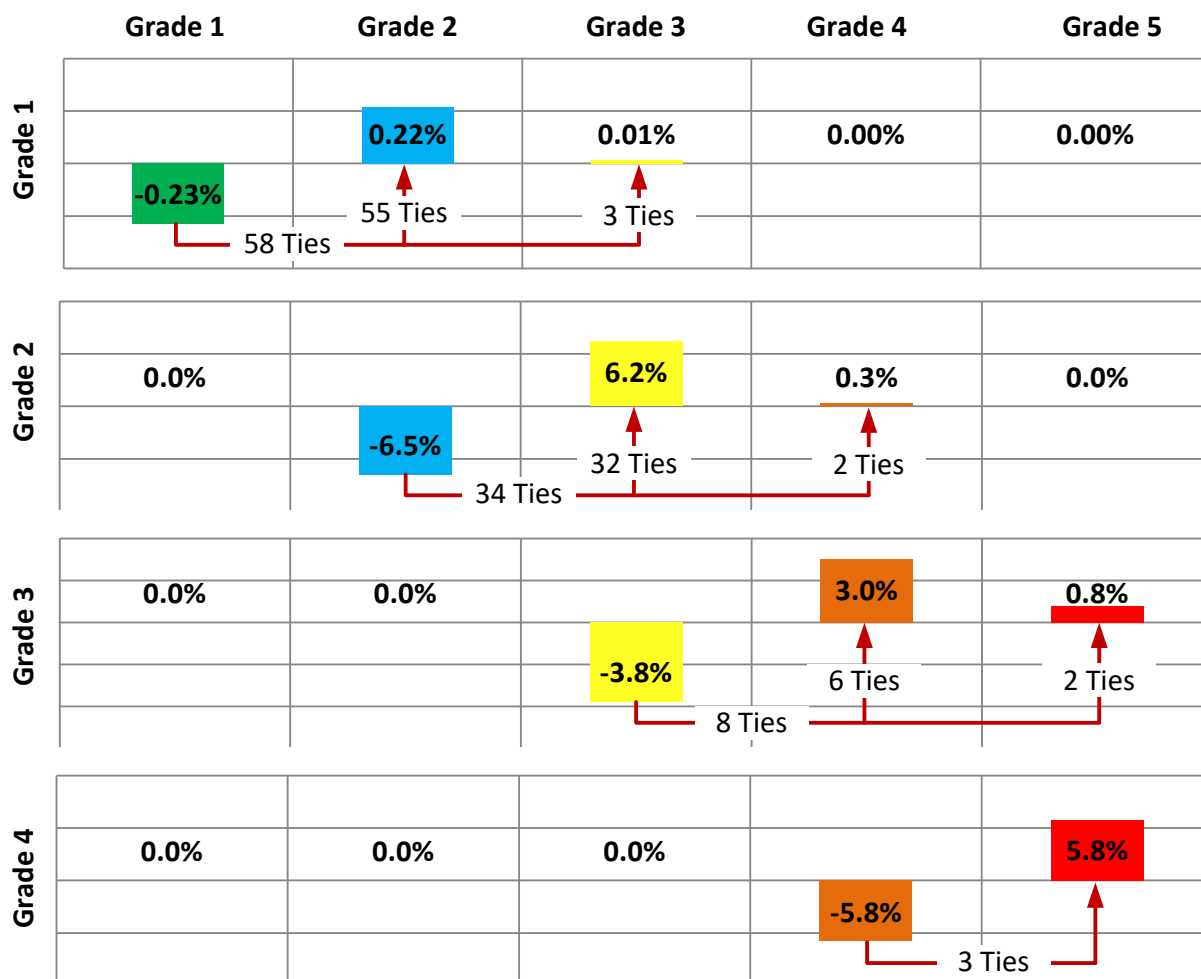


Figure 3-5. Percent Change in the Number of Ties of Each Grade Over a 1-Year Period

3.1.5 Number of Grade 4 or 5 Ties Per 39 Feet

This section examines the density of Grade 4 and 5 ties over 10 miles of track before and after Amtrak’s spot tie replacement activities during this study’s observation period. Figure 3-6 and

Figure 3-7 show the number of ties with a grade of either 4 or 5 per 39 feet over the ten miles of track listed in Table 2-3. The results in Figure 3-6 correspond to the status of the ties during the first imaging survey conducted in August 2012. The results of Figure 3-7 correspond to the status of the ties following the third imaging survey conducted in September 2013. In Figure 3-6 and Figure 3-7 the horizontal axis represents the location along the track over ten non-contiguous miles; the vertical axis then indicates the number of Grade 4 or 5 ties per 39 feet at each location.

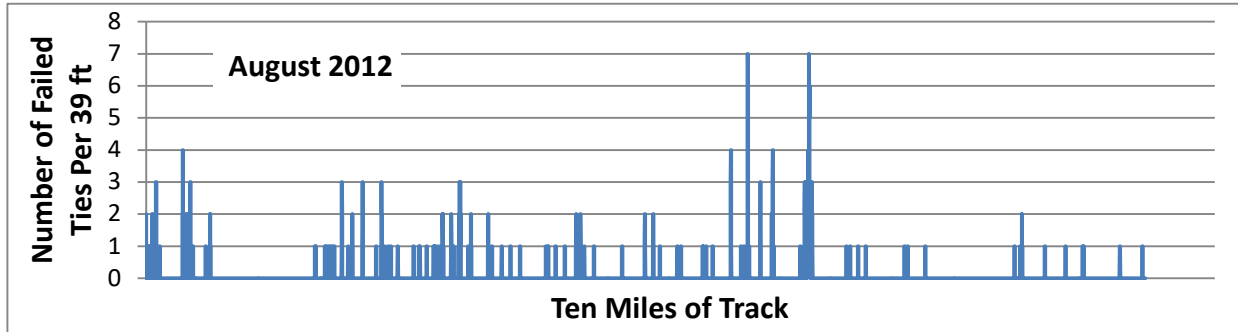


Figure 3-6. Number of Grade 4 or 5 Ties per 39 Feet Versus Tie Location - August 2012

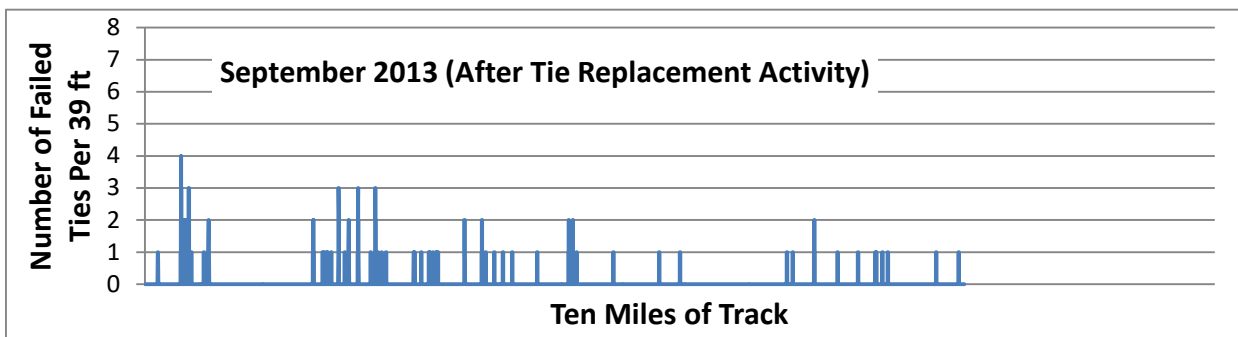


Figure 3-7. Number of Grade 4 or 5 Ties per 39 Feet Versus Tie Location—September 2013

3.2 Growth Rate Results—All Cracks Studied

This section presents crack growth rates across the entire population of studied cracks. The data presented in this section was gathered during two periods within a contiguous 13-month window. Data for the first period (Figure 3-8) reflects crack growth that occurred between imaging Surveys 1 and 2 conducted August 2012 and April 2013, respectively, while data for the second period (Figure 3-9) reflects crack growth that occurred between imaging Surveys 1 and 3 conducted August 2012 and September 2013. For reference, Table 3-1 summarizes the total number of cracks assessed during each of these two periods.

Table 3-1. Summary of Assessed Crack Population Sizes for Periods 1 and 3

Period	Number of Cracks Assessed
Period 1 – August 2012 to April 2013	1,022
Period 3 – August 2012 to September 2013	2,139

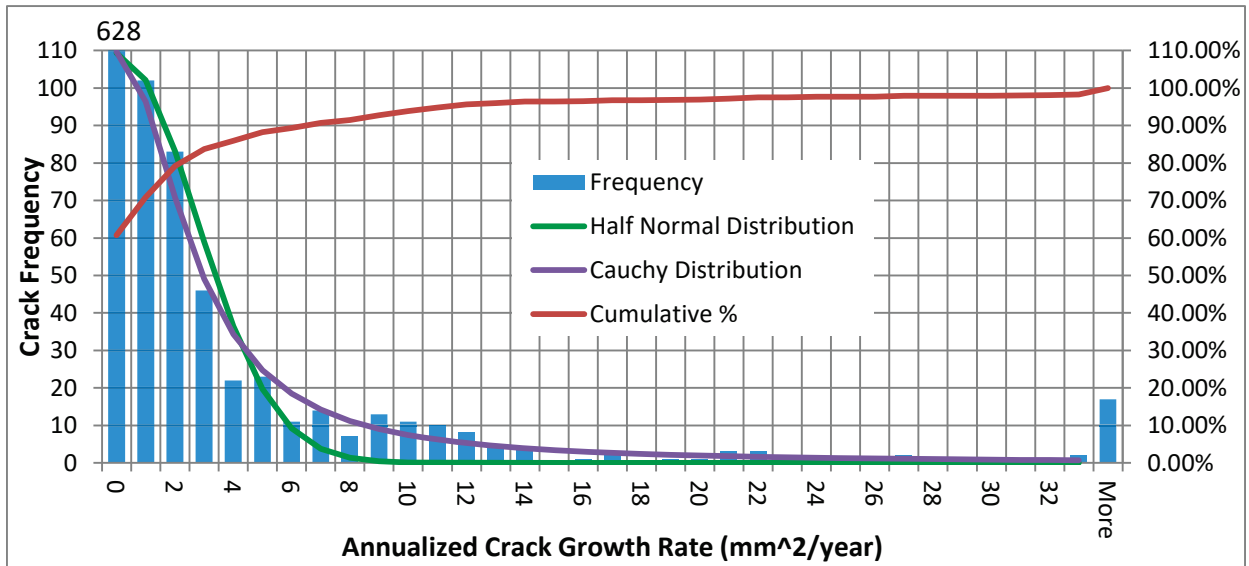


Figure 3-8. Crack Growth Rate Data for All Cracks Studied Between August 2012 and April 2013 (1,022 Cracks)

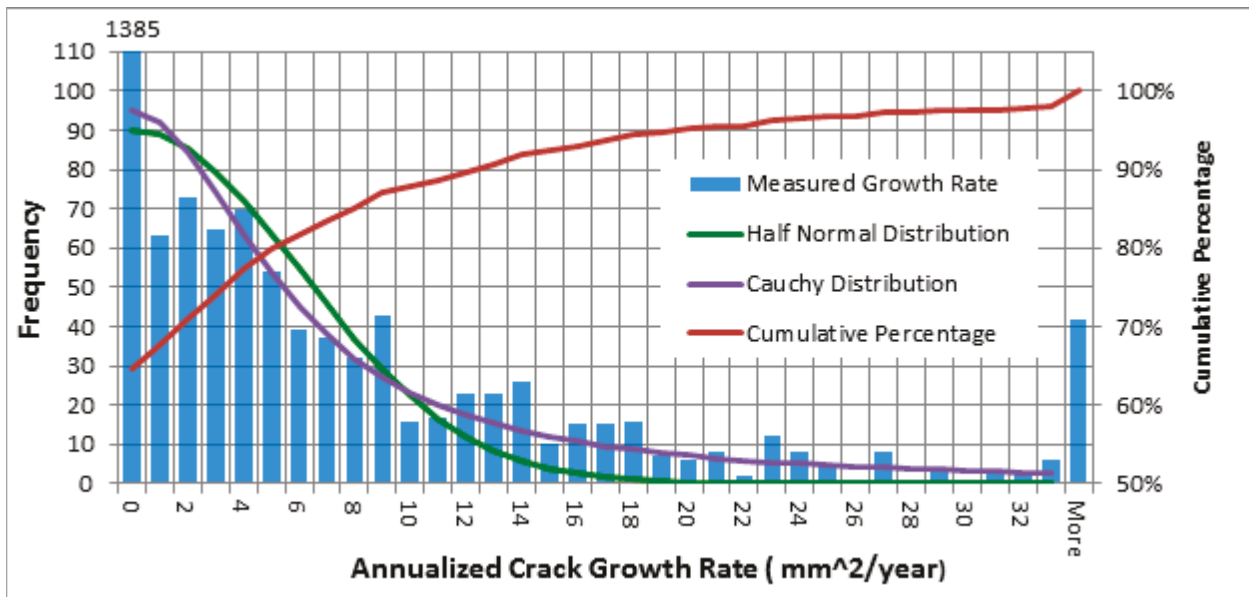


Figure 3-9. Crack Growth Rate Data for All Cracks Studied Between August 2012 and September 2013 (2,139 Cracks)

Many of the cracks studied in detail showed little or no growth. This minimal-growth subset is represented in Figure 3-8 and Figure 3-9 by including the actual number of cracks that lie in the “zero” bin (the left-most bin) above the bin’s histogram bar (values 628 and 1,385, respectively).

Figure 3-8 and Figure 3-9 include a cumulative percentage curve (in red), with its vertical axis shown on the right side of the graph. For reference, Figure 3-8 and Figure 3-9 also include curves for both a half-normal and a Cauchy distribution that have been fitted to the data. Both of these fitted curves closely approximate the underlying data for crack growth rates up to about the 87th percentile point, however, the Cauchy distribution does a better job of approximating the underlying data over all crack growth rates.

Table 3-2 summarizes the graphed results presented in Figure 3-8 and Figure 3-9 by showing the number (and percentage) of cracks that did and did not grow during Periods 1 and 3.

Table 3-2. Percentage of All Cracks Studied That Did and Did Not Grow

Period	Number of Cracks Assessed	Number (Percentage) of Cracks That Did Not Grow	Number (Percentage) of Cracks That Grew
Period 1	1,022	628 (61%)	394 (39%)
Period 3	2,139	1,385 (65%)	754 (35%)

Figure 3-10 shows the distribution of crack growth rates among the cracks that showed measurable growth between August 2012 and September 2013. The cumulative percentage curve shown in Figure 3-10 provides a basis for defining typical slow, medium, and fast growth rates among the studied cracks. Specifically, a typical slow growth rate (10th percentile) would be 2.7 mm²/year, a typical medium growth rate (50th percentile) would be 7.5 mm²/year, and a typical fast growth rate corresponding to the 90th percentile point would be 25.5 mm²/year.

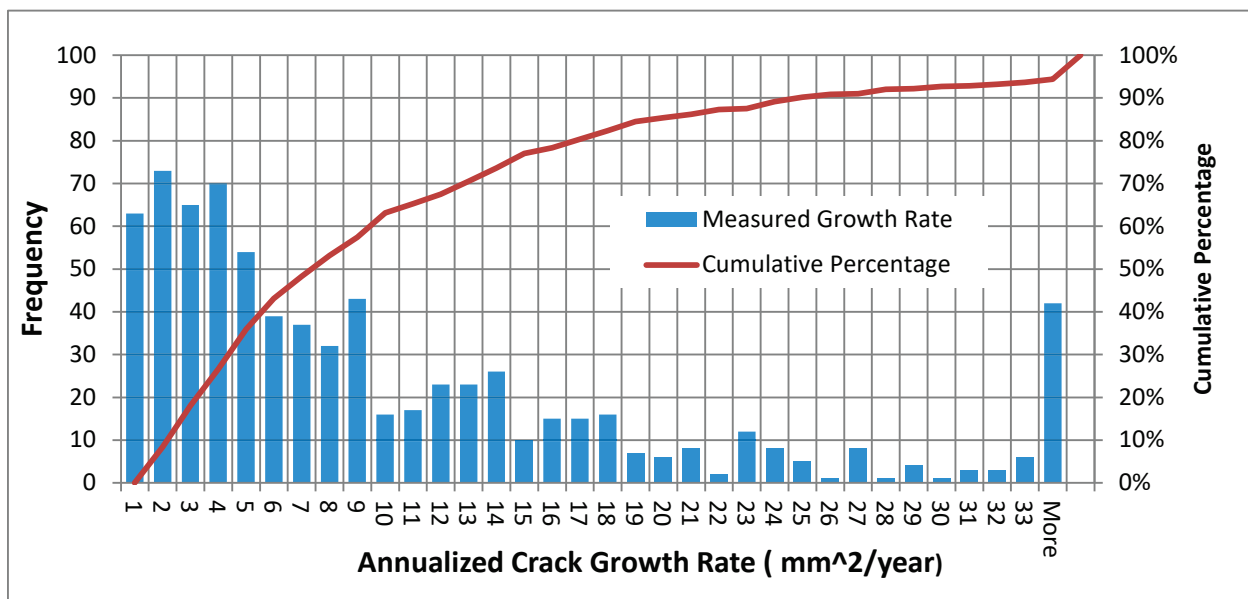


Figure 3-10. Distribution of Crack Growth Rates Among Cracks That Grew

3.3 Parametric Growth Rate Results

This section presents data which is used to assess whether or not various parameters influence crack growth rate. The parameters covered in this section include:

- Curvature
- Track Grade
- Posted Speed
- Crack Location
- Crack Size
- Tie Manufacturer
- Combined Influence

To assess each parameter, two or more sub-populations were extracted from the total population of cracks and then the crack growth rates of the extracted sub-populations were compared. Table 3-3 summarizes the number of cracks in each sub-population for each evaluated parameter.

Table 3-3. Sub-Population Sizes for Assessed Parameters

Parameter	Number of Cracks in Sub-Population
Curvature	
Non-Tangent Track	253
Tangent Track	499
Track Grade	
Neutral: $ \text{Grade} < 0.116$	278
Non-Neutral: $ \text{Grade} > 0.116$	476
Posted Track Speed	
High Range ($>125 - 150$ mph)	435
Low Range ($30 - \leq 125$ mph)	296
Crack Location	
Gauge Side	271
Field Side	483
Crack Size	
Small Cracks – < 35 mm ² (~3 in. long)	251
Medium Cracks – 35 mm ² to 70 mm ² (~6 in. long)	251
Large Cracks – greater than 70 mm ² ($> \sim 6$ in. long)	252
Tie Manufacturer	
Tie Manufacturer “A”	608
Tie Manufacturer “B”	144
Combined Factors	
Worst Case	148
Best Case	163

For each figure in this section, the data is presented in two formats: 1) a cumulative percentage curve and 2) a normalized frequency histogram. The cumulative percentage format is used to

assess whether or not a given parameter tends to influence crack growth rate more or less than a corresponding control parameter. Specifically, the horizontal separation between two cumulative percentage curves (i.e., the amount of white space between the curves) indicates the degree of influence that the non-control parameter has on crack growth rate. The frequency histograms, which are included with each figure in this section, are provided for reference purposes and they are useful for comparing the prevalence of specific growth rates between a control and a non-control group. The results in this section are quantified and summarized in tabular form in Section 4.2.

3.3.1 Growth Rate Versus Operating Conditions

This section presents Figure 3-11, Figure 3-12, and Figure 3-13 used to evaluate whether or not the following parameters related to operating conditions tend to impact crack growth rate.

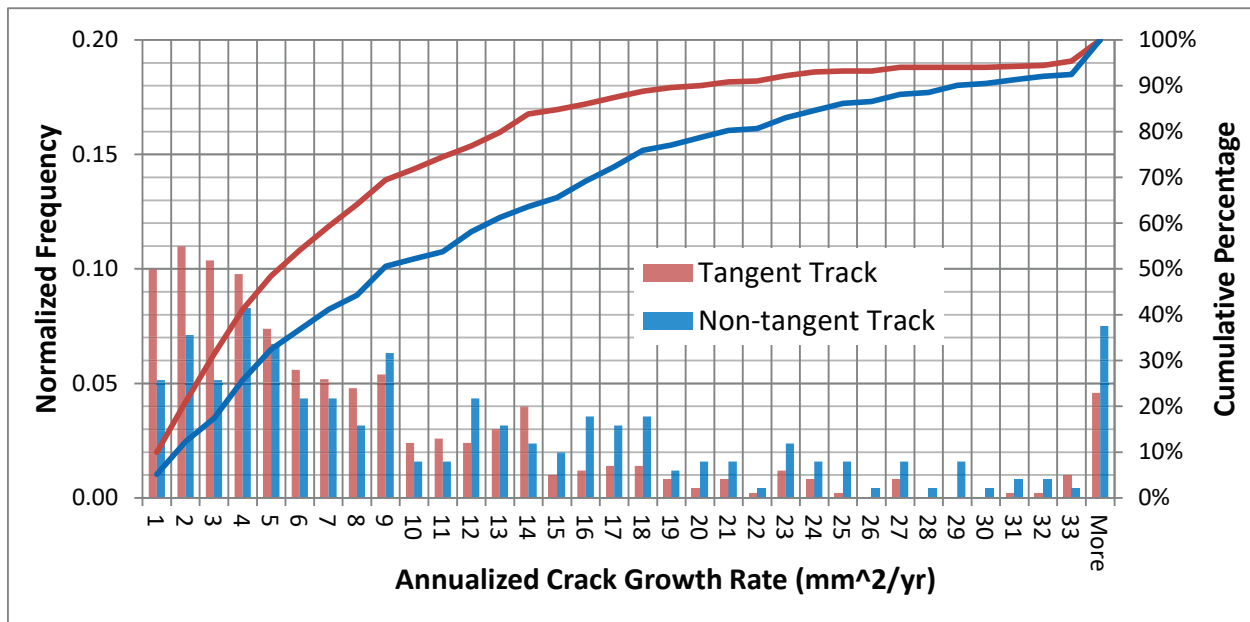


Figure 3-11. Crack Growth Rate Versus Curvature

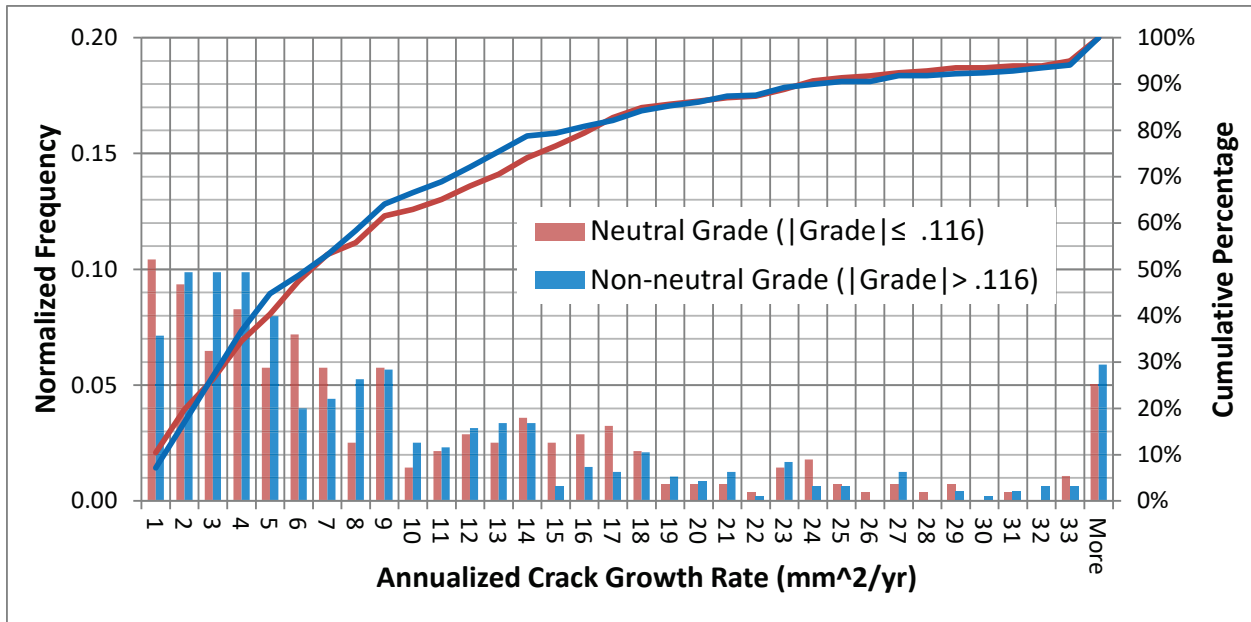


Figure 3-12. Crack Growth Rate Versus Track Grade

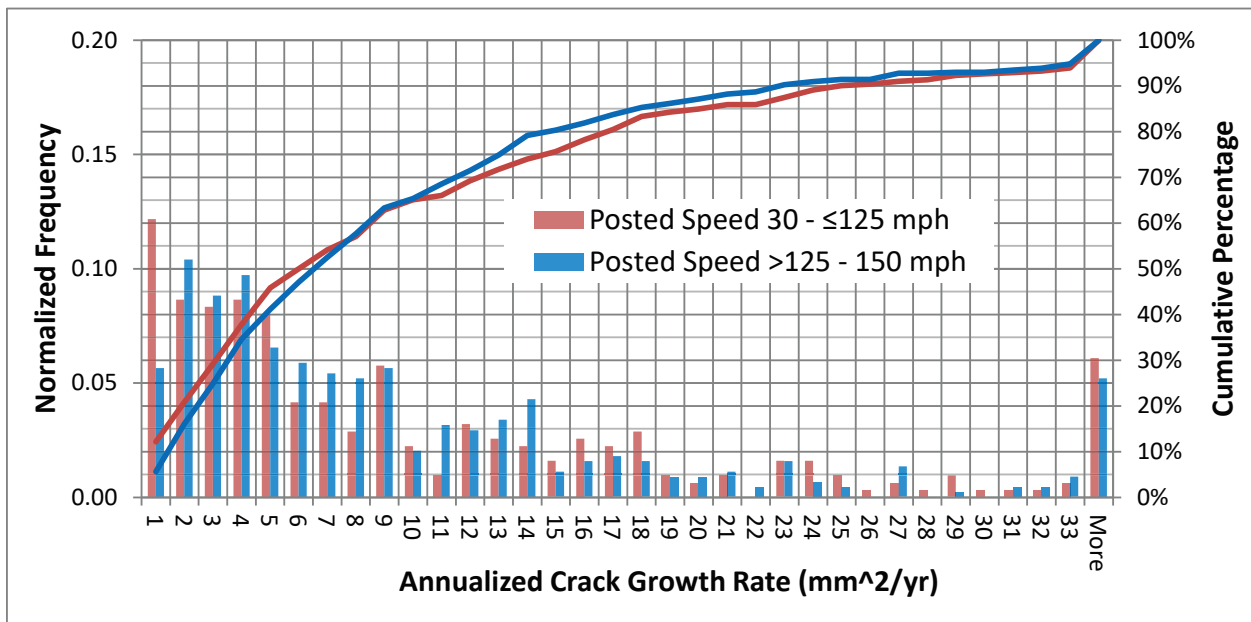


Figure 3-13. Crack Growth Rate Versus Posted Speed

3.3.2 Growth Rate Versus Position Along the Tie

This section presents evidence which may indicate that crack growth rates are influenced by whether a crack is located on the field or gauge side of a tie. Specifically, Figure 3-14, compares measured crack growth rates on the field side of the tie to those on the gauge side of the tie.

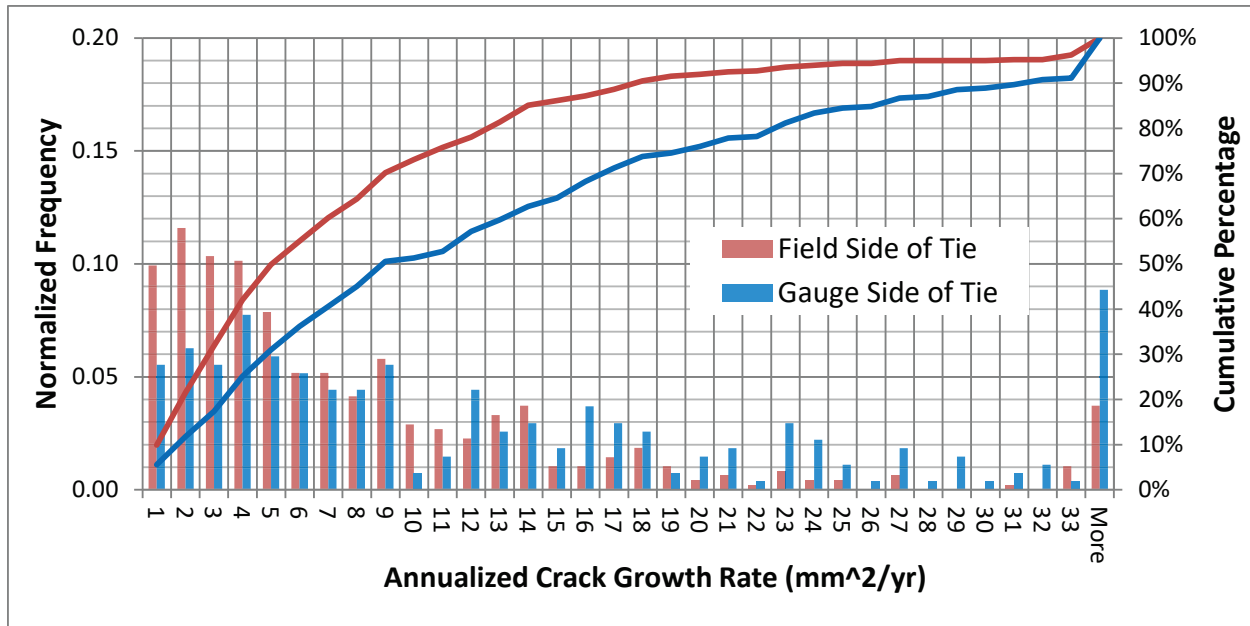


Figure 3-14. Crack Growth Versus Crack Location (Field Versus Gauge Side of Tie)

3.3.3 Growth Rate Versus Crack Size

The graph presented in this section is intended to help assess whether crack growth rate tends to be dependent on crack size. It compares crack growth using cumulative percentage curves and frequency histograms as described earlier in Section 3.3 and is based on dividing the sub-population of 754 cracks that grew between imaging Surveys 1 and 3 (August 2012 to September 2013) into three equal sub-populations comprised of small, medium, and large cracks. Small cracks are defined as those with a total area in the lower third of the population, medium cracks have a total area in the middle third of the population, and large cracks have a total area in the upper third of the population. The crack areas (in square millimeters) corresponding to each of these sub-populations is:

- Small cracks - $\leq 35 \text{ mm}^2$ (typical length ≈ 3 in)
- Medium cracks - $> 35 \text{ mm}^2$ to $\leq 70 \text{ mm}^2$ (typical length ≈ 3 to 6 in)
- Large cracks - $> 70 \text{ mm}^2$ (typical length greater than ≈ 6 in)

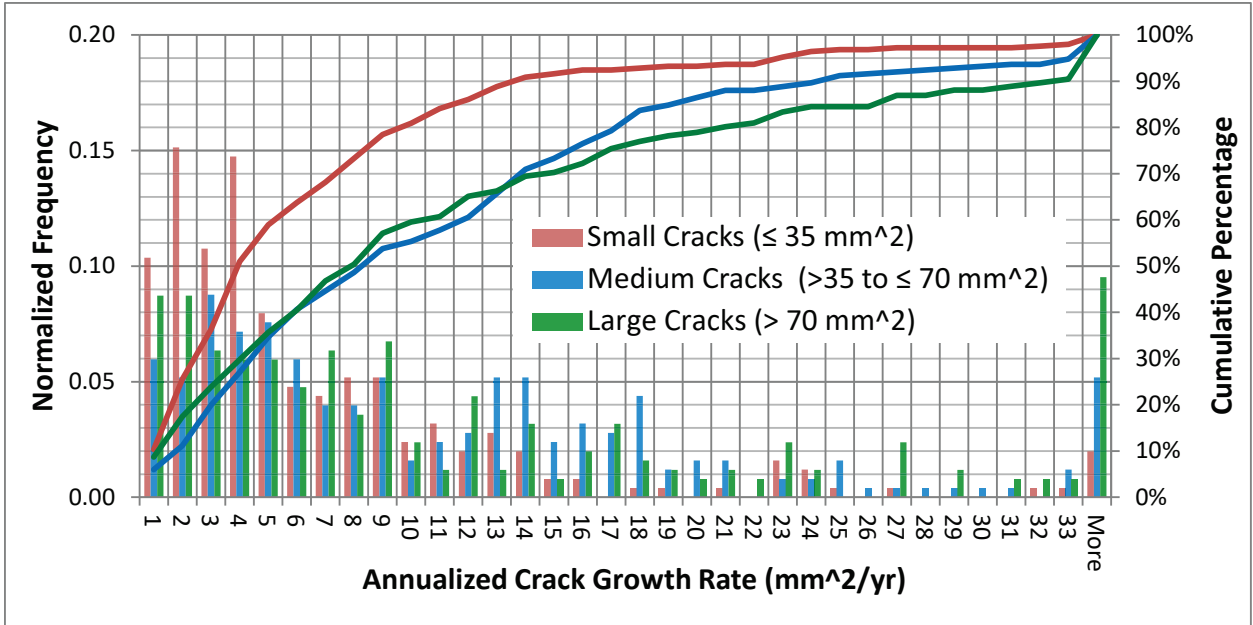


Figure 3-15. Comparison of Crack Growth Rate Versus Crack Size

3.3.4 Growth Rate Versus Combined Influence

The results in this section assess the impact that multiple, simultaneous factors have on crack growth rate. Specifically, the data in Figure 3-16 compares a subpopulation of cracks based on conditions associated with lower crack growth rates (favorable conditions) to a subpopulation based on conditions associated with higher crack growth rates (unfavorable conditions). Table 3-4 summarizes the two scenarios used to compile the data shown in Figure 3-16.

Table 3-4. Conditions Used to Assess the Impact of Simultaneous Factors on Growth Rate

Favorable Conditions	Unfavorable Conditions
Tangent Track	Curving Track
Tie Manufacturer "A" Only	Tie Manufacturers "A" and "B"
Small Cracks Only	Medium and Large Cracks
Field Side of Tie	Gauge Side of Tie

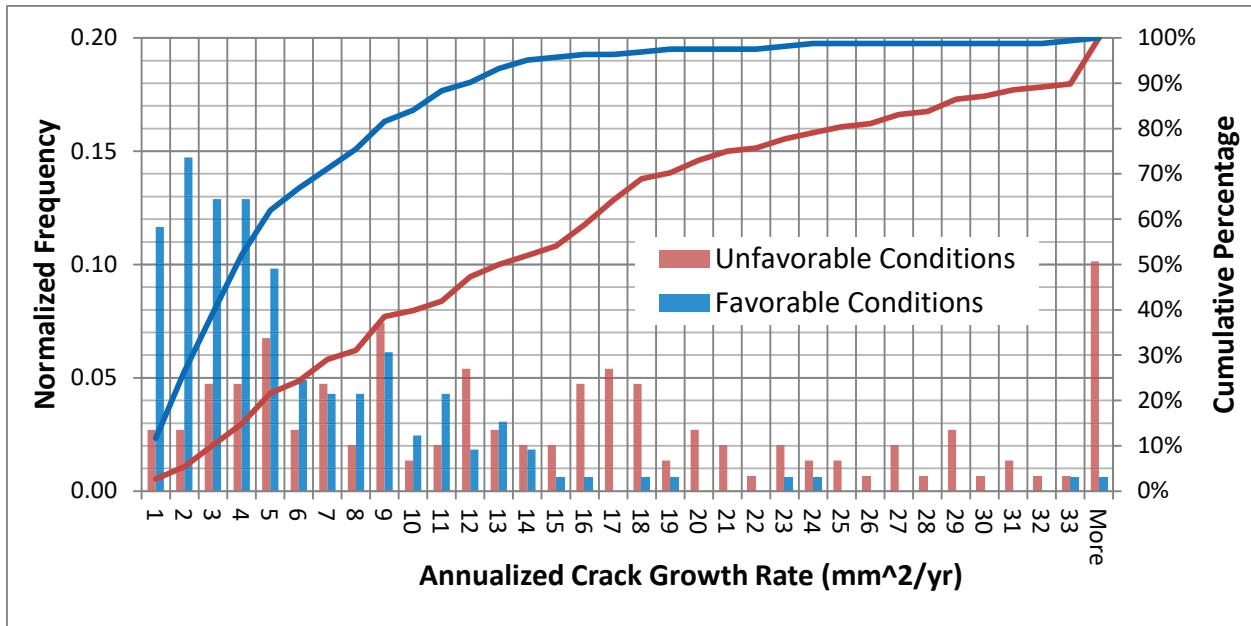


Figure 3-16. Crack Growth Rate Versus Favorable and Unfavorable Conditions

3.3.5 Growth Rate Versus Tie Manufacturer

This section presents data that assesses whether or not the tie manufacturer has a material impact on crack growth rate. The data presented in Figure 3-17 compares crack growth rates for a population of cracks found on ties manufactured by Tie Manufacturer “A” with growth rates corresponding to a population of cracks found on ties manufactured by Tie Manufacturer “B.”

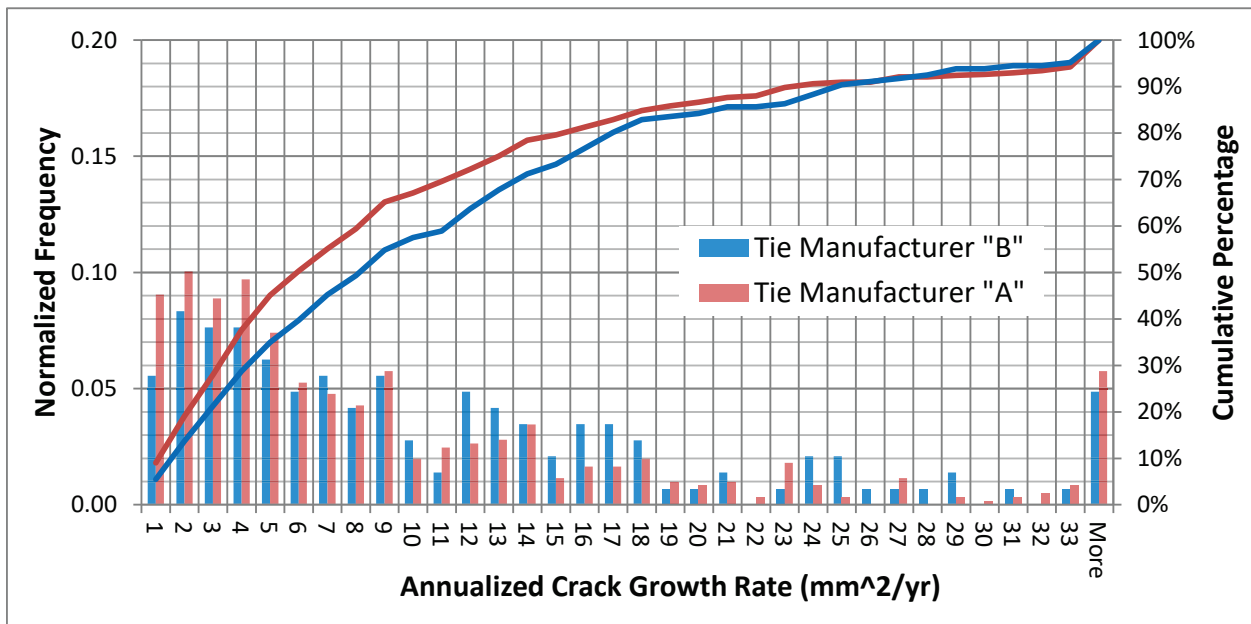


Figure 3-17. Crack Growth Rate Versus Tie Manufacturer

3.4 Heuristic Growth Rate and Frequency Results

This section provides a heuristic assessment of whether cracks tend to be more or less prevalent in specific regions along a tie.

3.4.1 Heuristic Growth Rate Versus Position Along the Tie

This subsection presents Figure 3-18, Figure 3-19, and Figure 3-20 that support a heuristic assessment of crack growth rate as a function of crack position along the tie.

All three graphs are scatter plots in which each point corresponds to a different crack (or crack cluster). A point's vertical position indicates the crack's growth rate, while the point's horizontal position indicates the crack's location along the tie. Points that lie along the base of the tie overlay shown in each graph correspond to cracks that did not exhibit growth. Extreme outlier growth rates are not included in these plots.

The data presented in Figure 3-18 includes ties manufactured by both Tie Manufacturer "A" and Tie Manufacturer "B." Figure 3-19 and Figure 3-20 are in the same format as Figure 3-18 but only include data corresponding to either Tie Manufacturer "A" or Tie Manufacturer "B," respectively. These latter two plots support a heuristic assessment of any crack growth rate trends that might depend on differences in the respective tie manufacturing processes.

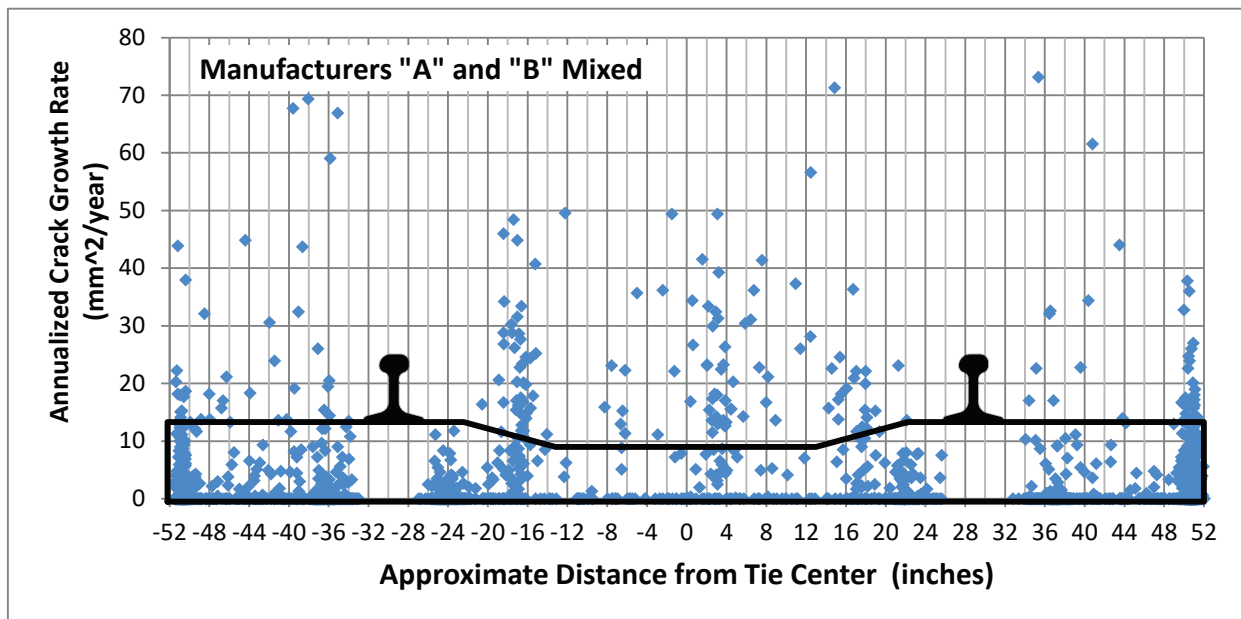


Figure 3-18. Crack Growth Rate Versus Position Along the Tie (Tie Manufacturers "A" and "B")

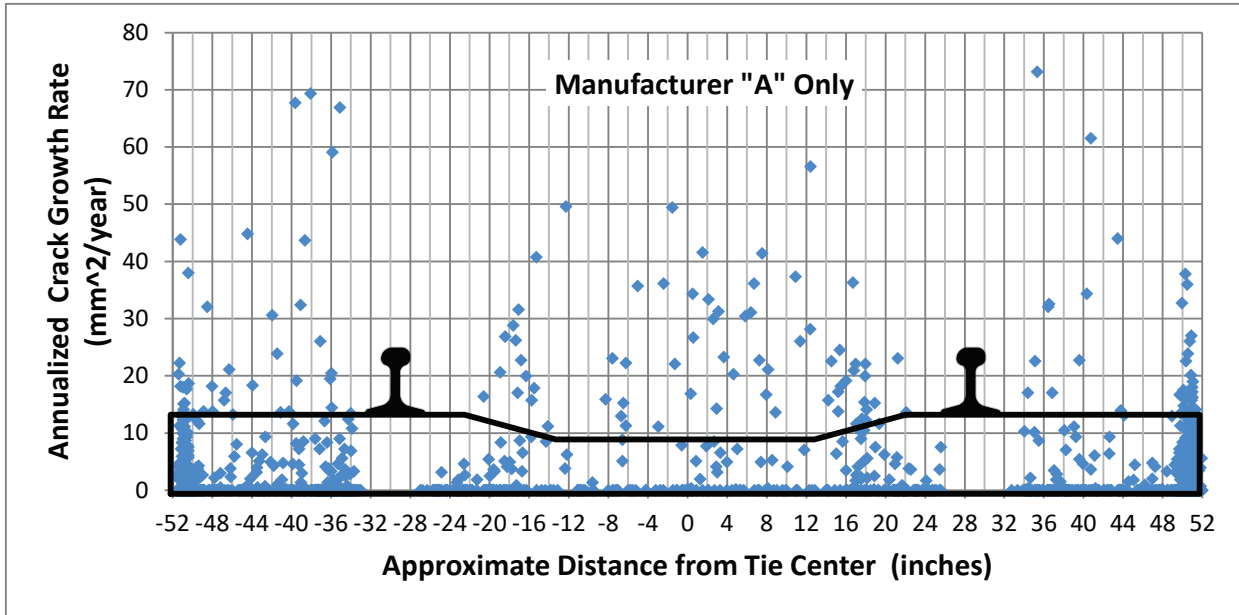


Figure 3-19. Crack Growth Rate Versus Position Along the Tie (Tie Manufacturer “A” Only)

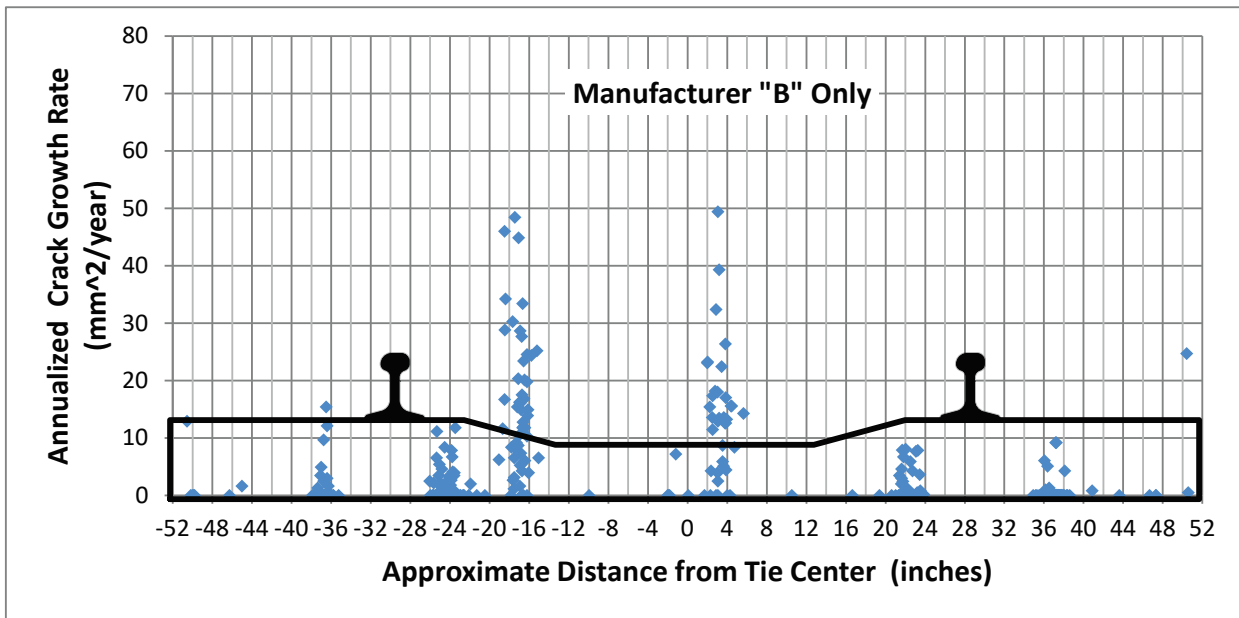


Figure 3-20. Crack Growth Rate Versus Position Along the Tie (Tie Manufacturer “B” Only)

3.4.2 Heuristic Crack Frequency Versus Position Along the Tie

This section presents Figure 3-21, Figure 3-22, and Figure 3-23 that support a heuristic assessment of whether cracks tend to be more or less prevalent in specific regions along a tie.

Each graph in this section is a frequency histogram that indicates the prevalence of cracks at each position across the length of a tie. Figure 3-21 presents normalized crack frequency as a function of position along the tie for both Tie Manufacturers “A” and “B.” Effectively, each vertical bar in Figure 3-21 indicates the percentage of a given manufacturer’s ties that have a crack at the bar’s approximate position along the tie. Thus, Figure 3-21 compares the prevalence of cracks as functions of both location and tie manufacturer. Figure 3-22 and Figure 3-23 present the same data shown in Figure 3-21, except the results for Tie Manufacturers “A” and “B” are shown on separate graphs so that the vertical scale for each tie manufacturer better matches the data for each tie manufacturer. The crack prevalence data presented in this section was derived from track bed images recorded during the first imaging survey in August 2012.

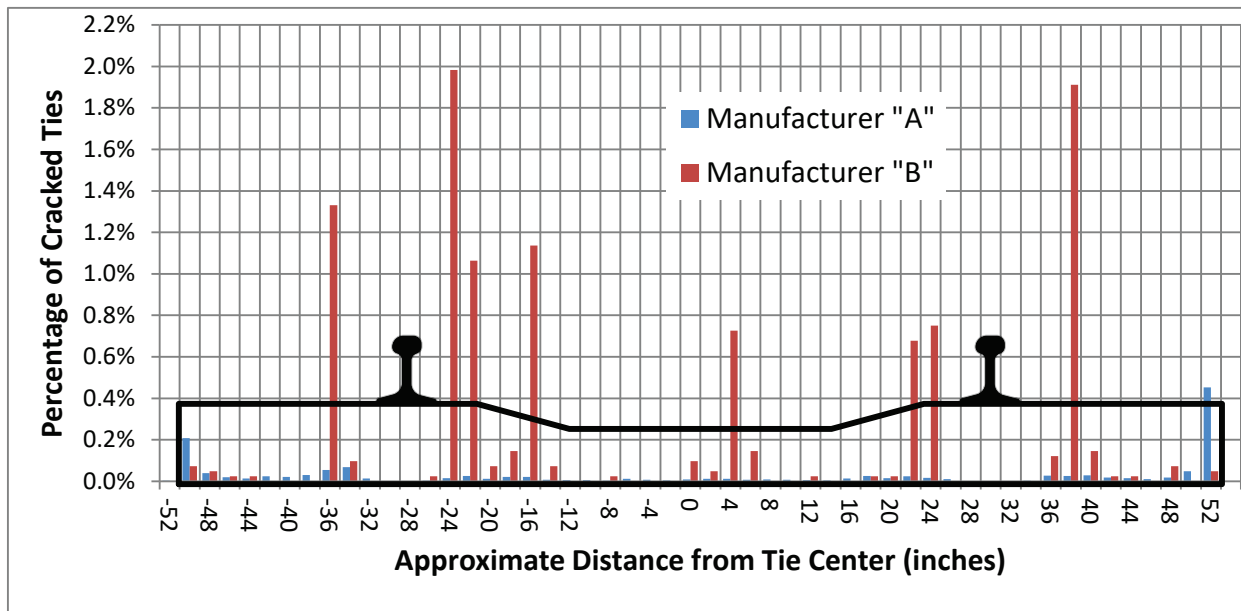


Figure 3-21. Normalized Crack Frequency Versus Position Along the Tie (Tie Manufacturers “A” and “B”)

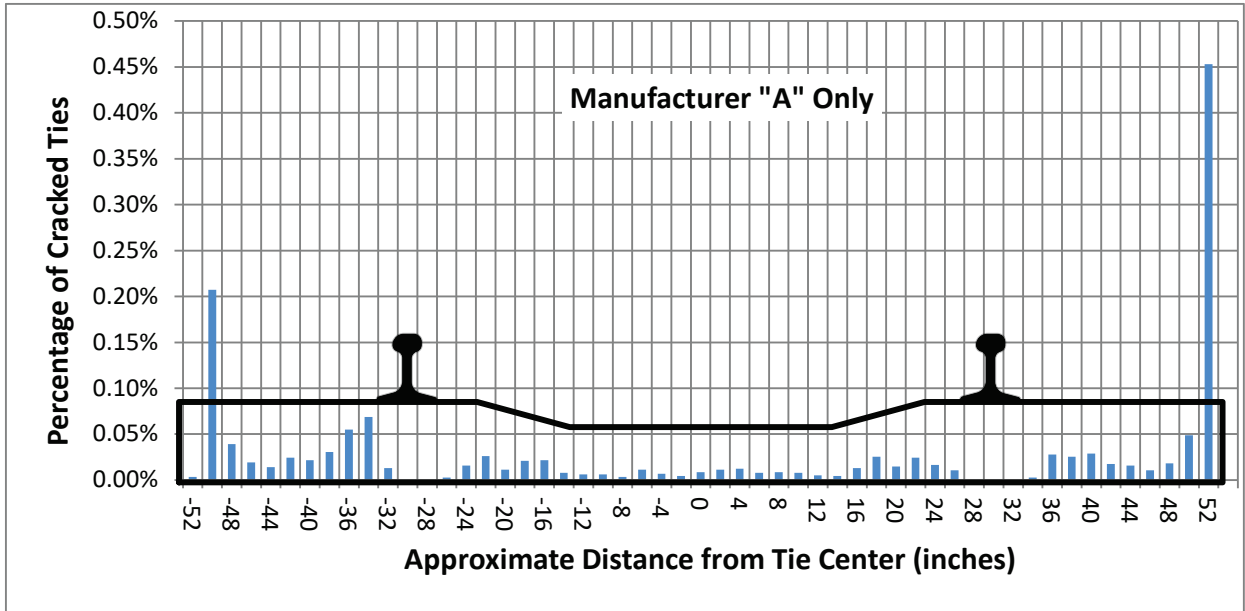


Figure 3-22. Crack Frequency Versus Position Along the Tie (Tie Manufacturer "A" Only)

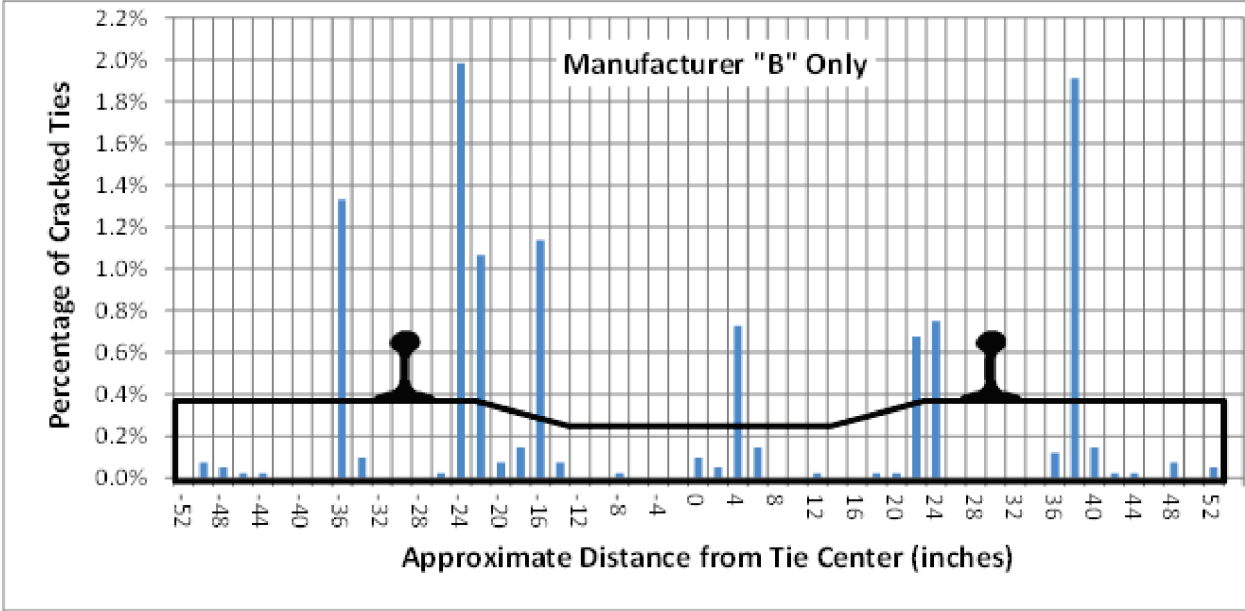


Figure 3-23. Crack Frequency Versus Position Along the Tie (Tie Manufacturer "B" Only)

4. Assessments

4.1 Tie Condition Assessment

This section assesses the tie condition results presented in Section 3.1 and makes recommendations pertaining to concrete tie inspection practices. The results in Section 3.1 are based on two separate tie evaluation efforts. The first effort examined the overall condition of approximately 26,000 ties spread across 10 miles within the study's test zone. During this evaluation, ties were graded on a scale of Grade 1–No Material Nonconformances through Grade 5–Ineffective for a population of approximately 26,000 ties. The ties were also examined to locate the following nonconformance types:

- Cracks
- Chips
- Crumbling
- Missing Fasteners

Figure 4-1 shows a typical example of each of the nonconformance types listed above.

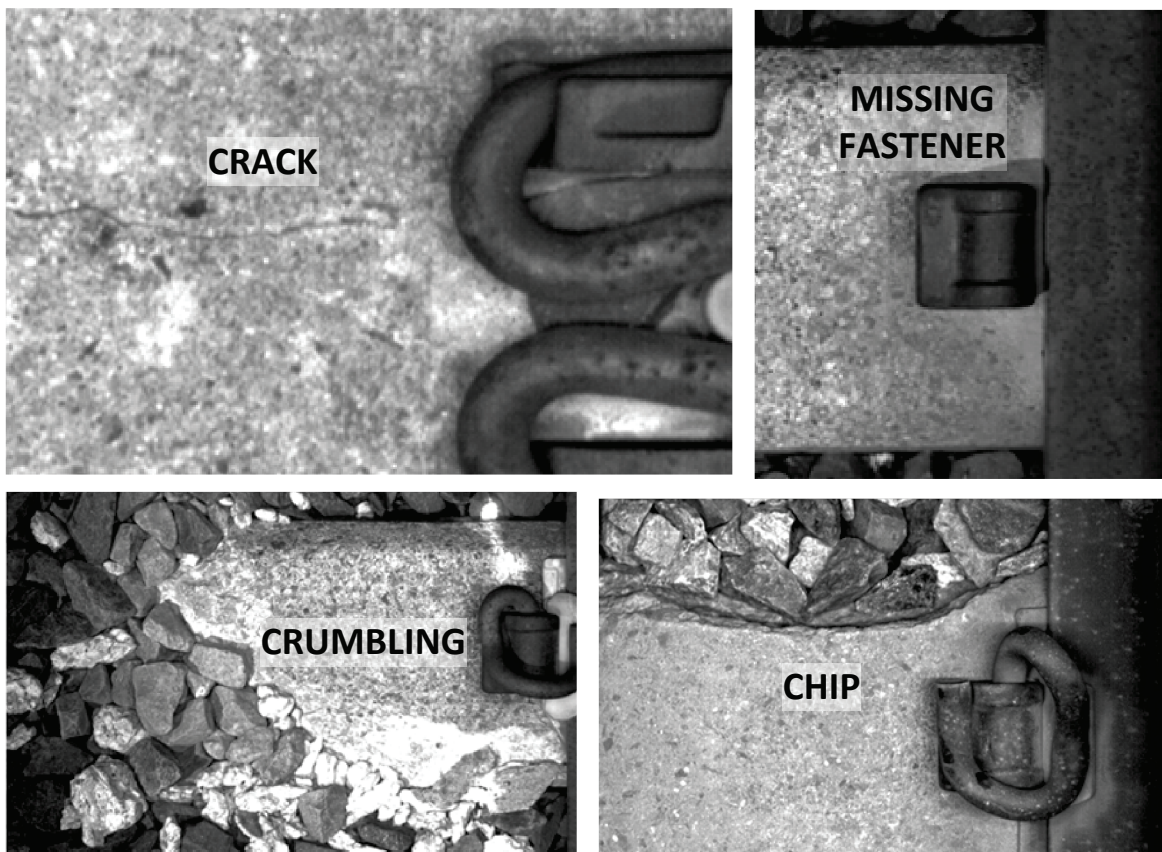


Figure 4-1. Typical Examples of the Nonconformance Types Assessed

The second tie evaluation effort in Section 3.1 involved classifying a set of approximately 1,000 already-identified cracks based on the categories listed in Table 4-1. For reference, an example image showing a crack in each category is included in Appendix A.

Table 4-1. List of Observed Crack Types

Crack Category	
1. Other Crack Types (Small)	6. Center Crack
2. Clip Crack	7. Other Crack Types (Large)
3. Edge Crack	8. Mid Shoulder Crack
4. End Crack	9. Mid Gauge Crack
5. Eroded Crack	10. Spider Crack

Most of the ties encountered during this study were in acceptable condition. Specifically, based on the distribution of tie grades presented earlier in Figure 3-4, the condition of approximately 99 percent of the ties assessed was found to be satisfactory (Grade 2 or less). Thus, the nonconforming ties shown in Figure 4-1 and in Appendix A are exceptions rather than the rule. This observation underscores that, at least in this study’s test zone, severely degraded ties were not prevalent.

Among the nonconformance types evaluated in this study, the results presented in Figure 3-1 indicate that cracks were the most prevalent type of nonconformance. Specifically, cracks accounted for 46 percent of the identified nonconformances. Chips were found to occur almost as frequently as cracks, accounting for 44 percent of the observed nonconformance pool. Chips were followed by crumbling at 6 percent and missing fasteners at 4 percent. Due to heightened levels of uncertainty that occur when nonconformance size approaches the limits of the imaging resolution, faint cracks were not included in this assessment. Thus, while the frequencies for both cracks and chips reported in Figure 3-1 are similar, it is estimated that the relative prevalence of cracks is being under-reported by at least 10 percent.

The observed distribution of nonconformance types on a mile-by-mile basis, presented in Figure 3-2, indicates that the prevalence of each nonconformance type varies considerably from one mile to the next. This suggests that the overall distribution of nonconformance types presented in Figure 3-1 would, in general, shift somewhat for differing blocks of miles. These observations also tend to de-emphasize the utility of sampled track bed inspection (i.e., random spot checking) to determine overall tie conditions.

In general, the distribution of crack types exhibited in Figure 3-3 demonstrates that the type and nature of the cracks observed tended to vary widely such that no crack mode (or small set of modes) emerged as clearly dominant. Instead, the distribution of various crack types varied gradually and without large changes in prevalence from one type to the next most prevalent type. This observation underscores the reality that automating crack detection in concrete ties is a nontrivial task; however, no result from this study provides any justification to warrant automatically classifying cracks found in concrete ties. Instead, efforts devoted to automated tie inspection should focus on detecting more substantial crack sizes as well as being able to quantify crack location and overall crack size.

The results shown in Figure 3-3 indicate that, among crack types, the most common type was observed to be early stage cracks, accounting for 20 percent of all cracks assessed. Related to this, the growth rate results shown in Figure 3-15 indicate that smaller cracks tend to grow at a slower absolute rate than larger cracks. The observation that early stage cracks are the most

prevalent form of crack is consistent with the growth rate trend that smaller cracks grow at a slower absolute rate than larger cracks, which would de-emphasize the importance of targeting smaller cracks during track bed inspections and emphasize the importance of targeting larger cracks. Here, the reasoning is that larger cracks are poised to cause a tie failure while slower-growing smaller cracks are not. Thus, the results of this study support a recommendation to de-emphasize smaller cracks during tie inspection based on the premise that they can be addressed once they become larger cracks.

The results of Figure 3-5 indicate that overall progression in concrete tie conditions was neither widespread nor severe. Specifically, the number of ties that advanced in grade during this study's longest period of observation (13 months) was not alarming, and most ties that did advance did so by only one grade level. Only a few ties advanced by two grade levels, and none of the assessed ties advanced by more than two grade levels.

4.2 Crack Growth Rate Assessment—All Cracks Studied

The growth rate results, summarized in Table 3-2, which correspond to all cracks examined during this study's longest observation period of 13 months, indicate that 65 percent of the cracks studied did not grow while 35 percent did grow. This means that no material change occurred over the course of just over 1 year in approximately two-thirds of the cracks studied in detail. Among cracks that did grow, the median (typical) growth rate was only 7.5 mm²/yr, equating roughly to a length growth rate of 0.6 in/yr. The growth rate of a typical fast-growing crack (e.g., a crack at the 90th percentile point) was found to be 25.5 mm²/yr, equating roughly to a length growth rate of 2.2 in/yr.

This same analysis was repeated for an even more severe scenario. Under the more severe scenario, unfavorable conditions were combined (see Figure 3-16) to yield a sub-population that reflected crack growth rates based on the available worst case conditions. A typical fast-growing crack (e.g., a crack at the 90th percentile) in this extreme subpopulation was found to grow at a rate of 33 mm²/yr or approximately 3 in. in length growth per year.

4.3 Parametric Crack Growth Rate Assessment

This section assesses whether or not each of the seven parameters presented earlier in Section 3.3 has a significant influence on crack growth rate. The assessment was performed two times. The first assessment included a mixture of ties manufactured by both Tie Manufacturer "B" and Tie Manufacturer "A." Parameters determined to exert a statistically significant influence on crack growth rate based on the first assessment were then reassessed a second time based on segregating Tie Manufacturers "A" and "B" ties such that the influence of tie manufacturer is isolated.

4.3.1 Growth Rate Assessment—Tie Manufacturer "B" and Tie Manufacturer "A" Ties Mixed

To support the assessment presented in this section, the results from Section 3.3 are summarized in Table 4-2 using the median growth rate to represent each subpopulation's overall growth rate tendency. In Table 4-2, the columns are described as follows:

Growth Rate of a Typical Crack – Values that correspond to the median growth rates for each subpopulation of studied cracks. Sub-population(s) in each category which exhibited higher crack growth rates are highlighted in bold.

Growth Rate Spread – Values which equal the difference between the maximum and minimum median growth rates among each set of compared parameters. To clarify, values in the “Growth Rate Spread” column quantify the amount of influence that a given parameter has on crack growth rate.

Two-Sigma Uncertainty – Values which indicate the portion of growth rate spread that can be due to measurement and sampling uncertainty given a confidence level of 95 percent.

Residual – Values used to assess whether a given growth rate spread is statistically significant. It is calculated by subtracting the value in the “Two-Sigma Uncertainty” column from the corresponding value in the “Growth Rate Spread” column. A difference in measured crack growth rate for a given parameter (e.g., curvature) is deemed statistically significant if the corresponding value in the “Residual” column is greater than zero.

The results of Table 4-2 indicate that the parameters “Combined Factors,” “Crack Size,” “Field vs. Gauge,” “Curvature,” and “Tie Manufacturer” exhibit a statistically significant influence on crack growth rate. Conversely, the parameters “Posted Speed” and “Track Grade” do not exhibit a statistically significant influence on crack growth rate.

Table 4-2. Summary of Crack Growth Rates for Assessed Parameters

Parameter	Growth Rate of a Typical Crack (mm ² /yr)	Growth Rate Spread (mm ² /yr)	Two-Sigma Uncertainty (mm ² /yr)	Residual (mm ² /yr)
Combined Factors Worst Case Best Case	13 3.8	9.2	2.4	6.8
Crack Size Small Crack ≤ 35 mm ² Medium Crack < 35 to ≤ 70 mm² Large Crack > 70 mm²	4 8.3 7.9	4.3	2.0	2.3
Field vs. Gauge Gauge Side Field Side	8.9 5	3.9	2.1	1.8
Curvature Non-Tangent Track Tangent Track	8.9 5.3	3.6	2.1	1.5
Tie Manufacturer Tie Manufacturer “B” Tie Manufacturer “A”	8.1 5.9	2.2	2.1	0.1

Parameter	Growth Rate of a Typical Crack (mm ² /yr)	Growth Rate Spread (mm ² /yr)	Two-Sigma Uncertainty (mm ² /yr)	Residual (mm ² /yr)
Posted Speed High Range (>125 - 150 mph) Low Range (30 - ≤125 mph)	6.5 6	0.5	2.0	-1.5
Track Grade Neutral Grade (Grade ≤ 116) Non-Neutral Grade (Grade > 116)	6.4 6.2	0.2	1.9	-1.7

4.3.2 Growth Rate Assessment—Ties for Manufacturers “A” and “B” Segregated

The growth rate results listed in the previous section indicate that the identity of the tie manufacturer has a statistically significant influence on crack growth rate. The same results also suggest that curvature, crack location, and crack size affect crack growth rate, however, these initial assessments are based on data sets that include ties manufactured by both Tie Manufacturer “A” and Tie Manufacturer “B.”

Table 4-3 compares the impact that curvature, crack location and crack size have on crack growth rate when both Tie Manufacturer “A” and Tie Manufacturer “B” ties are included versus the impact of those parameters when only Tie Manufacturer “A” ties are included. In Table 4-3, the Tie Manufacturer “A”-only subpopulation no longer includes the influence of the faster-growing cracks associated with the Tie Manufacturer “B” subpopulation. This supports a more direct assessment of the influence imparted by curvature, crack location, and crack size.

Values in the “Growth Rate Spread” column of Table 4-3 indicate the amount of influence that each parameter listed in the first column has on growth rate with and without Tie Manufacturer “B” ties included. The value in the “Difference Spread” column quantifies the amount of isolated influence that Tie Manufacturer “B” ties have on growth rate. In Table 4-3, values in the “Two-Sigma Uncertainty” column indicate the portion of the values in the “Difference Spread” column that can be due to measurement and sampling uncertainty given a confidence level of 95 percent. Finally, values in the “Residual” column of Table 4-3 are calculated by subtracting the value in the “Two-Sigma Uncertainty” column from the corresponding value in the “Difference Spread” column.

If the presence or absence of Tie Manufacturer “B” ties significantly influenced the results associated with a given parameter, then the corresponding value listed in the “Residual” column of Table 4-3 would be positive. Because all values in the “Residual” column are negative, the influences that curvature, crack location, and crack size have on crack growth rate do not significantly interact with the influence that tie manufacturer has on growth rate. Effectively, this analysis indicates that that curvature, crack location, and crack size tend to influence crack growth rate independent of tie manufacturer.

Table 4-3. Growth Rate Spread When Tie Manufacturer “B” Ties are Removed from Data Set

Parameter	Growth Rate Spread (mm ² /yr)		Difference Spread (mm ² /yr)	Two-Sigma Uncertainty (mm ² /yr)	Residual (mm ² /yr)
	Tie Manufacturer “A” Only	Tie Manufacturers “A” and “B”			
Field vs. Gauge	4.5	3.9	0.6	2.9	-2.3
Crack Size	4.45	4.3	0.15	2.8	-2.65
Curvature	3.7	3.6	0.1	2.9	-2.8

4.4 Assessment of Human and Machine Factors

This section assesses the effectiveness of the human and machine-based analysis approaches employed during this study. Without machine vision technology, this study would not have been practical. The study has demonstrated that reviewing track bed images in an office environment is an effective means of identifying relevant nonconformances in concrete ties, including cracks, chips, missing fasteners, and crumbling. In addition, image quality was adequate enough to assess many other potentially relevant nonconformances, such as rail base corrosion, standing water and fouled ballast where mud is present and the presence of vegetation that would interfere with railroad employees performing normal duties.

When track bed imaging was conducted at night, it was possible to cover 60 miles of track in 8 hours with a three-person crew. Given an optimized process, the corresponding time required to manually assess 60 miles of track bed image data would be approximately 2 hours per mile. Factoring in anticipated advances in machine vision algorithms, this 2-hour estimate could potentially drop by a factor of four within the next few years. In contrast, on-foot tie inspection requires between 3 and 4 man-hours per mile and is logistically more complicated due to the extended amount of foul time required.

To acquire quality track bed images at high speeds using machine vision technology, a densely focused beam of light is needed. With significant attention to detail, today’s LED technology is suitable for supporting image acquisition at revenue service speeds, however, there is room for improving light density. Increased light density would enhance machine vision-based concrete tie inspection by improving conditions for manual image reviews. It stands to reason that increasing light density would also benefit fully automated concrete tie inspection; however, this remains an open question.

During this study, a machine vision algorithm was used to detect and catalog concrete ties. The automatic tie detection performance was better than 99.9 percent reliable and met the needs of this study well, but automated algorithms for detecting cracks and other irregular nonconformances in concrete ties are less developed. As a result, track bed images were manually reviewed to locate and annotate the nonconformances admitted into this study, as discussed below.

The time required to manually inspect track bed images varied depending on nonconformance size. Locating small nonconformances, such as fine, early-stage cracks required approximately eight hours per mile per reviewer. Locating larger nonconformances, such as later-stage cracks, chips, crumbling, and missing fasteners required approximately 2 hours per mile per reviewer.

Manual image review was most effective when nonconformance size was larger than approximately five pixels, however, effectiveness declined as nonconformance size approached the limit of the imaging resolution. Effectively, manually locating fine-scale nonconformances in track bed images, such as faint cracks with a width near the limit of the imaging resolution, was determined to be unreliable. For this reason, faint cracks were ultimately excluded from this study.

The use of GPS-based location references and image review software provided a reasonably efficient means of manually aligning track bed image data. GPS references typically provided an initial registration accuracy on the order of ± 20 feet. Perfect tie-to-tie registration was achieved using either large- or fine-scale landmarks in the image data. Examples of large-scale landmarks that worked well included frogs and electrical equipment visible in the track bed image. Examples of fine-scale landmarks that worked well included semi-permanent staining on the tie surface and fixed granular patterns embedded in individual ties.

In conclusion, while aspects of machine vision still require additional development in order to more fully address the needs of the rail industry, current technology proved to be invaluable in meeting the objectives of this research.

5. Conclusion

The results presented by ENSCO, Inc. indicate that tie conditions in the high-speed passenger line progressed at non-alarming rates. During the 13-month period between the first and third imaging surveys, 65 percent of the assessed cracks showed no measurable growth, while 35 percent showed growth. Among the cracks that showed growth, the growth rate for a typical crack, as characterized by the median growth rate, was 7.5 mm²/yr, equating to an increase in crack length of roughly 0.6 in/yr. The two-sigma uncertainty associated with this growth rate due to measurement and sampling uncertainty is 1.9 mm²/yr.

Examining the situation from another perspective, the results of this study have shown that tie grades (on a scale of Grade 1—No Material Nonconformances through Grade 5—Ineffective for a population of approximately 26,000 ties) advanced during the study's longest observation interval of 13 months, however, the amount of advancement was slight. Specifically, only 0.23 percent (i.e., a fraction of 1 percent) of approximately 26,000 assessed Grade 1 ties advanced to a higher, or worse, grade level. Among the Grade 1 ties that advanced, approximately 96 percent advanced by one grade level while only approximately 4 percent advanced by two grade levels. None of the assessed Grade 1 ties advanced by more than two grade levels. Ties with an initial grade of 2 through 4 behaved similarly to Grade 1 ties in that most advanced by only one grade level, and none advanced by more than two grade levels.

Based on the amounts of degradation observed in this study, the interval of observation (13 months) equates to a brief snapshot in the total life of a typical concrete tie. This is reasonable if the expected lifetime of a concrete tie is 50 years or more. The main conclusion from this study, that concrete tie degradation rates are not alarming, is generally consistent with a high life expectancy for a typical concrete tie. However, it is not a contradiction for a non-trivial number of ties to fail sooner than the expected life of a typical tie. This study has shown, at least in part, why this would be the case, as further clarified next.

In this study, it has been shown that several factors influence concrete tie degradation rates. The results indicate that curvature, tie manufacturer, crack location, and crack size all influence the rate at which cracks grow, which means that all ties are not created equal and not all ties “live” an equal life. It is reasonable to note that not all ties last equally long, but because the duration of this study was brief compared to the anticipated life of a typical concrete tie, deriving a definitive answer to the life expectancy question from this study's results is not practical. Instead, the corresponding conclusion is simply that this study's results are consistent with an expected life of 50 years or more for a typical concrete tie.

Initially, the evidence that curvature influences concrete tie degradation rates would seem to be a basis for recommending changes to existing tie inspection practices; however, the amount of additional influence observed is not deemed significant. Cracks on curving track were shown to progress in length at roughly 0.6 in/yr versus 0.4 in/yr for tangent track, and while this difference was shown to be statistically significant, neither of these rates is high enough to justify a change in prevailing practices. A similar conclusion generally applies to all the parameters assessed under this study, effectively because the global trend is that observed crack growth rates are non-alarming in general.

Where safety is concerned, it is certainly justifiable to base decisions on worst case scenarios rather than typical scenarios. With this in mind, two analyses were conducted to examine the

behavior of typical “fast-growing” cracks. In the first scenario, a typical “fast-growing” crack was defined as a crack that grew at a rate equal to the 90th percentile point within a given crack population. Thus, a typical “fast growing” crack grew faster than 90 percent of all other cracks in a given population. The growth rate for a typical “fast growing” crack among all cracks studied was found to be 25.4 mm²/yr, which equates to approximately 2.2 in of length change per year. It was estimated that a typical “fast growing” crack originating near the tip of a tie shoulder (for example) would take a projected 6.5 years to begin entering the zone around the rail seat.

The second scenario was even more severe. Unfavorable conditions were combined to yield a sub-population reflective of crack growth rates that might exist under worst case conditions. A typical fast-growing crack in this “worst case” subpopulation was determined to grow at a rate of 33 mm²/yr, or approximately 3 in of length change per year. At this rate, the projected time for a crack to grow from the tip of a tie shoulder to the rail seat region was estimated to be 4.6 years.

Outlier growth rates larger than 33 mm²/yr were encountered during this study. However, outlier growth rates accounted for less than 3 percent of the studied population and corresponded exclusively to late stage cracks on ties already designated as ineffective. As a result, basing assessments on worst case median growth rates is adequately conservative because true worst case growth rates were only observed to occur after a tie’s ability to contribute to holding gauge was already severely compromised.

Where tie grading scales are concerned, the scale used in this study (refer to Appendix B) effectively supported the study’s objectives by allowing tie grade progression to be accurately tracked over time. In practice, tie grades are useful in determining compliance with FRA standards and identifying which ties need to be replaced. Both of these objectives could be met using a 2-point tie grading scale (such as Grade 1–Satisfactory, Grade 2–Ineffective); however, additional grade levels allow any ties that are beginning to degrade to be visible in a tie condition report. A tie grading scale with more than five grade levels would tend to complicate and slow the tie grading process, and also tends to be more expensive in practice. Conversely, a tie grading scale with fewer than three grade levels would not provide enough resolution to accurately convey tie conditions. Thus, tie grading scales with three to five grade levels are recommended.

Based on a comparison of machine vision-based concrete tie inspection to on-foot tie inspection, the machine vision-based approach offers a competitive advantage. This was even the case given that significant manual review of the track bed image is required today. As machine vision algorithms continue to evolve, machine vision’s existing competitive advantage is expected to grow.

Although this study provides a significant amount of additional information to provide increased understanding of concrete tie degradation in a high-speed corridor, many factors remain unknown. Some of those factors include:

- The progression rate of other failure modes (e.g., crumbling and chipping)
- The impact of tonnage on crack growth rates
- The impact of seasonal variations and different geographical regions on tie degradation
- Potential variations among additional tie manufacturers

This study also did not attempt to quantify crack depth. Therefore, the study's results do not address questions pertaining to how crack depth may impact crack growth rates. Effectively, many important caveats apply to the various conclusions and recommendations herein.

Consequently, the preliminary recommendations made in this report should be vetted over time under actual conditions corresponding to each individual railroad. With this in mind, a prudent strategy would be to gradually phase in any changes to existing tie inspection practices that are made based on the recommendations presented in this report.

In conclusion, the study's recommendations can be summarized as follows:

- Focus concrete tie assessments and replacement activities on later stage nonconformances while de-emphasizing less severe early stage nonconformances
- Grade concrete ties using a grading scale with three to five grade levels based on objective (quantifiable) criteria
- Leverage machine vision technology to assess concrete tie conditions

6. References

Tajaddini, A. (2006). *Video System for Joint Bar Inspection*. Washington DC: Federal Railroad Administration. Research Results, RR06-03. Available at: https://www.fra.dot.gov/eLib/details/L03528#p1_z5_gD_kVideo%20System%20for%20Joint%20Bar%20Inspection.

Abbreviations and Acronyms

AGR	Annualized Growth Rate
FRA	Federal Railroad Administration
GPS	Global Positioning System
GUI	Graphical User Interface
Amtrak	National Railroad Passenger Corporation
NEC	Northeast Corridor
RD&T	Office of Research, Development and Technology
RSS	Root of the Sum of the Squares

Appendix A.
Example Images Showing Observed Crack Types

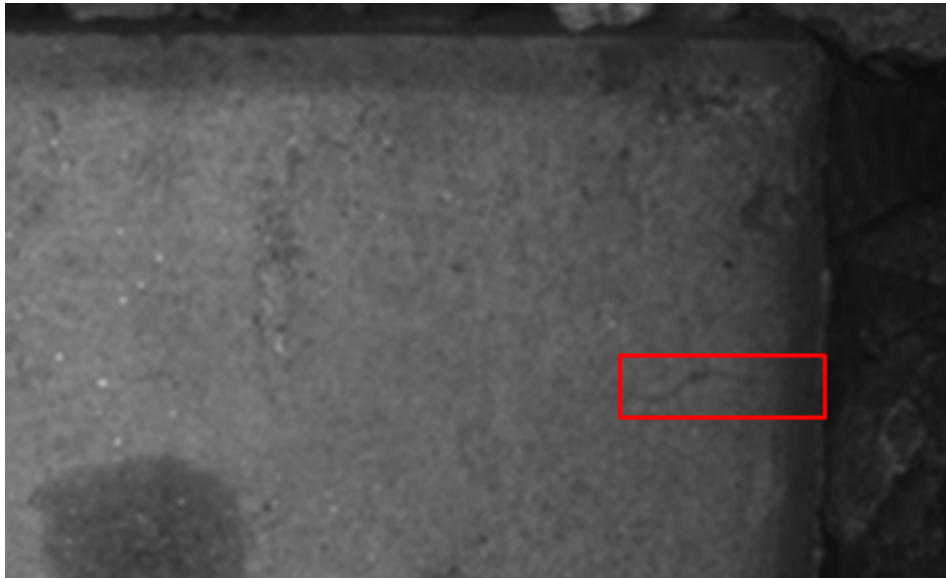


Figure A-1. Example of a Typical Other Crack Type (Small)



Figure A-2. Example of a Typical Clip Crack



Figure A-3. Example of a Typical Edge Crack



Figure A-4. Example of a Typical End Crack



Figure A-5. Example of a Typical Eroded Crack

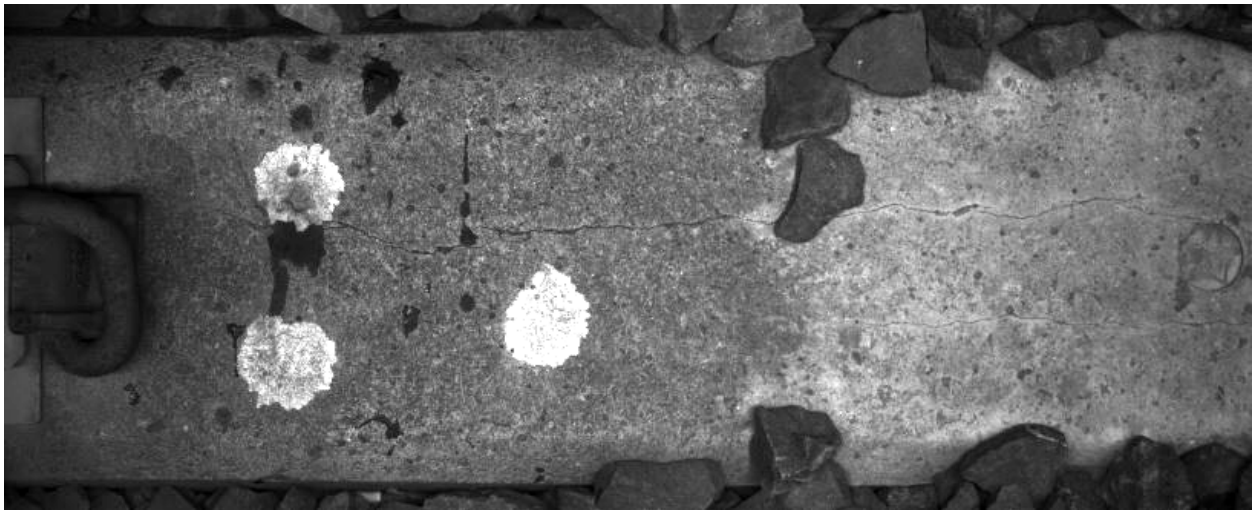


Figure A-6. Example of a Typical Center Crack

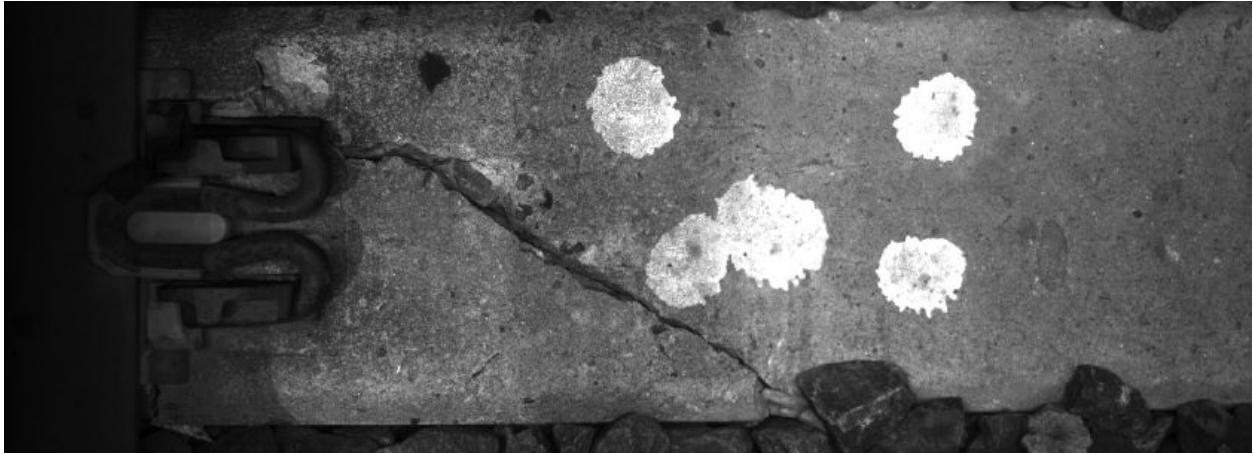


Figure A-7. Example of a Typical Other Crack Type (Large)

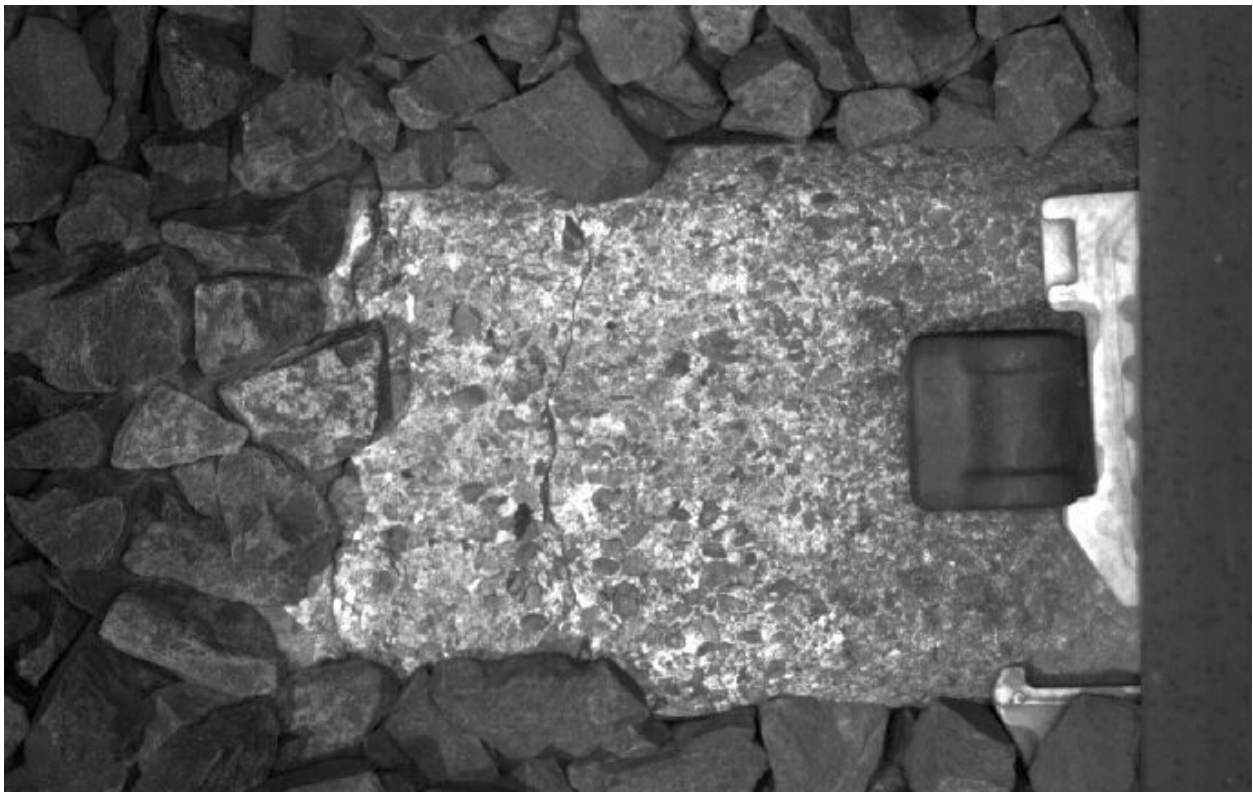


Figure A-8. Example of a Typical Mid Shoulder Crack



Figure A-9. Example of a Typical Mid Gauge Crack

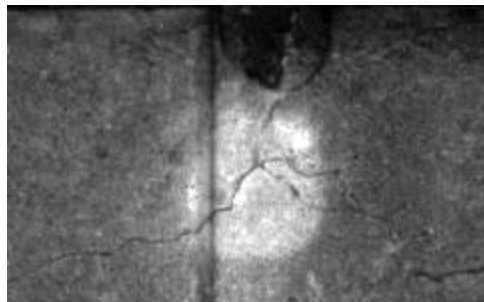


Figure A-10. Example of a Typical Spider Crack

Appendix B.

Tie Rating Guidelines Used in this Study

B.1 Scope

This appendix provides the study's guidelines for assigning numerical grades to concrete ties when track bed images are examined on a computer monitor.

B.2 Background

The primary function of a cross tie is to provide a rigid foundation for holding gauge (keeping the two rails of a railroad track in place under the load of a moving train). Ideally, a numerical grade assigned to a tie would indicate how much longer a tie can be expected to make meaningful contributions to holding gauge.

Missing Fasteners and Tie Grading

A tie must be affixed to the rail by a rail fastener in order to hold gauge and a missing, damaged, or improperly oriented rail fastener impairs the tie's ability to do so. However, a fastener anomaly is classified as a nonconformance in and of itself rather than a tie nonconformance. Thus, fastener anomalies have no impact on a tie's grade in this study.

Objective Tie Grading Guidelines

The tie grading guidelines presented here are based on a scale of Grade 1—No Material Nonconformances through Grade 5—Ineffective for a population of approximately 26,000 ties. The guidelines are based on objective criteria that can be numerically approximated or represented as a Boolean (Yes/No) value. The tie-grading guidelines in this appendix are based on the seven parameters listed below. When ties are graded on the parameters provided in Table B-1, a tie shall be given the lowest (best) grade. Best judgment was used to resolve ambiguous cases that did not clearly lie within the parameters set in Table B-1.

Objective tie grading parameters

- 1) Maximum width of a crack in, or with reasonable potential to enter, a rail seat zone or divide the tie between the rails.
- 2) Maximum percentage that a crack can extend perpendicular to a tie between the rails or through a rail seat zone.
- 3) Maximum sum of crack lengths in a tie.
- 4) Maximum width reduction in the rail seat zone or between the rails caused by a nonconformance.
- 5) Maximum number of exposed pre-tensioning wire sites.
- 6) Maximum percentage of tie shoulder in crumbled state, absent, or disconnected from tie.
- 7) Maximum number of rail seat zones impacted by a nonconformance.

Table B-1. Parameter Limits for Tie Grades Applied During This Study

Parameter	Parameter Description	Tie Grade				
		1	2	3	4	5
1	Maximum width of crack with potential to enter a rail seat zone or divide the tie between the rails	0 mm	2 mm	4 mm	6 mm	Not 1-4
2	Maximum percentage that a crack can extend perpendicular to a tie between the rails or through a rail seat zone	10%	20%	40%	60%	Not 1-4
3	Maximum sum of crack lengths in tie	3 in	9 in	18 in	27 in	Not 1-4
4	Maximum width reduction in rail seat zone or between the rails caused by a nonconformance	0 in	1 in	2 in	4 in	Not 1-4
5	Maximum number of exposed pre-tensioning wire sites	None	None	None	1 site	Not 1-4
6	Maximum percentage of tie shoulder in crumbled state, absent, or disconnected from tie	10%	20%	40%	60%	Not 1-4
7	Maximum number of rail seat zones impacted by a nonconformance	0	1	1	2	Not 1-4

B.3 Tie Grade Examples

B.3.1 Grade 1 Examples

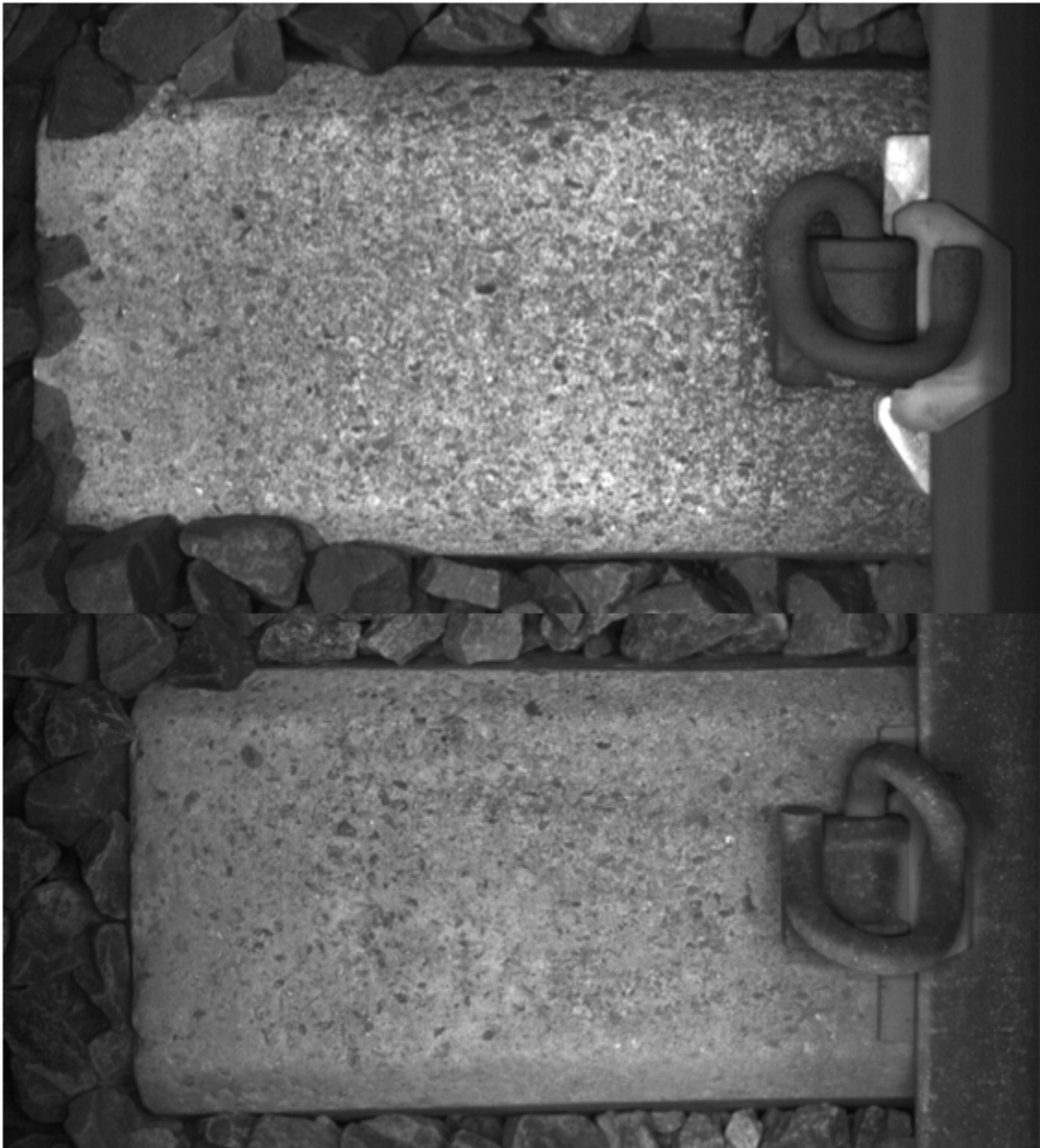


Figure B-1. Two Tie Shoulders in Excellent Condition—Tie Grade = 1



Figure B-2. Section of Tie Between the Rails in Excellent Condition —Tie Grade = 1



Figure B-3. Tie Shoulder with Minor Chip on One Corner—Tie Grade = 1



Figure B-4. Tie Shoulder with Surface Contamination—Tie Grade = 1



Figure B-5. Tie Shoulder Exhibiting Preliminary Signs of Crumbling Impacting Less Than 10 Percent of Shoulder—Tie Grade = 1



Figure B-6. Tie Shoulder with Inconsequential Surface Irregularities—Tie Grade = 1

B.3.2 Grade 2 Examples

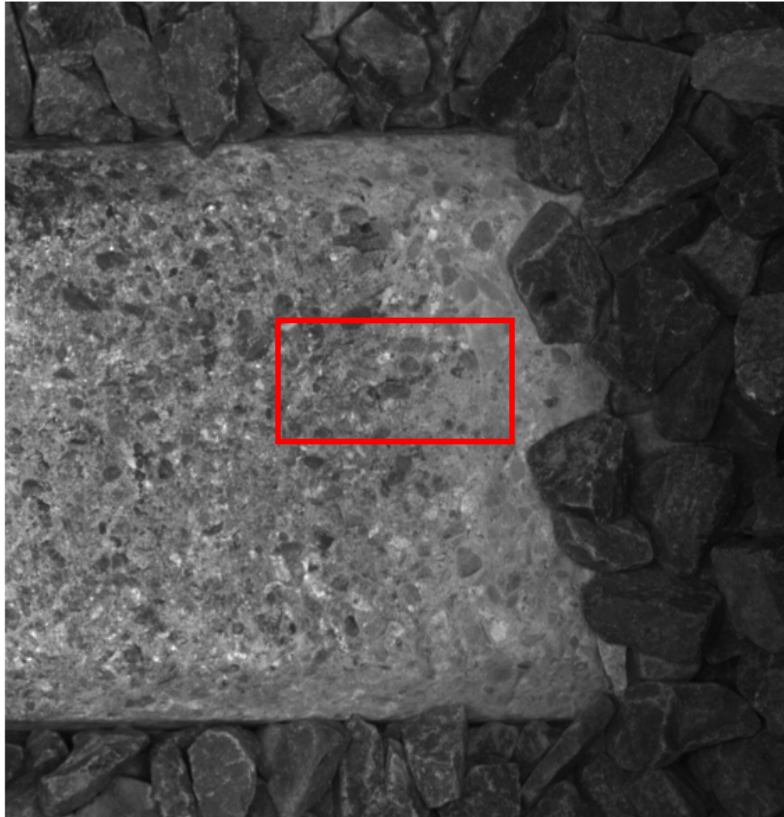


Figure B-7. Early-Stage Hairline Crack with Estimated Potential to Reach a Rail Seat Zone—Tie Grade 2

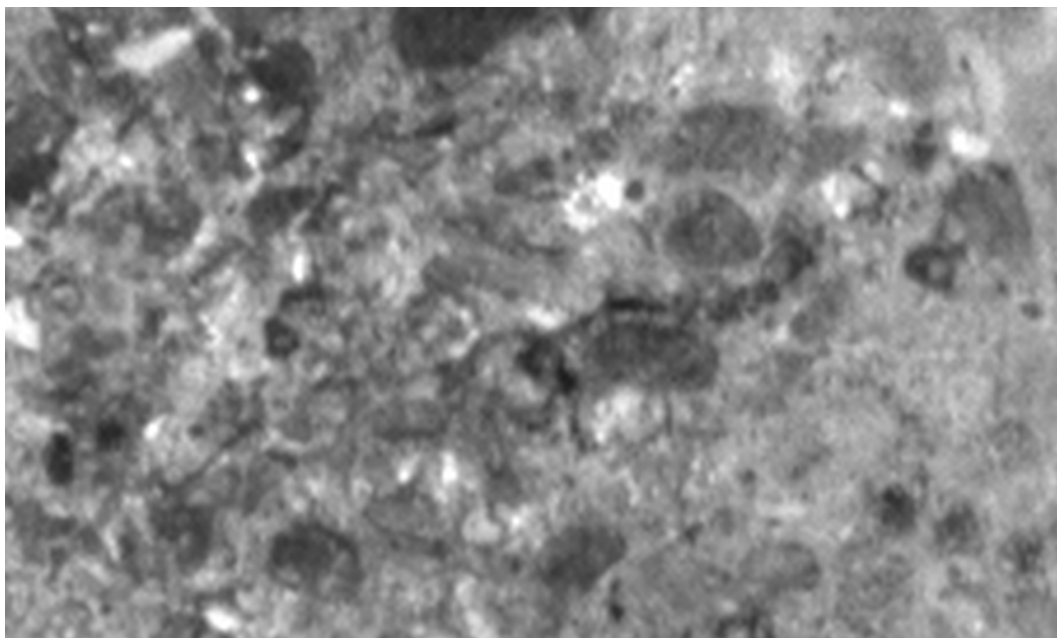


Figure B-8. Close-Up View of Early Stage Crack Shown in Figure B-7



Figure B-9. Tie Chip Not Reducing Width of Rail Seat Zone by More Than 1 Inch, One Rail Seat Zone Impacted by a Crack, and Total Crack Length Less Than 9 Inches—Tie Grade 2



Figure B-10. Marking Between the Rails (Two White Dots) Applied by Amtrak to Indicate a Tie Grade 2 for the Tie Shown in Figure B-9

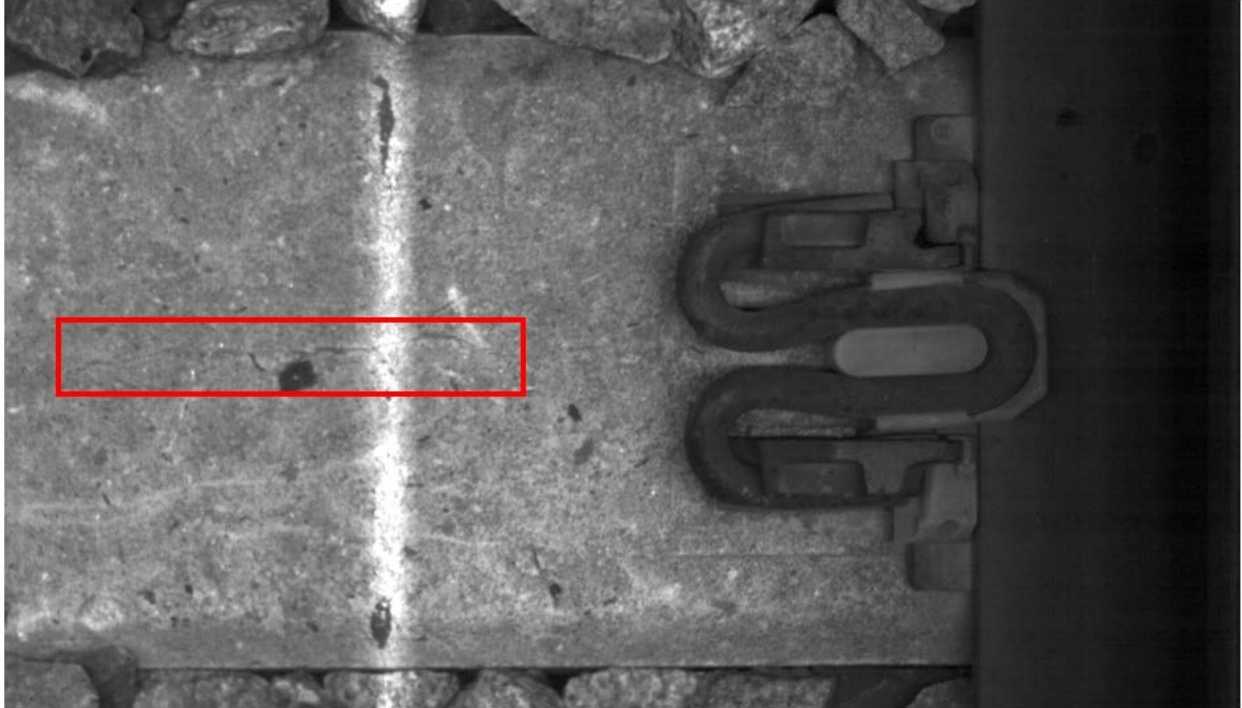


Figure B-11. Longitudinal Hairline Crack Between the Rails, Total Length Less Than 9 Inches—Tie Grade = 2 (This Tie is on the Border Between Grades 2 and 3)

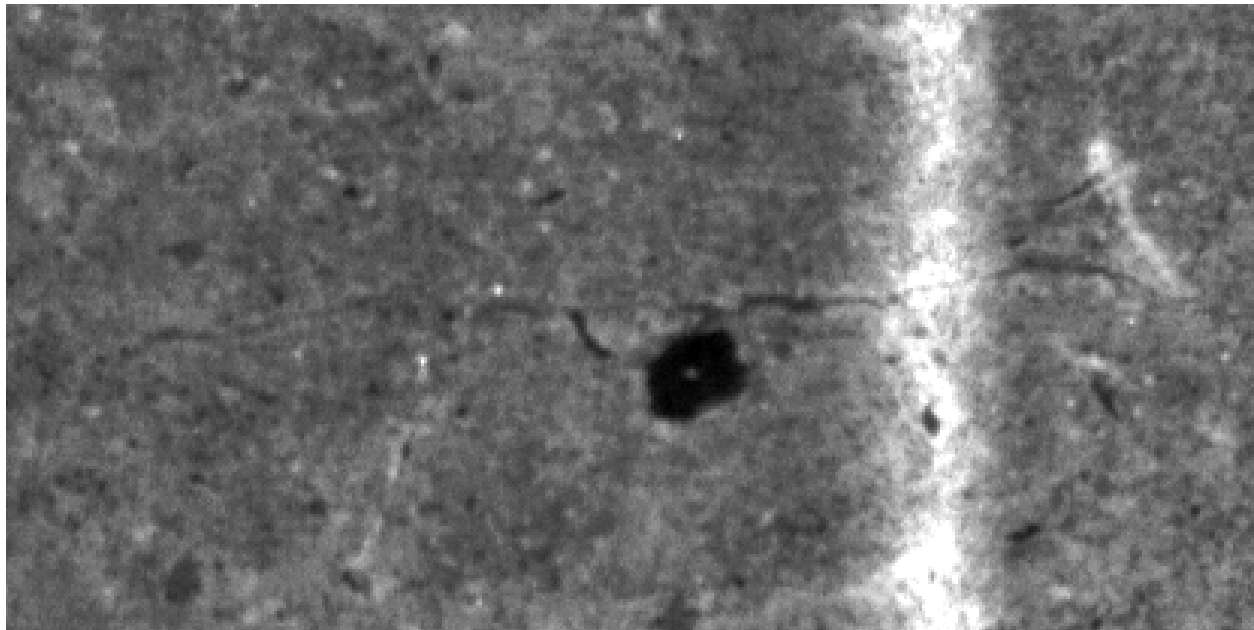


Figure B-12. Enlarged View of Hairline Crack Shown in Figure B-11

B.3.3 Grade 3 Examples

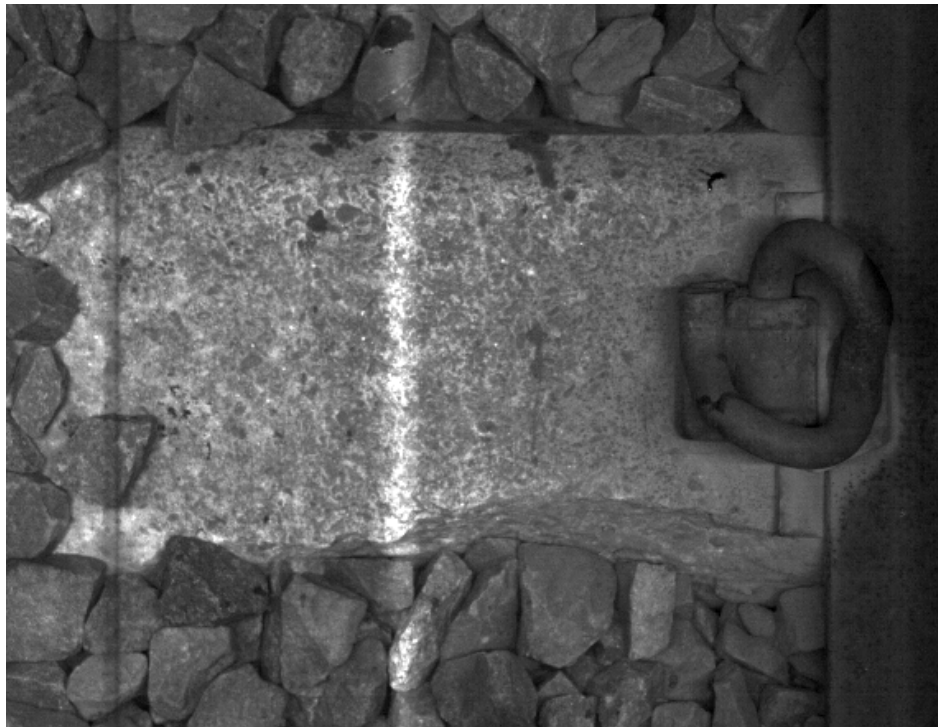


Figure B-13. Nonconformance Reducing Tie Width in Rail Seat Zone by More Than 1 Inch but Less Than 2 Inches—Tie Grade = 3

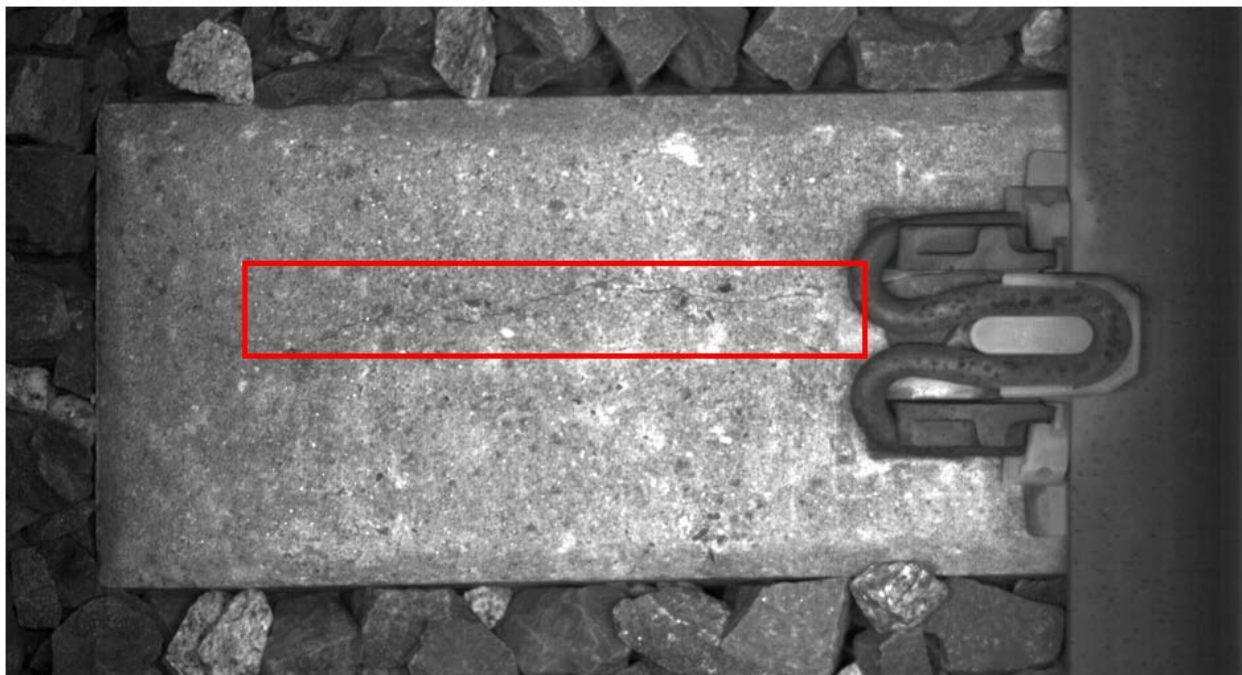


Figure B-14. Tie with Center Crack, Total Crack Length Greater Than 9 Inches—Tie Grade = 3

B.3.4 Grade 4 Examples



Figure B-15. Tie with One Pre-Tensioning Wire Exposure Site—Tie Grade = 4

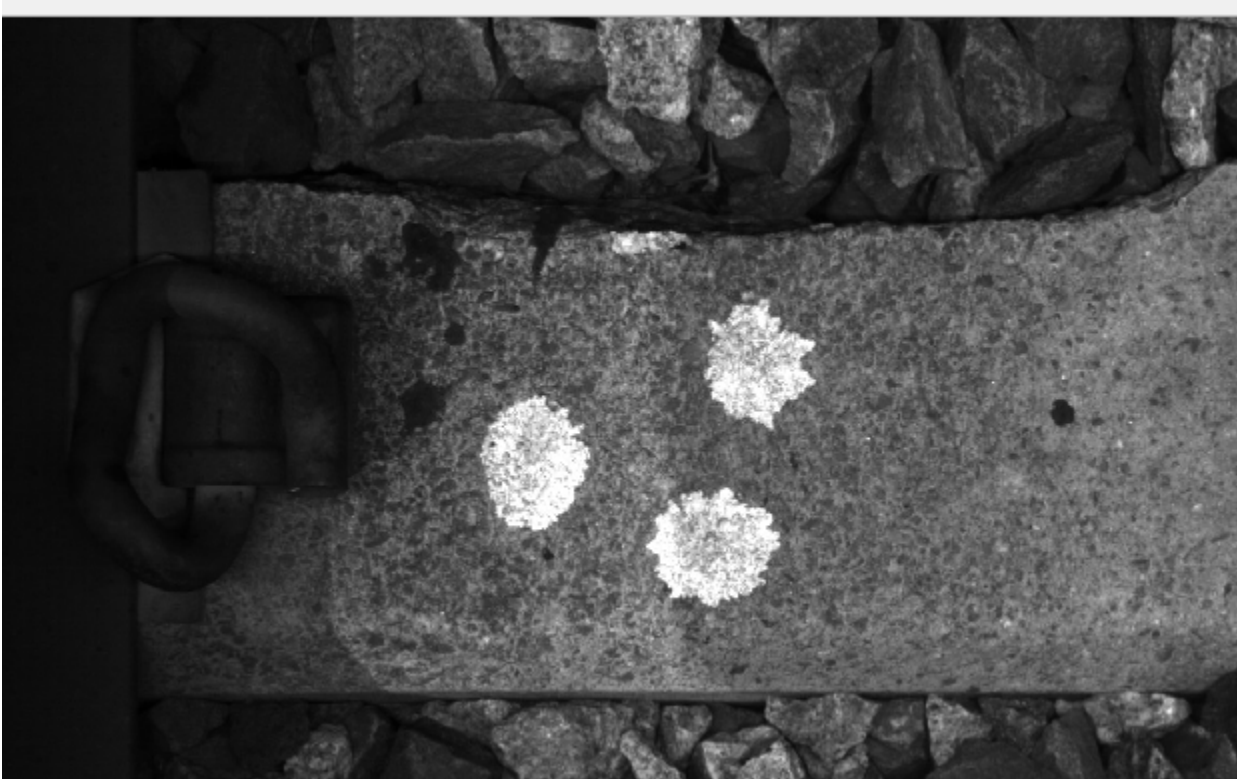


Figure B-16. Tie Width Reduced by More Than 2 Inches Between the Rails—Tie Grade = 4

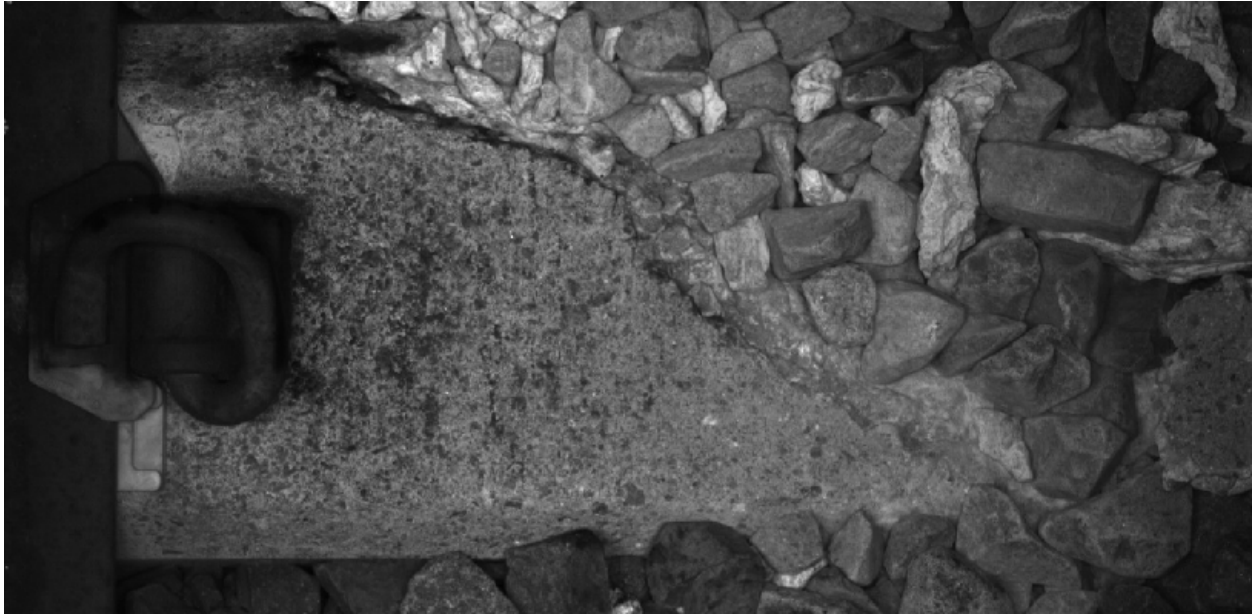


Figure B-17. More than 40 Percent but Less Than 60 Percent of Tie Shoulder Absent, Rail Seat Zones Still Intact—Tie Grade = 4

B.3.5 Grade 5 Examples

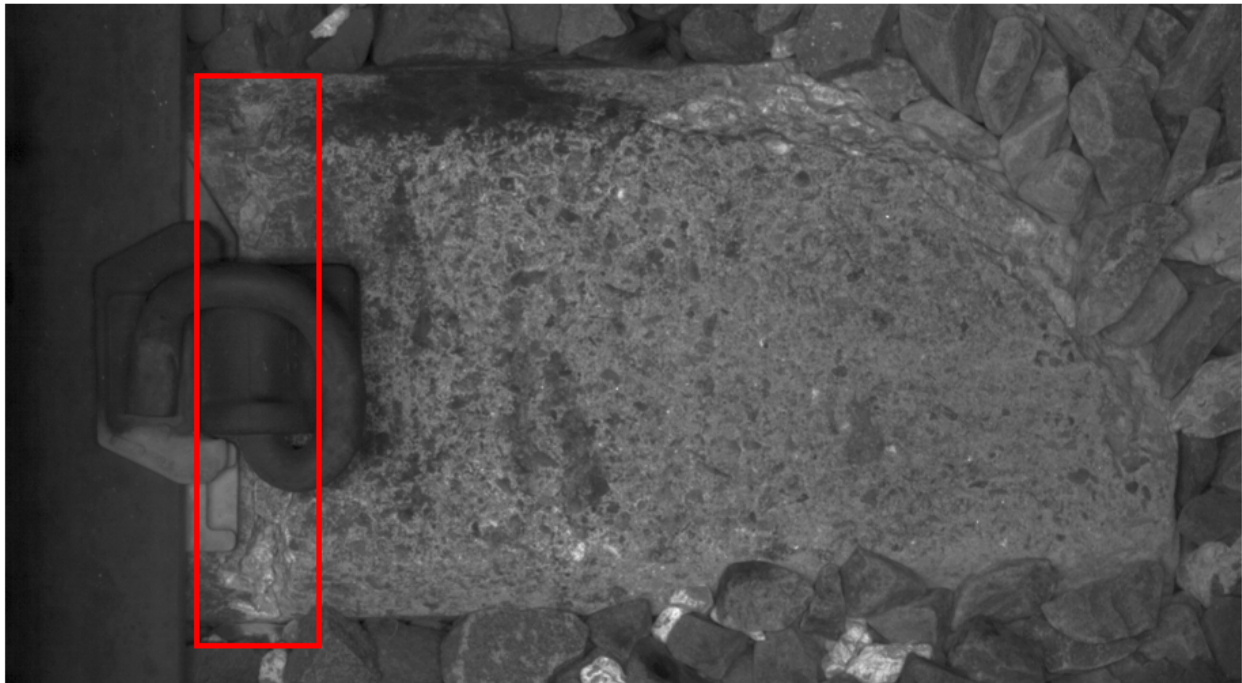


Figure B-18. Crack Passing Perpendicular to Tie Through Rail Seat Zone Spanning More Than 60 Percent of Tie's Width—Tie Grade = 5

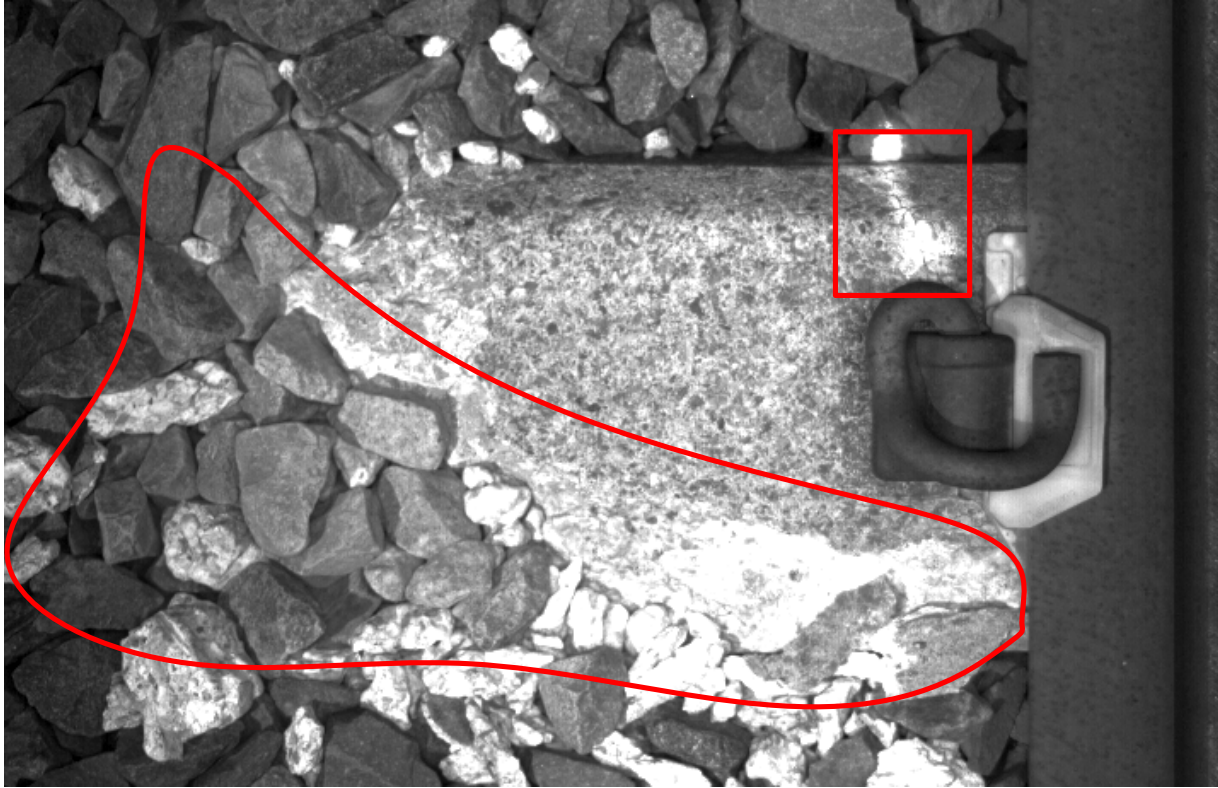


Figure B-19. More Than 60 Percent of Tie Shoulder in Crumbled State—Tie Grade = 5

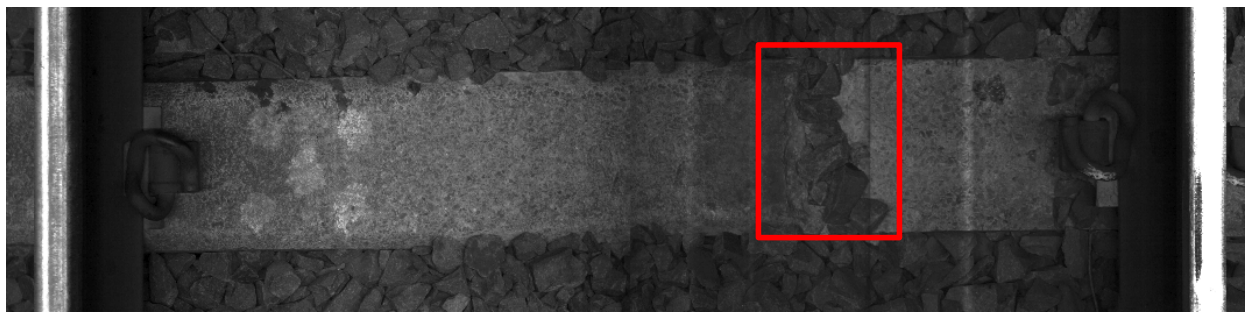


Figure B-20. Crack Perpendicular to Tie Between the Rails Spanning More Than 60 Percent of Tie's Width—Tie Grade = 5



Figure B-21. More Than 60 Percent of Tie Shoulder in Crumbled State—Tie Grade = 5

Appendix C. Preliminary and Final Software Customization Efforts

C.1 Phase 1 Software Overview of Operation

The software development portion of this study was divided into two phases. This section walks through a typical user experience and shows how the Phase 1 software enhancements were used.

After the user launches the software and specifies a track bed image file, a view similar to Figure C-1 appears.

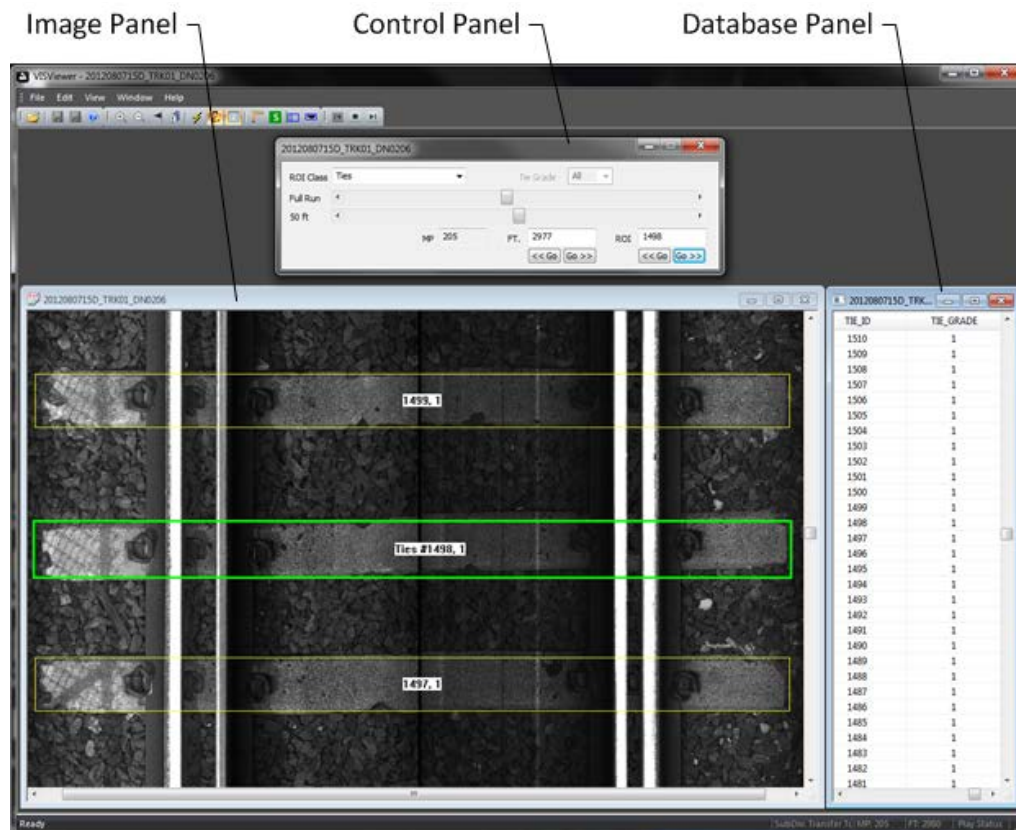


Figure C-1. Typical Screen Configuration Used When Locating Defects in Concrete Ties

The view in Figure C-1 has three panels. The image panel allows the user to see any desired portion within a continuous track bed image, the control panel is new and supports efficient navigation through large image files and finally, the database panel displays metadata corresponding to each tie, or other identified defect regions, within an image.

After opening an image file, a user will typically arrange the panels above to establish a preferred layout on the screen and then save the layout for repeated use. As an example, Figure C-2 shows a layout commonly used when manually searching for hairline cracks in concrete ties. In this layout, the user has taken advantage of two, side-by-side monitors and has zoomed in to show an enlarged view of one end of a tie. When looking at a portion of a tie on a dual-monitor setup, the tie appears as it would be seen by a track walker who is bending over to view it from a height of about 3 feet. A horizontal scroll bar supports left-to-right panning, which allows the

user to inspect an entire tie while zoomed in. After inspecting a given tie, a user will typically press either the up or down arrow key to automatically advance to the next tie. The ability to advance from one tie to the next is enabled by a pre-existing machine vision algorithm that automatically draws an approximate bounding box around each tie. The tie currently being evaluated (i.e., the active tie) is shown with a green border; all other ties are shown with a yellow border. Zooming and other operations, such as entering a tie grade, apply to the active tie.

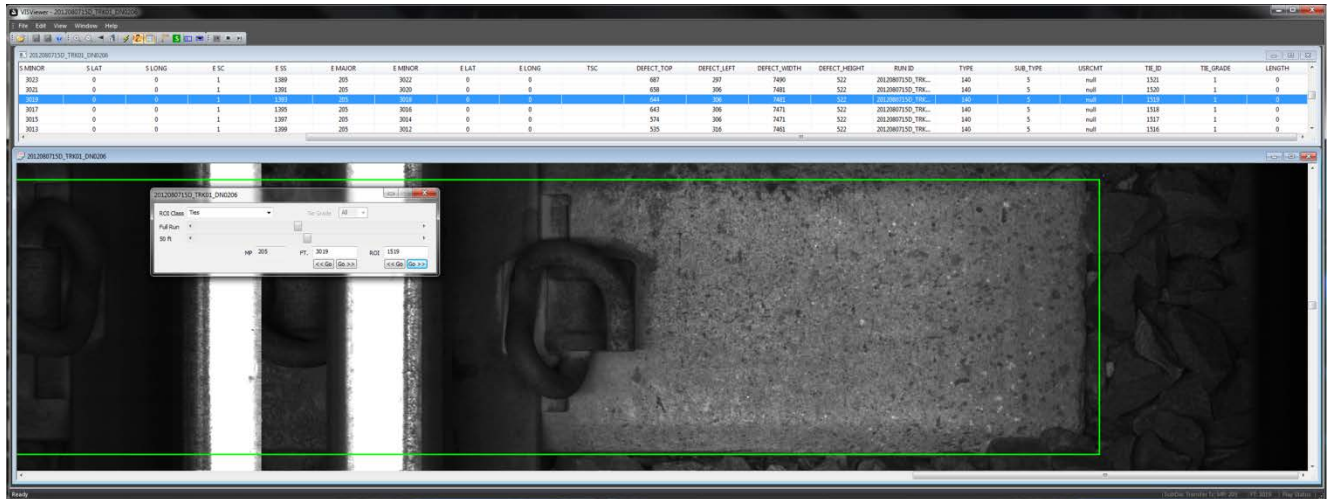


Figure C-2. Typical Screen Configuration Used When Locating Defects in Concrete Ties

Upon locating a cracked or defective tie (Figure C-3), the user is able to drag a rectangle around the defective zone and assign a defect name to the zone by selecting from a dropdown menu. Then the software stores the marked location and selected defect name in the database table shown in Figure C-1. Drawing a box around a defect region allows the region to be automatically cropped by a separate computer program called the Defect Outlining Tool (described next).

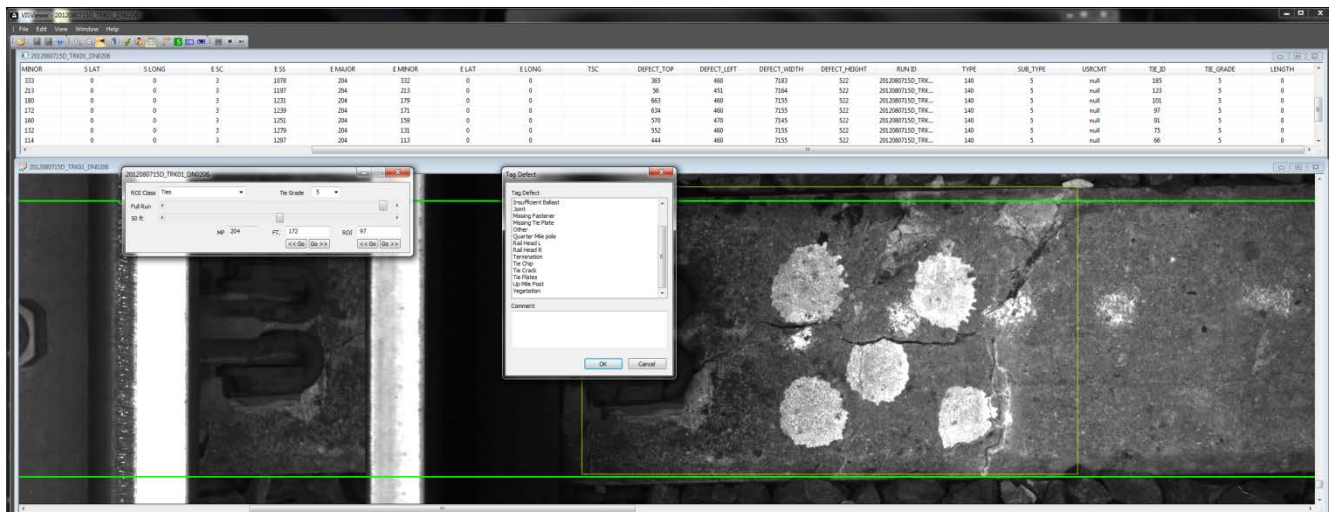


Figure C-3. Example of Marking a Cracked Tie Region with a Bounding Box Using the Subject Software

After cracked or otherwise defective regions in a given track bed image file have been manually

marked, each identified region is automatically cropped by the Defect Outlining Tool (mentioned above) and automatically named using a convention that provides traceability back to the tie where the crop was taken from the original track bed image. After the defective regions have been cropped, the user can employ the Defect Outlining Tool to draw a precise outline around a defect region so that the defect's area can be accurately determined by a computer. Figure C-4 shows an example of a crack that has been outlined using the Defect Outlining Tool. For reference, Figure C-5 shows a zoomed-in view of a portion of the same outlined crack.

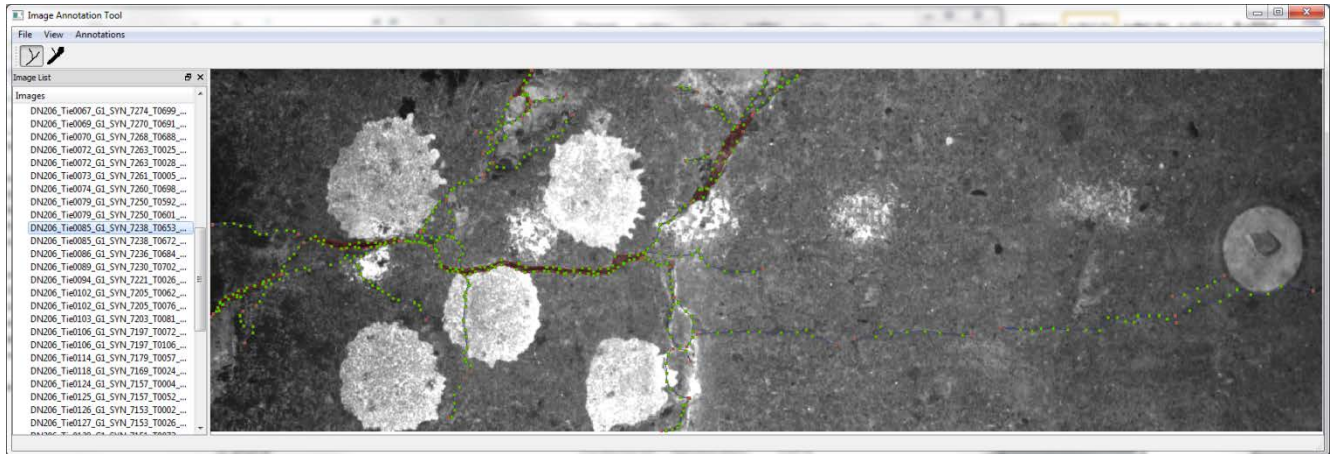


Figure C-4. Example Showing Human-Entered Outlines Around Cracks in a Defective Tie

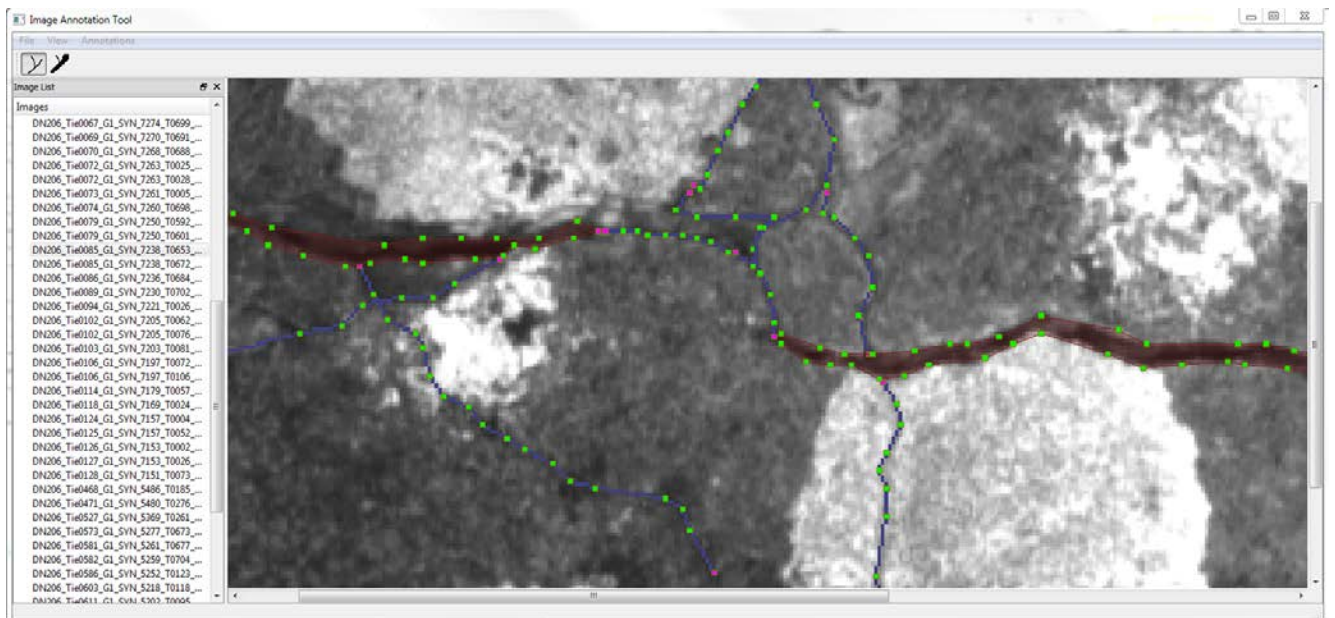


Figure C-5. Close-Up View of a Portion of the Cracked Tie Shown in Figure C-4

During Phase 2 of the software effort, the ability to automatically count the number of pixels inside an outlined region will be added to the Defect Outlining Tool, and the pixel count will provide an accurate measure of the total area occupied by each marked defect. The area measurements produced by the Defect Outlining Tool will ultimately allow accurate defect

progression rates to be determined on a tie-by-tie basis, which will permit the progression rates produced by the Defect Outlining Tool to serve as primary inputs that achieve project goals.

C.2 Phase 2 Software Overview of Operation

This section presents a typical user experience that demonstrates how Phase 2's software enhancements are combined with the software's pre-existing capabilities. After launching the software and specifying a track bed image file, the user will see a typical view, such as that shown in Figure C-6.

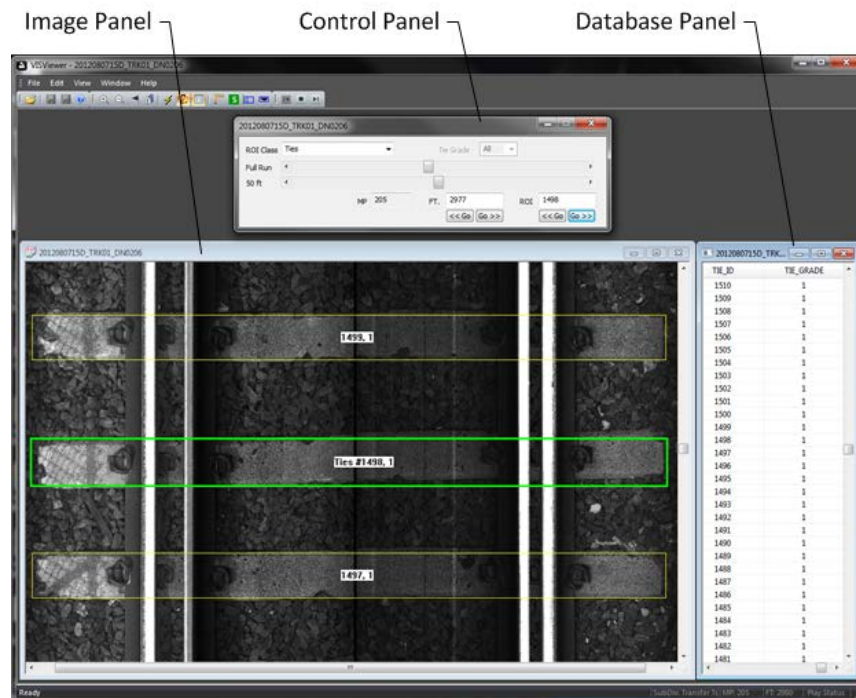


Figure C-6. Image Panel, Control Panel, and Database Panel for Phase 1 Software

As shown previously (and in Figure C-6), the software's graphical user interface (GUI) consists of three main components: 1) an image panel, 2) a control panel, and 3) a database panel. The image panel allows the user to scroll through a continuous track bed image. The control panel supports efficient navigation through large image files and has the ability to filter the types of nonconformances displayed in the image panel. Finally, the database panel allows a user to go directly to a specific nonconformance (or other region) in the image panel by selecting the region's entry in the table.

After nonconformances have been identified in a given image file, the software allows the image file to be aligned with a second image file corresponding to the same mile of track. To align two images, the user opens the first image and locates the mile post reference marker (see the green box on left side of Figure C-7). In this study, mile post reference markers are automatically inserted into image files based on GPS data that identifies and locates the physical mile posts in the real world. The GPS data allows the virtual mile posts to be inserted with approximately ± 12 feet of accuracy. After locating the mile post reference marker in the first image, the user opens the second image. Next, the user locates the mile post reference marker in the second image (see green box on right side of Figure C-7). Under ideal conditions, the reference markers in both

images would be adjacent to the same tie. However, due to inherent inaccuracies in GPS, the initial reference ties typically do not match. To correct this problem, the user scrolls up and down in either (or both) images to locate a pair of matching ties near the initial reference markers. After a pair of matching ties is located, the user repositions the reference markers accordingly. Then the software automatically renumbers all ties below the reference marker in each image. The user then repeats the same process to align the mile post reference markers at the end of the current mile.

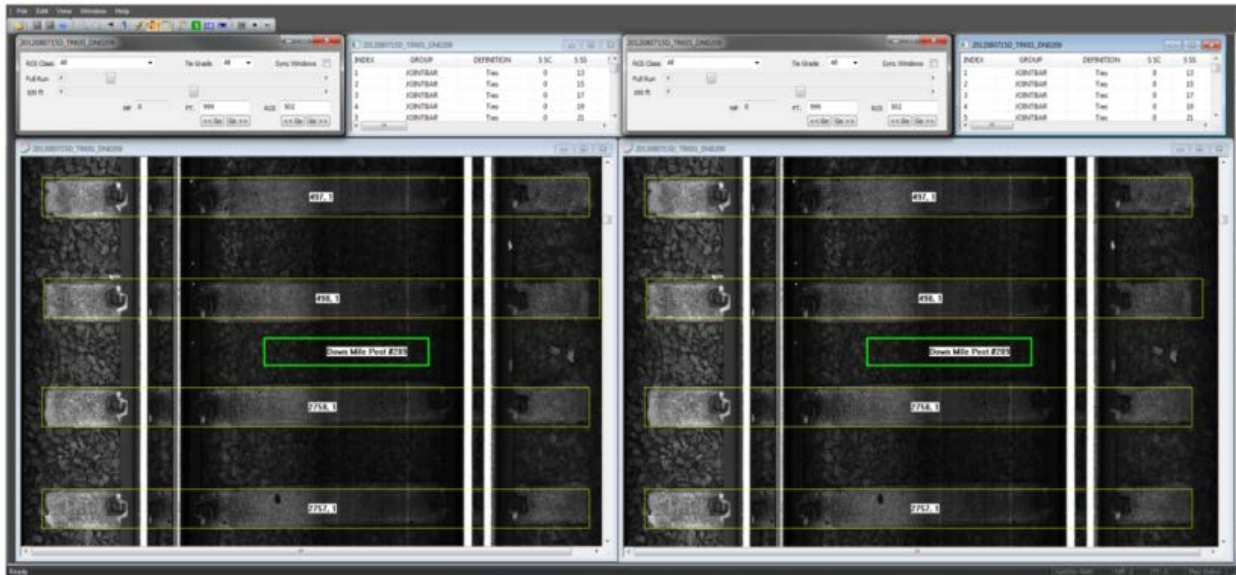


Figure C-7. Side-By-Side Track Bed Viewing Supported by the Phase 2 Software

Under ideal conditions, the alignment process would be complete at this point. However, in practice, the user employs the control panel navigation feature to verify/reconcile correct tie counts at multiple points throughout both image files. This final step ensures that the automatic tie detection found a match for all ties in both images.

Once all tie numbers match a given pair of image files, those files and the corresponding database tables containing tie boundaries are uploaded to a centralized server. A separate software tool, referred to as the Rail Vision Client (developed through support from the Computer Vision Laboratory at the University of Maryland, College Park), assigns infrastructure parameters to each detected tie based on the tie's known mile post and foot location. In this study, infrastructure parameters include: curvature, grade, tonnage, speed, traffic type, tie manufacturer, and year of installation.

After images have been uploaded, the Rail Vision Client application is used to manually review each tie and determine if the tie contains a nonconformance of interest (e.g., cracks, chipping, or surface erosion). Figure C-8 shows the Rail Vision Client configured to support manually locate nonconformances. Upon locating a nonconformance, an annotation tool within the Rail Vision Client is used to draw an outline around the nonconforming region. (An enlarged view of an annotated nonconformance is shown in Figure C-9.) The software then uses the outline coordinates to compute the area of the nonconforming region. Each annotation is ultimately transferred to the same nonconforming region on a matching tie from a subsequent image of the

tie. The user is then able to update the annotation boundary to account for any changes that have occurred over time. The point-by-point annotations entered by a user allow the software to accurately estimate a nonconformance progression rate as the change in nonconforming area divided by the elapsed time between imaging dates.



Figure C-8. GUI for University of Maryland Rail Vision Client Used in this Study to Annotate and Track Nonconformances

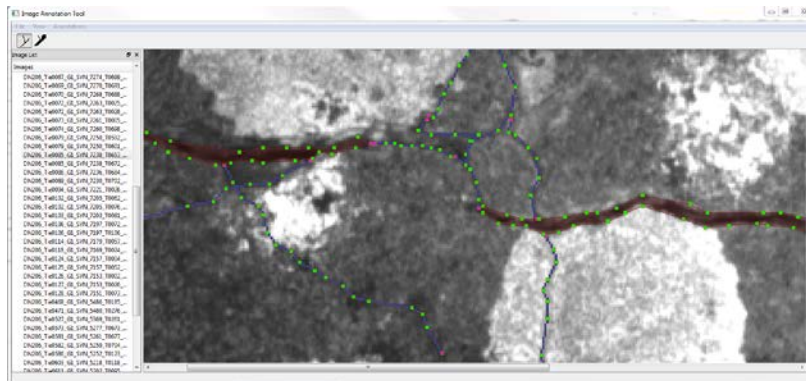


Figure C-9. Close-Up View of an Annotated Crack in a Concrete Tie